https://ntrs.nasa.gov/search.jsp?R=19750022031 2020-03-22T20:55:17+00:00Z

ECH LIBRARY KAFB, NM
0061236

NASA CONTRACTOR REPORT

NASA CR-2543

LOAN COPY: RETURN TO
AFWL TECHNICAL LIBRARY
KIRTLAND AFB, N. M.

PREDICTION OF UNSTEADY AERODYNAMIC LOADINGS CAUSED BY LEADING EDGE AND TRAILING EDGE CONTROL SURFACE MOTIONS IN SUBSONIC COMPRESSIBLE FLOW - ANALYSIS AND RESULTS

W. S. Rowe, M. C. Redman, F. E. Ehlers, and J. N. Sebastian

Prepared by
BOEING COMPANY
Seattle, Wash. 98124
for Langley Research Center

NATIONAL AERONAUTICS AND SPACE ADMINISTRATION • WASHINGTON, D. C. • AUGUST 1975

9 SEP 975
Technical Library
AF Weapons Laboratory

TECH LIBRARY KAFB, NM

0061236

1. Report No.	2. Government Accession No.	3. Recipient's Catalog No.
NASA CR-2543		

4. Title and Subtitle
PREDICTION OF UNSTEADY AERODYNAMIC LOADINGS CAUSED BY LEADING EDGE AND TRAILING EDGE CONTROL SURFACE MOTIONS IN SUBSONIC COMPRESSIBLE FLOW-ANALYSIS AND RESULTS

5. Report Date: August 1975

6. Performing Organization Code:

7. Author(s)
W. S. Rowe, M. C. Redman, F. E. Ehlers, and J. D. Sebastian

8. Performing Organization Report No.:

10. Work Unit No.:

9. Performing Organization Name and Address
The Boeing Commercial Airplane Company
P. O. Box 3707
Seattle, Washington 98124

11. Contract or Grant No.: NAS1-12020

13. Type of Report and Period Covered: Contractor Report

12. Sponsoring Agency Name and Address
National Aeronautics and Space Administration
Washington, D.C.

14. Sponsoring Agency Code:

15. Supplementary Notes
Final report.

16. Abstract

A theoretical analysis and computer program has been developed for the prediction of unsteady lifting surface loadings caused by motions of leading edge and trailing edge control surfaces having sealed gaps. The final form of the downwash integral equation has been formulated by isolating the singularities from the non-singular terms and using a preferred solution process to remove and evaluate the downwash discontinuities in a systematic manner. Comparisons of theoretical and experimental pressure data are made for several control surface configurations. The comparisons indicate that reasonably accurate theoretical pressure distributions and generalized forces may be obtained for a wide variety of control surface configurations.

Spanwise symmetry or antisymmetry of motion, and up to six control surfaces on each half span can be accommodated.

17. Key Words (Suggested by Author(s))	18. Distribution Statement
Flutter, Wing-Control-Surface Flutter, Aeroelasticity, Structural Dynamics, Aerodynamics, Unsteady Aerodynamics	Unclassified-Unlimited Subject Category 02 Aerodynamics

19. Security Classif. (of this report)	20. Security Classif. (of this page)	21. No. of Pages	22. Price*
Unclassified	Unclassified	152	$6.25

*For sale by the National Technical Information Service, Springfield, Virginia 22151

CONTENTS

PREDICTION OF UNSTEADY AERODYNAMIC LOADINGS CAUSED BY LEADING EDGE AND TRAILING EDGE CONTROL SURFACE MOTIONS IN SUBSONIC COMPRESSIBLE FLOW--ANALYSIS AND RESULTS

By

W. S. ROWE, M. C. REDMAN

F. E. EHLERS and J. D. SEBASTIAN

Boeing Commercial Airplane Company

SUMMARY

A theoretical analysis and computer program has been developed for the prediction of unsteady lifting surface loadings caused by motions of leading edge and trailing edge control surfaces having sealed gaps. The final form of the downwash integral equation has been formulated by isolating the singularities from the non-singular terms and using a preferred solution process to remove and evaluate the downwash discontinuities in a systematic manner. Comparisons of theoretical and experimental pressure data are made for several control surface configurations. The comparisons indicate that reasonably accurate theoretical pressure distributions and generalized forces may be obtained for a wide variety of control surface configurations.

INTRODUCTION

Historically, much effort has been expended to adapt conventional oscillating lifting-surface solution techniques to wings with control surfaces. Extensive use has been made of the reverse flow theorem (reference 1) to construct an analytical upwash function that is used in reverse flow to produce "equivalent" generalized forces. The generated upwash function is obtained by the expedient of smoothing over, in one way or another, the slope discontinuities and corresponding singularities within the pressure functions. The "equivalent" upwash function does not match the control surface slope accurately at all points, but does produce reasonable "indirect" generalized forces. The usefulness of this method deteriorates when the "direct" hinge-moment term is to be determined.

The work of reference 2 is one of the few subsonic methods developed to determine the 'direct' surface loadings using pressure terms that are capable of correctly representing the known singularity functions around the boundaries of the control surface. However, it was found that solutions obtained from the method of reference 2 were highly sensitive to the relative location and number of control point collocation stations used in the analysis. The sensitivity may be attributed to the particular solution process being applied that assumes that discontinuous downwash distributions may be approximated by a linear combination of polynomial represented downwash sheets that satisfy the boundary conditions at a select set of control points. Changing the control point locations by relatively small amounts results in large changes in the unsteady loadings. consequently, the method requires calculation of downwashes at many stations and seeking solutions in a least-squares-error sense.

Solution sensitivity remained until pressure distributions were developed (reference 3) that identify the functional distribution and singularity strengths required to produce identical mathematical downwash discontinuities contained in the kinematic distribution. A preferred solution process was developed by subtracting the discontinuous mathematical downwash distribution from the discontinuous kinematic distribution resulting in smooth downwash distribution for which standard lifting-surface solutions could be applied. The resulting loadings would then be relatively insensitive to the locations and number of control points used in the analysis.

The present work represents an extension of the analytical methods suggested in reference 3 to provide a capability of numerically predicting the unsteady loadings caused by control surface motions that is relatively insensitive to locations of collocation stations on the surface. Documentation of the computer program design, usage, and limitations is provided in reference 4.

SYMBOLS

All quantities are dimensionless except as indicated.

a_{nm}	Unknown coefficient of assumed pressure modes, equation 69
b [length]	Local semichord
b_0 [length]	Reference length
c	Local chord length nondimensional with respect to b_0
$\hat{C}$	Variable used in spanwise pressure modification function, equation 49
$f(\eta)$	Spanwise pressure difference distribution, equations 56 and 69
$g(\xi,\eta)$	Chordwise pressure difference distribution, equations 56 and 65
$H_j(x,y)$	Mode shape of mode j (see equation 5 for dimensions)
i	$\sqrt{-1}$
$K(x,\xi,y,\eta)$	Kernel function, equation 6
k	Reduced frequency = $\frac{\omega b_0}{V}$
$\underline{k}$	Index variable, equation 73
M	Mach number
$\bar{M}$	Number of downwash stations on a downwash chord
$\bar{N}$	Number of downwash chords on semispan
$\bar{n}$	Index variable, equation 69
P_ℓ [Force/area]	Pressure on lower surface
P_u [Force/area]	Pressure on upper surface
ΔP [Force/area]	Pressure difference, $P_\ell - P_u$ (positive upward)

ΔP_j [(Force/area)/unit q_j]	Surface pressure difference in mode j
q_j	Generalized coordinate amplitude for mode j
Q_{ij}	Generalized forces (see equation 77 for dimensions)
Q^s_{ij}	Sectional generalized forces (see equation 76 for dimensions)
R	$\sqrt{x_0^2 + \beta^2 y_0^2}$
S [length]	Semispan
s	Nondimensional semispan, S/b_0
V [length/time]	Free stream velocity
$\frac{w}{V}$	Kinematic angle of attack or nondimensional normalwash
$\overline{W}$	$\frac{w}{V}$
$\overline{w}_j$	$w_j/q_j e^{i\omega t}$
x,y,z	Coordinates nondimensional with respect to b_0
$\underline{x}$	Local chordwise coordinate $(x - x_m)/(b/b_0)$
x_m	Nondimensional coordinate of the mid-chord line
x_ℓ	Nondimensional coordinate of the leading edge
x_t	Nondimensional coordinate of the trailing edge
x_0	$x - \xi$
x_{cs}	Streamwise coordinate of hingeline at side edge of control surface
$x_{\ell s}$	Streamwise coordinate of planform leading edge at side edge of control surface
$\bar{\bar{x}}$	Local coordinate for full chord control surface, equation 46
$\tilde{x}$	Local coordinate for trailing edge control surface, equation 42

y_0		$y-\eta$
y_s		Spanwise coordinate of control surface side edge
Z_s		Surface deflection (see equation 4 for dimensions)
β		$\sqrt{1-M^2}$
β_h		$\sqrt{\beta^2 + \tan^2 \Lambda_c}$
β_ℓ		$\sqrt{\beta^2 + \tan^2 \Lambda_\ell}$
ΔC_p		Non-dimensional pressure difference between lower and upper surfaces $(P_\ell - P_u)/(\frac{1}{2} \rho V^2)$
Λ_c	[radian]	Sweep angle of the control surface hingeline, positive swept back
Λ_ℓ	[radian]	Sweep angle of leading edge, positive swept back on right hand side
ξ_c		Hingeline coordinate at span station η
ξ, η, ζ		Dummy variables for (x,y,z)
$\Theta_H(\eta)$	[radian]	Rotation angle of control surface hingeline at (η), measured in the plane perpendicular to the y-axis and positive trailing edge up
χ		Multiplication symbol
ρ	[mass/length^3]	Density of the fluid
t	[time]	Time
ω	[1/time]	Circular frequency of oscillation
Θ		Chordwise angular coordinate, equation 69
ϕ		Spanwise angular coordinate, equation 69

ANALYTICAL FORMULATION

The Integral Equation and Its Elements

This report describes the procedures used in calculating generalized aerodynamic forces existing on a lifting surface caused by motions of leading edge or trailing edge control surfaces in subsonic flow. The analysis is applicable to planform configurations having full span or multiple partial span control surfaces located anywhere along the leading or trailing edge of the planform.

The analysis coordinate system is defined in figure 1 for a typical trailing edge and/or leading edge control surface configuration:

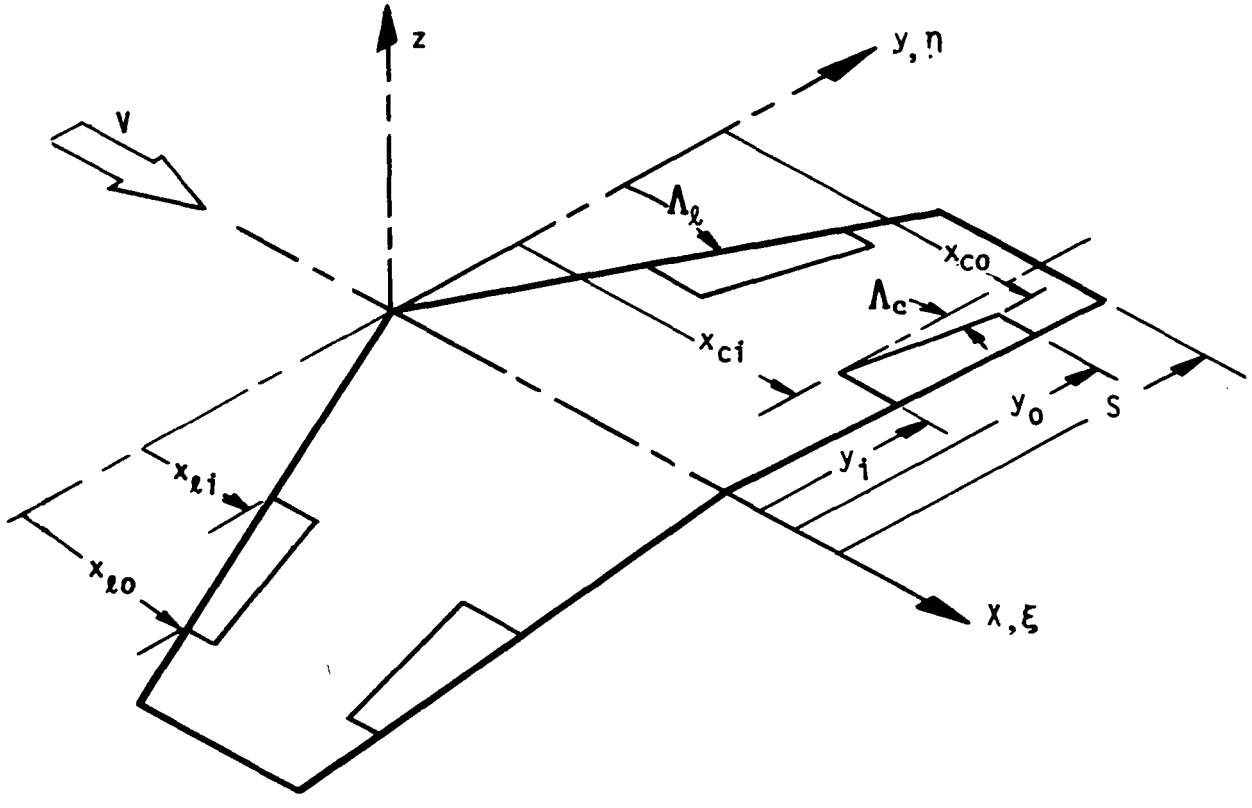

Figure 1 - Coordinate System Definition

Solutions are obtained by evaluating the downwash-pressure integral equation that has been derived from the linearized potential equation (1).

$$\nabla^2\phi(x,y,z,t) - \frac{1}{a^2}\left[V\frac{\partial}{\partial x} + \frac{\partial}{\partial t}\right]^2 \phi(x,y,z,t) = 0 \qquad (1)$$

The downwash-pressure integral equation derived in reference 5 provides the basis for the analytical formulations used in developing numerical methods for predicting unsteady loadings on lifting surfaces.

The general form of the integral equation derived in reference 5 and used throughout this discussion is given by the expression

$$\frac{w_s}{V} = \frac{1}{4\pi\rho V^2} \iint_{surface} \Delta P(\xi,\eta)\, K(x,\xi,y,\eta)\, d(b_0\xi)\, d(b_0\eta) \qquad (2)$$

where

$\frac{w_s}{V}$ represents the kinematic downwash caused by motions of the lifting surface

$\Delta P(\xi,\eta)$ represents the pressure difference between the upper and lower surface and is the only unknown in the equation

$K(x,\xi,y,\eta)$ represents the kernel function that defines the normalwash at x,y due to a pulsating pressure doublet at ξ,η.

Solutions of the integral equation are obtained by assuming that the lifting surface deflection shape, Z_s, may be represented by a finite sum of discrete mode shapes that are deflecting in a sinusoidal manner. That is, the deflection shape is assumed to be represented by

$$Z_s = \sum_j H_j(x,y)\, q_j\, e^{i\omega t} \qquad (3)$$

where Z_s has dimensions of length and is a function of time.

$H_j(x,y)$ is the deflection shape of the *jth* mode

q_j is the generalized coordinate defining how much of the *jth* mode is contained in Z_s.

The dimension of the product $H_j(x,y)q_j$ is in units of length. That is, if $H_j(x,y)$ has a dimension of length, then q_j is non-dimensional, or if $H_j(x,y)$ is non-dimensional, then q_j has units of length.

The kinematic downwash term of equation (2) is developed from the surface motion definition and is given as

$$w_s = \frac{DZ_s}{Dt} = -\left[\frac{\partial}{\partial t} + V\frac{\partial}{\partial(b_0 x)}\right] Z_s$$

$$\frac{w_s}{V} = \sum_j -\left[\frac{\partial H_j(x,y)}{\partial(b_0 x)} + \frac{i\omega H_j(x,y)}{V}\right] q_j\, e^{i\omega t}$$

$$\frac{w_s}{V} = \sum_j \left(\frac{\overline{w}_j}{V}\right) q_j\, e^{i\omega t} \qquad (4)$$

The total pressure difference between upper and lower surfaces is also dependent upon the modal displacement and is given as

$$\Delta P = P_\ell - P_u$$

$$\Delta P = \sum_j (\Delta P_j)\, q_j\, e^{i\omega t} \qquad (4a)$$

where $\Delta P_j = \frac{\partial(\Delta P)}{\partial\, q_j}$ (i.e., ΔP_j is per unit q_j)

The final form of the downwash integral equation is obtained by inserting the expressions for the kinematic downwash and pressure difference into equation (2) and removing the $q_j e^{i\omega t}$ term from both sides of the equation that results in the expression

$$-\left[\frac{\partial H_j}{\partial(b_0 x)} + \frac{i\omega H_j}{V}\right] = \frac{1}{4\pi\rho V^2} \iint_{surface} \Delta P_j(\xi,\eta)\, K(x,\xi,y,\eta)\, d(b_0\xi)\, d(b_0\eta) \qquad (5)$$

The pressure distribution $\Delta P_j(\xi,\eta)$ is the only unknown function within the integral equation and its dimensionality is established by noting that the product of $K(x,\xi,y,\eta)\,d(b_0\xi)d(b_0\eta)$ is non-dimensional and $(1/4\pi\rho V^2)$ has dimensional units of (1/(Force/area)) which requires that the dimensions of $\Delta P_j(\xi,\eta)$ is equal to the product of (Force/Area) times the dimensions of the kinematic downwash term.

That is, if $H_j(x,y)$ is dimensional, then the kinematic downwash is non-dimensional and results in having $\Delta P_j(\xi,\eta)$ take on dimensions of (Force/Area). However, if $H_j(x,y)$ is non-dimensional, then the kinematic downwash has dimensions of (1/length) which results in having dimensions of $\Delta P_j(\xi,\eta)$ defined as (Force/Area)/length .

The subscript (j) is omitted in the remaining sections, up to the section on generalized forces, with the understanding that the pressure terms being determined are those terms necessary to satisfy the *jth* mode shape boundary conditions.

The $K(x-\xi,y-\eta,M,k)$ term of equation (2) represents the kernel function of the integral equation that describes the surface normalwash at (x,y) due to a pulsating pressure doublet located at (ξ,η). The kernel function is defined as

$$K(x-\xi,y-\eta,M,k) = e^{-i\frac{\omega}{V}(x-\xi)} \lim_{z\to 0} \frac{\partial^2}{\partial z^2} \int_{-\infty}^{x-\xi} \frac{\exp\frac{i\omega}{V\beta^2}\left(\lambda - M\left[\lambda^2+\beta^2(y-\eta)^2+\beta^2z^2\right]^{\frac{1}{2}}\right)}{\left[\lambda^2+\beta^2(y-\eta)^2+\beta^2z^2\right]^{\frac{1}{2}}} d\lambda \qquad (6)$$

Reduction of equation (6) into a form easily evaluated by routine numerical procedures has been accomplished by Watkins, Runyan, and Woolston (reference 6) and presented in non-dimensional form by considering the variable as being referenced to some chosen length (b_0) and introducing the reduced frequency parameter $k = b_0\omega/V$ the function becomes

$$K(x-\xi,y-\eta,M,k) = \frac{e^{-ikx_0}}{b_0^2 y_0^2}\left\{-k|y_0|\left[K_1|ky_0|+i\frac{\pi}{2}\left(I_1|ky_0|-L_1|ky_0|\right) - i\right.\right.$$

$$\left. - i\int_0^h \left[\tau/(1+\tau^2)^{1/2}\right]\exp\left(ik|y_0|\tau\right)\,d\tau\right]$$

$$\left.\left. - x_0/(x_0^2+\beta^2y_0^2)^{1/2}\cdot\exp\left(\frac{ik}{\beta^2}\left[x_0-M(x_0^2+\beta^2y_0^2)^{1/2}\right]\right)\right\} \qquad (7)$$

where

$$h = \left[x_0-M(x_0^2+\beta^2y_0^2)^{1/2}\right]/\beta^2y_0$$

Singularities contained in equation (7) have been identified and are isolated in the following form

$$K(x,\xi,y,\eta) = K_{ns}(x,\xi,y,\eta) + K_s(x,\xi,y,\eta) \qquad (8)$$

where $K_{ns}(x,\xi,y,\eta)$ is the non-singular part of the kernel function.

The singular part is identified as

$$K_s(x,\xi y,\eta) = \frac{e^{-ikx_0}}{b_0^2}\left\{-\frac{1}{y_0^2}\left[1+x_0/(x_0^2+\beta^2y_0^2)^{1/2}\right] + ik/(x_0^2+\beta^2y_0^2)^{1/2}\right.$$

$$\left. - \frac{k^2}{2}\,\ell n|(x_0^2+\beta^2y_0^2)^{1/2}-x_0| - \frac{k^2}{2\beta^2}\left[x_0/(x_0^2+\beta^2y_0^2)^{1/2} - M\right]\right\} \qquad (9)$$

This expression contains the dipole, inverse square root, and logarithmic singularities identified in reference (6). The last term of equation (9) is not singular. However, it is included since special means are required in

evaluating the downwashes in regions near the downwash chord that are produced by this term.

Insertion of the above definitions into the downwash integral equation results in the following expression that is to be evaluated over the surface to satisfy the boundary condtions.

$$4\pi\rho V^2 \frac{w}{V} = \iint \Delta P(\xi,\eta)\, K_{ns}(x,\xi y,\eta)\, d(b_0\xi)d(b_0\eta)$$

$$- \iint \Delta P(\xi,\eta)\, e^{-ikx_0}\, \frac{1}{y_0^2} \left[1+x_0/(x_0^2+\beta^2 y_0^2)^{\frac{1}{2}}\right] d\xi d\eta$$

$$+ ik \iint \Delta P(\xi,\eta)\, e^{-ikx_0}/(x_0^2+\beta^2 y_0^2)^{\frac{1}{2}}\, d\xi d\eta$$

$$- \frac{k^2}{2} \iint \Delta P(\xi,\eta)\, e^{-ikx_0}\, \ell n|(x_0^2+\beta^2 y_0^2)^{\frac{1}{2}} - x_0|\, d\xi d\eta$$

$$- \frac{k^2}{2\beta^2} \iint \Delta P(\xi,\eta)\, e^{-ikx_0} \left[x_0/(x_0^2+\beta^2 y_0^2)^{\frac{1}{2}} - M\right] d\xi d\eta \qquad (10)$$

The first integral represents the contribution to the downwash at (x,y) due to the non-singular part of the kernel function. The general shape of $K_{ns}(x,\xi,y,\eta)$ is usually quite smooth for low Mach numbers and is due to the strong sinusoidal characteristic of e^{-ikx_0} in the expression. However, the chordwise characteristics change quite rapidly for Mach numbers greater than $M = 0.85$ as is demonstrated in figure 2 that represents the chordwise variation in the imaginary part of $K_{ns}(x,\xi,y,\eta)$ with Mach number. The $(x-\xi)$ coordinate of figure 2 represents the chordwise difference between the pulse sending point located at (ξ,η) and the downwash station (x,y).

Since the functional distributions of K_{ns} are quite different forward and aft of the downwash station the chordwise integration interval is subdivided into two intervals $x_\ell \leq \xi \leq x$ and $x \leq \xi \leq x_t$ to provide an accurate evaluation of the chordwise integral.

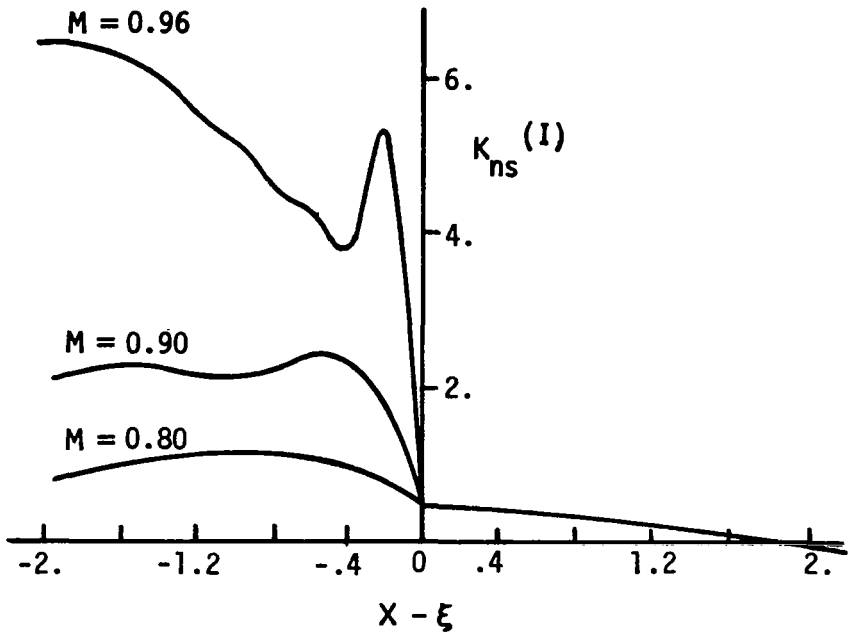

Figure 2 — Chordwise Variation of $K_{ns}^{(I)}$ as a Function of Mach Number for $y-\eta=0.05$, $k=0.7854$

The second, third, and fourth integrals of equations represent the downwash contributions due to the dipole, inverse square root, and logarithmic singularity terms respectively. The last integral does not contain a singularity in the spanwise direction, however, special procedures are required to evaluate its downwash contribution since a finite discontinuity exist for values of $\eta \rightarrow y$.

Evaluation of the Dipole Term

The downwash contribution due to the dipole term is evaluated using the method suggested by Hsu (reference 7). The dipole integral of equation (10) is given as

$$\overline{w}^{dp} = -\int_{-s}^{s}\int_{x_\ell}^{x_t} \Delta P(\xi,\eta) e^{-ikx_0} \frac{1}{(y-\eta)^2}\left[1+(x-\xi)/\left((x-\xi)^2+\beta^2(y-\eta)^2\right)^{1/2}\right] d\xi d\eta \qquad (11)$$

The downwash contribution due to the dipole term is determined by considering the normalwash at a point (x,y,ε) that is located just off the surface shown in figure 3.

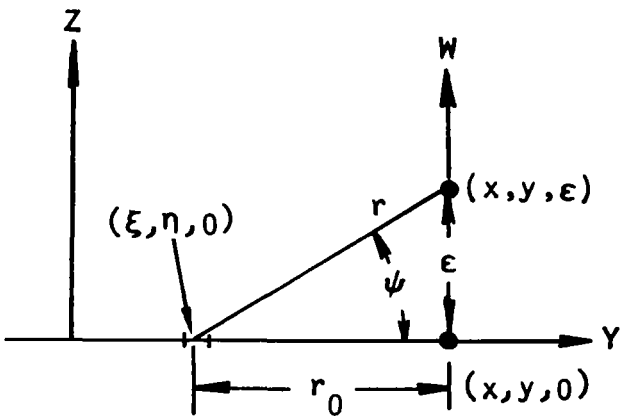

Figure 3 — Coordinate System Used in the Kernel Function Derivation

The kernel function describing the normalwash at (x,y,ε) due to a pressure pulse at $(\xi,\eta,0)$ is given by

$$K(x,\xi,y,\eta) = e^{-ikx_0}\left[\frac{1}{r}\frac{\partial E_0}{\partial r} + \sin^2\psi\left(\frac{\partial^2 E_0}{\partial r^2} - \frac{1}{r}\frac{\partial E_0}{\partial r}\right)\right] \qquad (12)$$

where $$E_0 = \int_{-\infty}^{h} e^{ik\lambda} (r^2+\lambda^2)^{-1/2} \, d\lambda$$

$$h = (x_0-MR)/\beta^2; \quad R = (x_0^2+\beta^2 r^2)^{1/2}; \quad x_0 = x-\xi$$

The dipole portion of the kernel is

$$K^{dp} = + e^{-ikx_0} \frac{1}{r^2} (1+x_0/R) \, (-1 + 2 \sin^2\psi)$$

Using the geometric properties of figure 3 that define

$$r^2 = r_0^2+\epsilon^2; \quad r_0 = y_0 = y-\eta; \quad \sin \psi = \frac{\epsilon}{r}, \quad R = (x_0^2+\beta^2 r_0^2)^{1/2}$$

The dipole portion then takes on the definition

$$K^{dp} = - e^{-ikx_0} \frac{(r_0^2-\epsilon^2)}{(r_0^2+\epsilon^2)^2} \left(1+x_0/R_0+0(\epsilon^2)\right) \tag{13}$$

where the terms represented by $0(\epsilon^2)\to 0$ as $\epsilon \to 0$.

The normalwash at $(x,y,0)$ is obtained by a limiting process allowing $\epsilon \to 0$ after the normalwash integral has been evaluated as indicated by the following:

$$\overline{w}^{dp}(x,y,0) = \lim_{\epsilon\to 0} - \int_{-s}^{s} \frac{(y_0^2-\epsilon^2)}{(y_0^2+\epsilon^2)^2} (s^2-\eta^2)^{1/2} \int_{x_\ell}^{x_t} \frac{\Delta P(\xi,\eta)}{(s^2-\eta^2)^{1/2}} e^{-ikx_0} [1+x_0/R_0] d\xi d\eta \tag{14}$$

Following the development of reference 7, let $G(x,y,\eta)$ be the chordwise integral

$$G(x,y,\eta) = \int_{x_\ell}^{x_t} \frac{\Delta P(\xi,\eta)}{(s^2-\eta^2)^{1/2}} e^{-ikx_0} \quad (1+x_0/R_0)\, d\xi \tag{15}$$

and as $\eta \to y$ this integral becomes

$$\lim_{\eta \to y} G(x,y,\eta) = G(x,y,y)$$

One of the singularities is then subtracted from equation (14) that results in the expression

$$\overline{W}^{dp}(x,y,0) = \lim_{\epsilon \to 0} \left\{ - \int_{-s}^{s} y_0 \frac{(y_0^2-\epsilon^2)}{(y_0^2+\epsilon^2)^2} (s^2-\eta^2)^{1/2} \frac{[G(x,y,\eta)-G(x,y,y)]}{y-\eta}\, d\eta \right.$$

$$\left. - G(x,y,y) \int_{-s}^{s} \frac{(y_0^2-\epsilon^2)}{(y_0^2+\epsilon^2)^2} (s^2-\eta^2)^{1/2}\, d\eta \right\} \tag{16}$$

The finite part of the second integral is

$$\lim_{\epsilon \to 0} - \int_{-s}^{s} \frac{(y_0^2+\epsilon^2)}{(y_0^2+\epsilon^2)^2} (s^2-\eta^2)^{1/2}\, d\eta = \pi$$

The first integral in equation (16) is also singular. However, it may be evaluated using Cauchy integrals provided that the term

$$\frac{[G(x,y,\eta) - G(x,y,y)]}{y - \eta}$$

exists in the limit as $\eta \to y$ and takes on a definition of the first derivative of $G(x,y,\eta)$ with respect to η.

The need of applying Cauchy integral procedures to equation (16) may be circumvented by subtracting an additional singularity.

Defining

$$H(x,y,\eta) = (s^2-\eta^2)\,\frac{[G(x,y,\eta) - G(x,y,y)]}{y - \eta} \tag{17}$$

and let

$$H(x,y,y) = \lim_{\eta\to y} H(x,y,\eta)$$

$$= -\,(s^2-y^2)\,\frac{\partial}{\partial\eta}\,[G(x,y,\eta)]_{\eta=y}$$

then

$$\overline{w}^{dp}(x,y,0) = \lim_{\varepsilon\to 0}\left\{-\int_{-s}^{s} y_0\,\frac{(y_0{}^2-\varepsilon^2)}{(y_0{}^2+\varepsilon^2)^2}\,\frac{1}{(s^2-\eta^2)^{\frac{1}{2}}}\,\frac{[H(x,y,\eta) - H(x,y,y)]}{y - \eta}\,d\eta\right.$$

$$\left. - H(x,y,y)\int_{-s}^{s} y_0\,\frac{(y_0{}^2-\varepsilon^2)}{(y_0{}^2+\varepsilon^2)^2}\,\frac{1}{(s^2-\eta^2)^{\frac{1}{2}}}\,d\eta\right\} + \pi G(x,y,y) \tag{18}$$

The second integral limits out to zero as $\varepsilon\to 0$ and equation (18) takes on the integral form of

$$\overline{w}^{dp}(x,y,0) = -\int_{-s}^{s}\frac{1}{(s^2-\eta^2)^{\frac{1}{2}}}\left\{(s^2-\eta^2)\,\frac{[G(x,y,\eta)-G(x,y,y)]}{(y-\eta)^2} - \frac{(s^2-y^2)G'(x,y,y)}{y-\eta}\right\}d\eta$$

$$+ \pi\, G(x,y,y) \tag{19}$$

It should be noted that, as $\varepsilon\to y$, the integrand of equation (19) tends to take on the definition of a second derivative of $G(x,y,\eta)$ with respect to η.

However, the second derivative does not exist since the integrand is singular at the downwash chord $\eta = y$. An example of this singular characteristic when $\eta \rightarrow y$ is shown in figure 4 which represents a plot of the spanwise integrand of equation (19) applied to the analysis planform shown in the sketch.

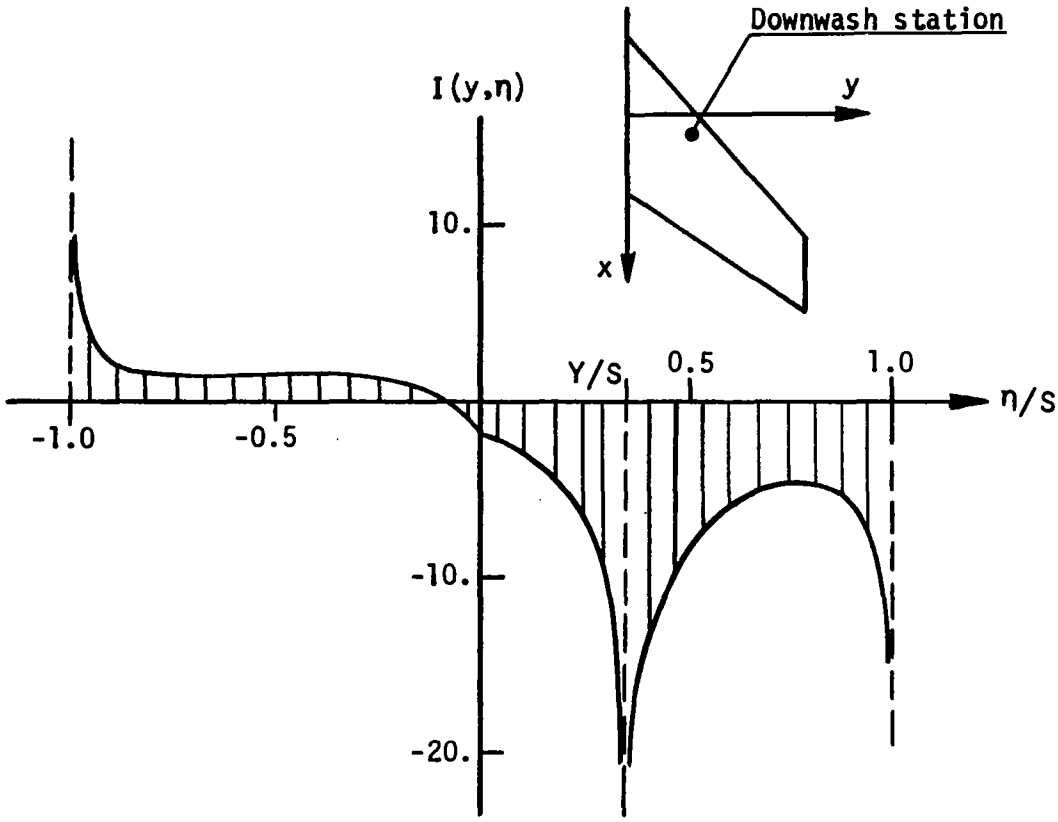

Figure 4 — Spanwise Variation of the Integrand of Equation (19) Displaying the Singularity at the Downwash Chord.

In the following section, the singularity just described is identified as being logarithmic in its character and numerical evaluation of equation (19) will be accomplished using logarithmic quadrature integration functions. Also, the following section contains a description of how the spanwise integrand may be modified to provide a non-singular distribution that may be readily evaluated by Legendre-Gauss integration quadrature functions.

IDENTIFICATION OF SPANWISE SINGULARITIES

The spanwise singularity contained within the integrand of the dipole downwash term was first identified by Multhopp (reference 8) in the development of the steady state lifting surface solution. The technique developed by Multhopp has been extended by Laschka (reference 9) to make it applicable for use in non-steady lifting surface solutions.

The functional expression of the additional singularity contained within the dipole downwash term may be obtained by developing a Taylor series expansion of $\Delta P(\xi,\eta)^{-ikx_0}$ about the downwash station and performing the resulting chordwise integration. That is, let $\Delta P(\xi,\eta)e^{-ikx_0}$ be approximated by spanwise-chordwise Taylor series given by

$$\Delta P(\xi,\eta)e^{-ikx_0} = \Delta P(x,y) + (\eta-y)\frac{\partial}{\partial\eta}\left[\Delta P(\xi,\eta)^{-ikx_0}\right]_{\substack{\eta=y\\ \xi=x}} + (\xi-x)\left[\frac{\partial}{\partial\xi}\left[\Delta P(\xi,y)e^{-ikx_0}\right]_{\xi=x} + (\eta-y)\frac{\partial^2}{\partial\xi\partial\eta}\left[\Delta P(\xi,\eta)e^{-ikx_0}\right]_{\substack{\eta=y\\ \xi=x}}\right] + \cdots \qquad (20)$$

The singularity in the spanwise integrand is identified by inserting equation (20) into the dipole chordwise integral of equation (10) and performing the indicated integration that results in the spanwise integral given as

$$I^{dp} = -\int_{-s}^{s}\frac{1}{y_0^2}\left[\frac{\partial}{\partial\xi}\left[\Delta P(\xi,y)e^{-ikx_0}\right]_{\xi=x} + (\eta-y)\frac{\partial^2}{\partial\xi\partial\eta}\left[\Delta P(\xi,\eta)e^{-ikx_0}\right]_{\substack{\eta=y\\ \xi=x}}\right]\chi$$

$$\left[\left[\frac{\beta^2}{2}y_0^2\ell n\beta^2y_0^2\right] + \begin{matrix}\text{Regular}\\ \text{Terms}\end{matrix}\right]d\eta \qquad (21)$$

Thus, the additional singularity is identified as being logarithmic in character which is amenable to integration by use of logarithmic integration quadrature functions.

The third integrals of equation (10) also contain a spanwise singularity that is proportional to $\ell n\beta^2(y-\eta)^2$. The singularity is identified by inserting the Taylor series expansion of equation (20) into the third downwash term and performing the chordwise integration that results in a spanwise integral given as

$$I^{(3)} = ik \int_{-s}^{s} \left[\Delta P(x,y)+(\eta-y) \frac{\partial}{\partial \eta}\left[\Delta P(\xi,\eta)e^{-ikx_0}\right]_{\substack{\xi=x \\ \eta=y}} \right] \left[\ell n\beta^2(y-\eta)^2 + \begin{matrix}\text{Regular} \\ \text{Terms}\end{matrix} \right] d\eta \quad (22)$$

The fourth integral of equation (10) has a spanwise singularity that may be identified by redefining the logarithmic part of the kernel function to have the following form for $\xi<x$

$$\ell n\left[\left((x-\xi)^2+\beta^2(y-\eta)^2\right)^{1/2} - (x-\xi)\right] = \ell n\beta^2(y-\eta)^2 - \ell n\left[\left((x-\xi)^2+\beta^2(y-\eta)^2\right)^{1/2} + (x-\xi)\right]$$

Insertion of this expression into the chordwise integral results in the equation for $I^{(4)}$ of

$$I^{(4)} = -\frac{k^2}{2} \int_{-s}^{s} \left[\ell n\beta^2(y-\eta)^2 \int_{x_\ell}^{x} \Delta P(\xi,y)e^{-ikx_0}\, d\xi + \begin{matrix}\text{Regular} \\ \text{Terms}\end{matrix} \right] d\eta \quad (23)$$

Once the singularities have been identified they may be subtracted out of the integrand and analytically evaluated outside of the integral.

Figure 5 shows the very smooth spanwise distributions of the integrand $I(y,\eta)$ obtained for the dipole term by subtracting out the identifiable singularities of equation (21). Removal of the singularities allows the use of Legendre-Gauss quadrature formulas to evaluate the spanwise integral using only a very small number of quadrature stations. As in any singularity subtraction process, localized gradients may appear that may require additional subdivision of the integration interval to accurately evaluate the integral.

It should be noted that there is a slope discontinuity yet existing at the downwash station and this may be smoothed by subtracting additional terms of the Taylor series expansion.

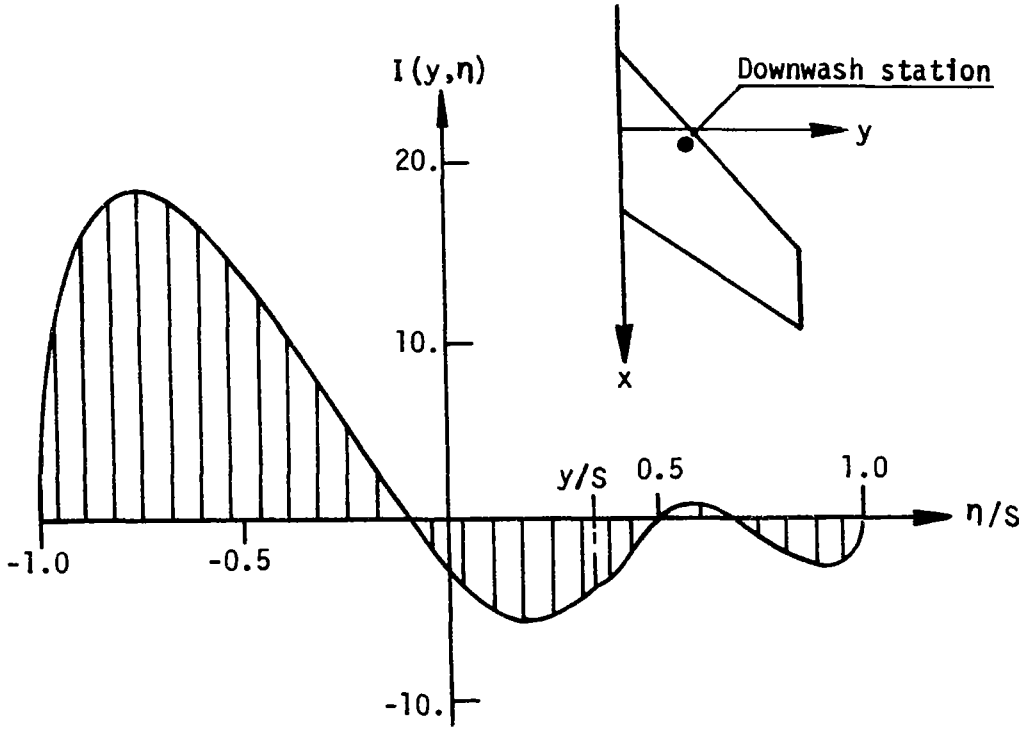

Figure 5 — Spanwise Variation of Integrand of Equation (19) with Singularities of Equation (12) Removed from the Integrand

As a consequence of the above there are several options open to the analyst in evaluating the spanwise portions of the downwash integral and are:

(1) ignore the logarithmic singularity since it is of relatively low order,

(2) subtract the singularities out of the expression and analytically evaluate their downwash contribution, and

(3) apply numerical integration quadrature functions that can evaluate the logarithmic term at the downwash chord.

Numerical investigations have been performed to determine the validity in using any one of the three integration options within the control surface program. The analysis planform shown in figure 6 is a rectangular wing having a full span flap deflected in steady flow. The deflection shape and step function downwash distribution are also displayed to show the discontinuity that must be matched by the mathematical downwash calculation of the integral equation. The assumed pressure distribution used in the analysis is composed of a chordwise singularity term $\ell n(\xi - x_c)^2$ and other modifying terms required to satisfy the boundary conditions along the planform edges.

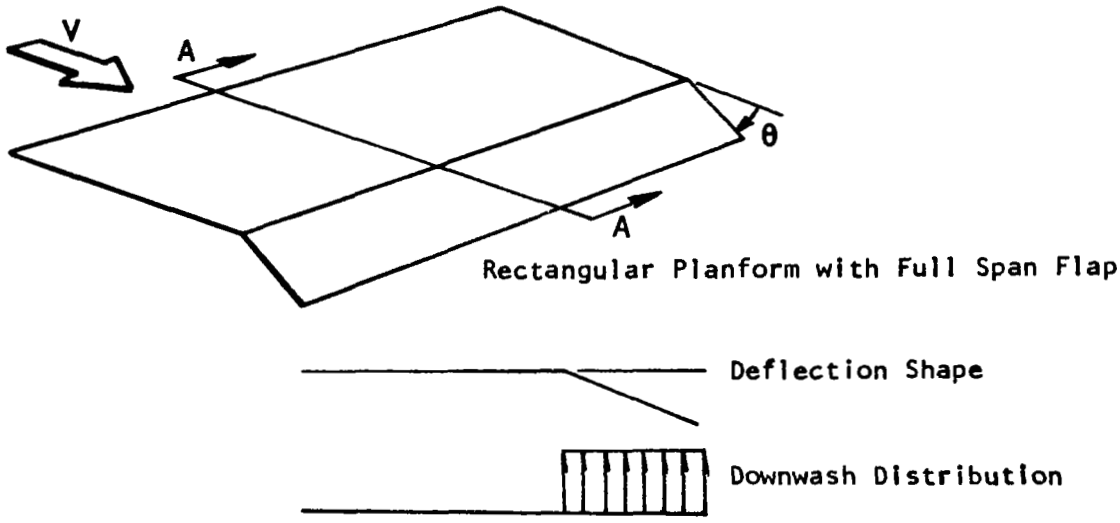

Figure 6 — Analysis Planform Used to Evaluate Effect of Spanwise Singularities on Downwash Distribution

Results of applying option (1) to evaluate the spanwise integral of equation (19) are shown in figure 7. The integral is evaluated using the interdigiting process suggested in reference 7 where a single Gauss-Mehler quadrature function is applied over the complete span of the planform. The singularity at the downwash chord is not recognized by this integration procedure and consequently the resulting chordwise downwash distribution is smooth and continuous across the hingeline. It appears that lifting surface solutions obtained using option (1) will not provide a satisfactory mathematical representation of the boundary conditions for physical wing-control surface combination.

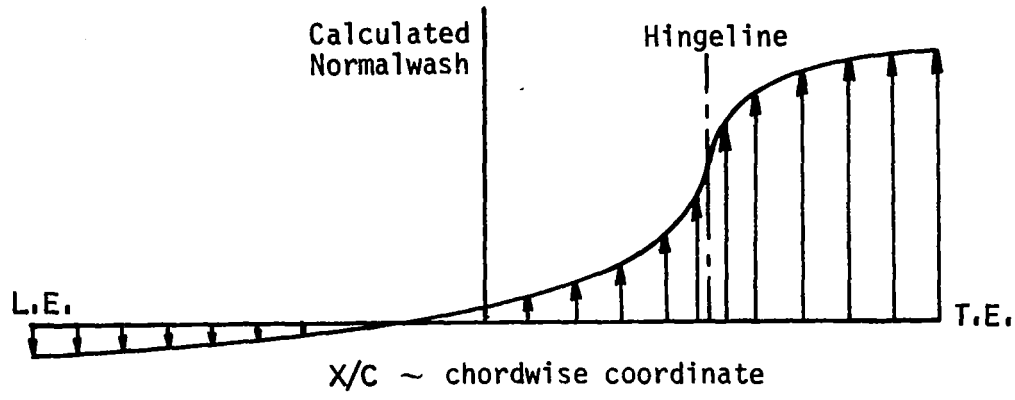

Figure 7 — Chordwise Downwash Distribution at Mid-Span Station Resulting from Applying Option (1) (logarithmic singularity ignored)

Figure 8 presents the results using the second option where the singularity is treated by approximating the pressure terms by a Taylor series expansion and removing the singularity from the spanwise integrand. Equation (19) has been modified by subtracting the singularities (identified in equation (21)) and evaluating their effect outside of the integral.

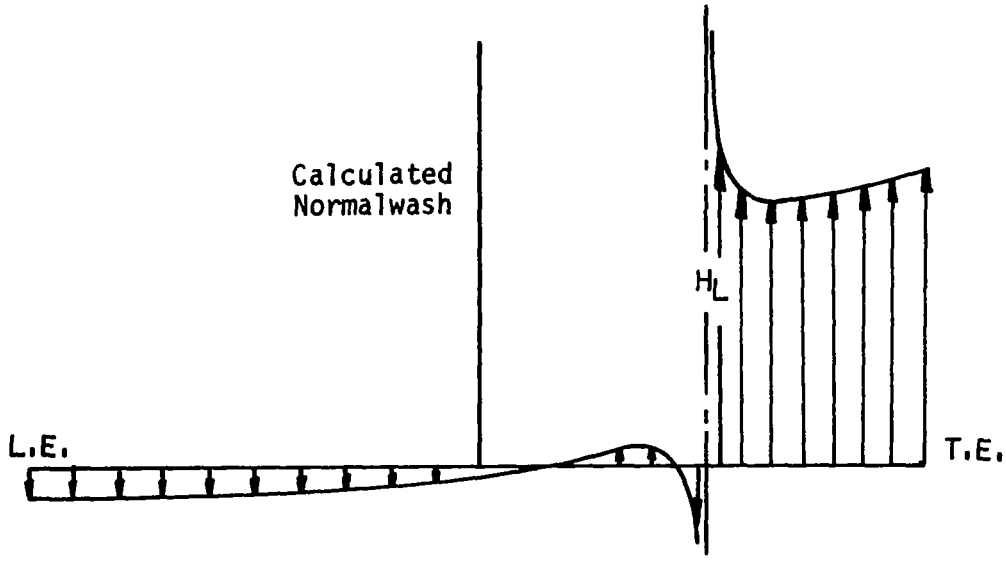

Figure 8 — Chordwise Downwash Distribution Resulting from Applying Option (2) (logarithmic singularity is subtracted and evaluated separately)

The downwash distribution appears to be reasonable at large distances from the hingeline; however, the downwash becomes singular at the hingeline. This is to be expected since the pressure term used in the analysis to provide the step function change in boundary conditions across the hingeline is proportional to $\ell og|\xi-x_c|$, which cannot be approximated by a Taylor series in the vicinity of the singularity at $\xi=x_c$.

The downwash distribution shown in figure 8 indicates that the downwash collocation stations are to be restricted to chordwise locations that are spaced well away from hingeline where large downwash gradients are developed. This restriction may not be satisfied for analyses of wings having small percent chord control surfaces.

This restriction may be removed by applying option (3) where the spanwise integral is evaluated by subdividing the integration interval, $-s\leq\eta\leq s$, into several subintervals and applying quadrature formulas appropriate to the functional characteristics of the integrand.

Results of applying option (3) to evaluate equation (19) are shown in figure 9. The integration interval has been divided into subregions and appropriate quadrature formulas have been applied in the subregions, *i.e.*, square root quadrature formulas applied at ends of the interval, logarithmic quadrature formulas used on either side of the downwash station, and Legendre quadratures applied within the remaining integration intervals.

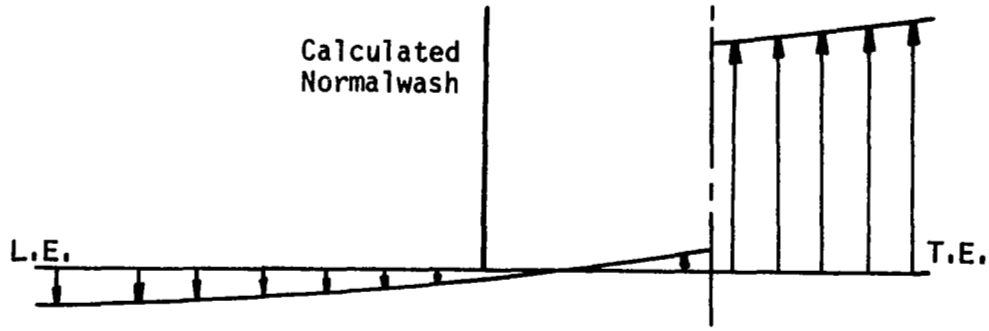

Figure 9. Chordwise Downwash Distribution Resulting from Applying Option (3) (logarithmic singularity evaluated by appropriate quadrature formulas)

The resulting downwash distribution (figure 9) does contain the step function change across the hingeline necessary to satisfy the boundary conditions and does not exhibit any large gradients near the hingeline that may cause solution sensitivities for analysis of small chord control surfaces.

Additional numerical investigations of calculated downwash distributions have been accomplished to identify the specific integration technique that would provide the least error in calculated downwash values for stations near the leading edge where large pressure gradients appear in the solution process. An assumed pressure function that is inversely proportional to the square root of the distance from the leading edge was applied to a rectangular planform having an aspect ratio of six. Figure 10 represents the steady state chordwise downwash distributions obtained at the mid semispan station using option 2 and option 3. The distributions appear to be similar for stations located at large distances from the leading edge, however, the option 2 distribution

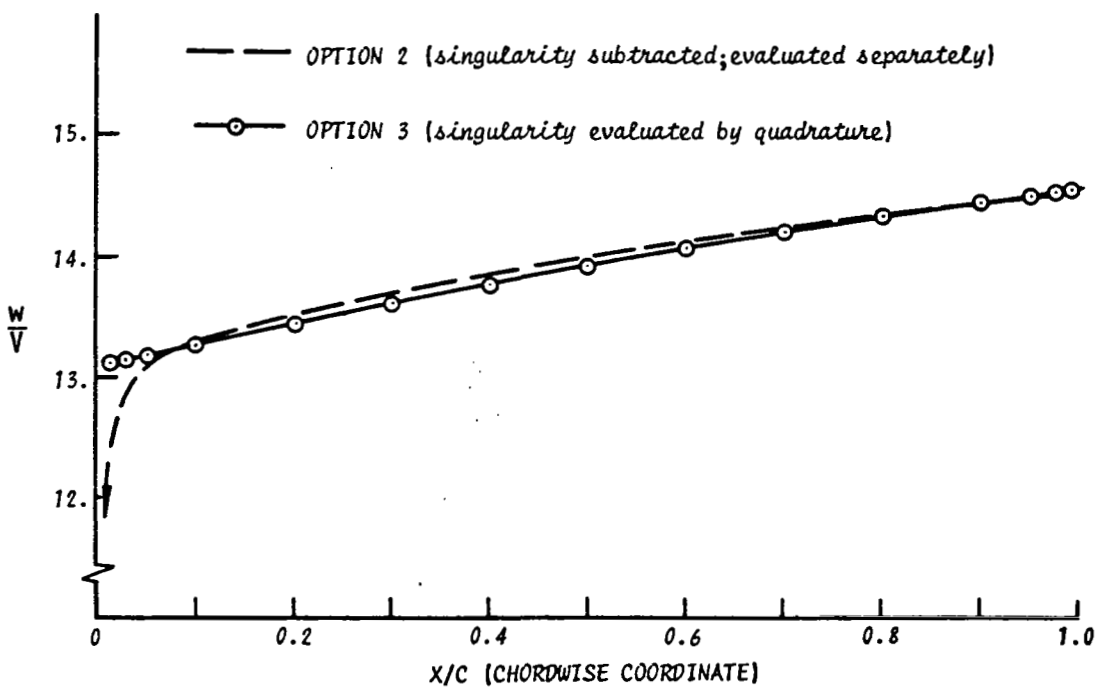

Figure 10 — Chordwise Downwash Distribution for Inverse Square Root Pressure Function Resulting from Applying Option 2 and Option 3.

(where the logarithmic singularity is subtracted from the integrand and evaluated separately) is tending to become singular near the leading edge. Again, this tendency for the calculated downwashes to become singular is expected since the Taylor series expansion of the inverse square root does not exist at the leading edge. The distribution obtained by applying appropriate quadrature formulas to the spanwise integrand (option 3) appears to be continuous for all regions including stations near the leading edge.

Consequently, it appears that application of option 3 will provide solutions that will not be sensitive to the relative location of downwash collocation stations for analysis of either small percent chord control surface configurations or for analysis of standard lifting surface configurations.

The above numerical investigations have been accomplished for the steady flow condition by evaluating equation (19) having the reduced frequency, k, set equal to zero. The following section establishes the numerical methods used to evaluate the downwashes for sinusoidal unsteady motion.

Evaluation of the Unsteady Downwash Integral

The downwash integral for unsteady motion is evaluated using a modification of the procedure suggested by Hsu (reference 7) where two singularities are subtracted and evaluated outside of the integral. The procedure previously described to evaluate the downwash due to the dipole term is modified by changing the definition of $H(x,y,\eta)$ of equation (17) to become

$$H(x,y,\eta) = \left[\frac{G(x,y,\eta) - G(x,y,y)}{y - \eta}\right] \tag{24}$$

such that

$$H(x,y,y) = \lim_{\eta \to y} H(x,y,\eta) = \left.\frac{\partial G(x,y,\eta)}{\partial \eta}\right|_{\eta=y} = G'(x,y,y) \tag{25}$$

Then equation (19) may be written in the revised form of

$$\overline{W}^{dp}(x,y,0) = -\int_{-s}^{s}(s^2-\eta^2)^{\frac{1}{2}}\left\{\frac{G(x,y,\eta)-G(x,y,y)}{(\eta-y)} - G'(x,y,\eta)\Big|_{\eta=y}\right\}\frac{d\eta}{(\eta-y)}$$

$$+ \pi\, G(x,y,y)-G'(x,y,\eta)\Big|_{\eta=y}\int_{-s}^{s}(s^2-\eta^2)^{\frac{1}{2}}\frac{d\eta}{(\eta-y)} \qquad (26)$$

and this is returned to another form using the definitions of $\Delta P(\xi,\eta)$ and the dipole kernel that results in

$$\frac{\overline{W}^{dp}}{4\rho V^2} = -\int_{-s}^{s}(s^2-\eta^2)^{\frac{1}{2}}\left\{\int_{x_\ell}^{x_t}\overline{\Delta P}(\xi,\eta)e^{ikx_0}\left[-\frac{1}{(y-\eta)^2}\left[1+\frac{x_0}{\sqrt{x_0^2+\beta^2y_0^2}}\right]\right]d\xi\right.$$

$$\left. + 2\int_{x_\ell}^{x}\frac{\overline{\Delta P}(\xi,\eta)e^{-ikx_0}\,d\xi}{(y-\eta)^2} - \frac{G'(x,y,\eta)\Big|_{\eta=y}}{(y-\eta)}\right\}d\eta$$

$$+ \pi\, 2\int_{x_\ell}^{x}\overline{\Delta P}(\xi,y)e^{-ikx_0}\,d\xi + \pi\, y\, G'(x,y\eta)\Big|_{\eta=y} \qquad (27)$$

where $\overline{\Delta P}(\xi,\eta) = \Delta P(\xi,\eta)/(s^2-\eta^2)^{\frac{1}{2}}$

$$G'(x,y,\eta)\Big|_{\eta=y} = \frac{\partial}{\partial\eta}\left\{\int_{x_\ell}^{x_t}\overline{\Delta P}(\xi,\eta)e^{-ik(x_0)}\left[1+\frac{x_0}{\sqrt{x_0^2+\beta^2y_0^2}}\right]d\xi\right\}_{\eta=y}$$

The downwashes due to the non-singular part of the kernel function are evaluated using Gauss-Legendre integration quadrature functions. The final form used to evaluate the downwash integral is given as follows:

$$\int_{-s}^{s} (s^2-\eta^2)^{\frac{1}{2}} \int_{x_\ell}^{x_t} \overline{\Delta P}(\xi,\eta) K(x,\xi,y,\eta)\, d(b_0\xi) d(b_0\eta) =$$

$$\int_{-s}^{s} (s^2-\eta^2)^{\frac{1}{2}} \left[f(\eta) \left\{ C_s(y,\eta) + C_{ns}(y,\eta) \right\} + f(y) \frac{\overline{G}(x,y,y)}{(y-\eta)^2} - \frac{G'(x,y,\eta)\Big|_{\eta=y}}{y-\eta} \right] d\eta$$

$$+ \pi\ G(x,y,y) + \pi\, y\, G'(x,y,\eta)\Big|_{\eta=y} \qquad (28)$$

where

$$\overline{\Delta P}(\xi,\eta) = \frac{\Delta P(\xi,\eta)}{(s^2-\eta^2)^{\frac{1}{2}}} = f(\eta)\ g(\xi,\eta)$$

$f(\eta)$ is the spanwise assumed pressure distribution divided by $(s^2-\eta^2)^{\frac{1}{2}}$.

$g(\xi,\eta)$ is the assumed chordwise pressure distribution.

$C_s(y,\eta)$ represents the chordwise integral due to the singular part of the kernel function

$$C_s(y,\eta) = \qquad (29)$$

$$= \int_{x_\ell}^{x_t} g(\xi,\eta) e^{-ik(x-\xi)} \left\{ \frac{1}{(y-\eta)^2} \left[1 + \frac{x-\xi}{\sqrt{(x-\xi)^2+\beta^2(y-\eta)^2}} \right] + \frac{ik}{\sqrt{(x-\xi)^2+\beta^2(y-\eta)^2}} \right.$$

$$\left. - \frac{k^2}{2} \log \left[\sqrt{(x-\xi)^2+\beta^2(y-\eta)^2} - (x-\xi) \right] - \frac{k^2}{2\beta^2} \left[\frac{x-\xi}{\sqrt{(x-\xi)^2+\beta^2(y-\eta)^2}} - M \right] \right\} d\xi$$

$C_{ns}(y,\eta)$ represents the chordwise integral due to the non-singular part of the kernel function

$$C_{ns}(y,\eta) = \int_{x_\ell}^{x_t} g(\xi,\eta)\, K(x,\xi,y,\eta)_{ns}\, d\xi \tag{30}$$

$$G(x,y,y) = f(y)\, 2 \int_{x_\ell}^{x} g(\xi,y)\, e^{-ik(x-\xi)}\, d\xi \tag{31}$$

$$G'(x,y,\eta)\Big|_{\eta=y} = \frac{\partial}{\partial\eta}\left\{ f(\eta) \int_{x_\ell}^{x_t} g(\xi,\eta) e^{-ik(x-\xi)} \left[1 + \frac{x-\xi}{\sqrt{(x-\xi)^2+\beta^2(y-\eta)^2}} \right] d\xi \right\}_{\eta=y} \tag{32}$$

The chordwise integrals of equations (29), (30), and (31) are numerically evaluated by subdividing the integration interval into small regions and applying integration quadrature formulas appropriate to the functional characteristics of the integrand. The spanwise integration interval of equation (28) is also subdivided into small integration intervals that includes an interval around the downwash chord where logarithmic integration quadrature formulas are applied to evaluate the spanwise singularity previously identified.

Evaluation of the spanwise derivative defined by equation (32) may be accomplished following the rule for differentiating a definite integral providing the integrand $g(\xi,\eta)$ does not contain terms that are singular. Special procedures are developed to evaluate equation (32) for the case of having pressure functions that have an inverse square root singularity at the leading edge or having a logarithmic singularity at the hingeline and are given as follows.

The chordwise integral for the case of having a pressure function that has an inverse square root singularity at a swept leading edge is given by

$$I = f(\eta) \int_{x_\ell}^{x_t} \frac{1}{\sqrt{\xi - x_\ell}} g(\xi,\eta) e^{-ik(x-\xi)} \left[1 + \frac{x-\xi}{\sqrt{(x-\xi)^2+\beta^2(y-\eta)^2}} \right] d\xi \qquad (33)$$

It is required to evaluate $\left.\frac{\partial I}{\partial \eta}\right|_{\eta=y}$ and may be accomplished by forming a Taylor series expansion of the last term of the integrand about $\eta=y$; that is

$$\left[1 + \frac{x-\xi}{\sqrt{(x-\xi)^2+\beta^2(y-\eta)^2}} \right] \cong \left[1 + \frac{x-\xi}{|x-\xi|} \right] - \frac{(\eta-y)^2}{2} \frac{\beta^2}{(x-\xi)^2} + \cdots \qquad (34)$$

and apply a transformation to reduce the integrand to an easily integrated form by letting

$$\tau = \xi - x_\ell$$

then

$$d\xi = d\tau$$

$$I = f(\eta) e^{ikx_\ell} \int_0^{x_t - x_\ell} \frac{1}{\sqrt{\tau}} g(\tau+x_\ell,\eta) e^{-ik(x-\tau)} \left[1 + \frac{x-(\tau+x_\ell)}{|x-(\tau+x_\ell)|} \right] d\xi$$

$$- f(\eta) e^{-ikx_\ell} \int_0^{x_t - x_\ell} \frac{1}{\sqrt{\tau}} g(\tau+x_\ell,\eta) e^{-ik(x-\tau)} \frac{(\eta-y)^2}{2} \frac{\beta^2}{(x-(\tau+x_\ell))^2} d\xi \qquad (35)$$

The last integral of the above expression will not contribute to the derivative value when evaluated at $\eta=y$ and may be neglected in the derivative calculation.

Following the rule for differentiating a definite integral and applying the chain rule

$$\frac{\partial F(U(\eta),\eta)}{\partial \eta} = \frac{\partial F}{\partial U}\frac{\partial U}{\partial \eta} + \frac{\partial F}{\partial \eta}$$

and noting that

$$\frac{\partial\left[1 + \frac{z}{|z|}\right]}{\partial z} = -\,2\,\delta(z)$$

where

$\delta(z)$ is the Dirac delta function.

then the expression for the spanwise derivative becomes upon applying the inverse transform

$$\left.\frac{\partial I}{\partial \eta}\right|_{\eta=y} = \left.\frac{\partial f(\eta)}{\partial \eta}\right|_{\eta=y} 2 \int_{x_\ell}^{x} \frac{1}{\sqrt{\xi - x_\ell}}\, g(\xi,y)\, e^{-ik(x-\xi)}\, d\xi$$

$$+ f(y)\, 2 \int_{x_\ell}^{x} \frac{1}{\sqrt{\xi - x_\ell}} \left[\frac{\partial g(\xi,\eta)}{\partial \xi}\frac{\partial x_\ell}{\partial \eta} + \frac{\partial g(\xi,\eta)}{\partial \eta}\right]_{\eta=y} e^{-ik(x-\xi)}\, d\xi$$

$$+ f(y)\, 2ik \int_{x_\ell}^{x} \frac{1}{\sqrt{\xi - x_\ell}}\, g(\xi,y)\, e^{-ik(x-\xi)}\, d\xi$$

$$- f(y)\, 2\, \frac{\partial x_\ell}{\partial \eta} \frac{1}{\sqrt{x - x_\ell}} g(x,y) \qquad (36)$$

A similar expression may be obtained for a chordwise integral that contains a logarithmic singularity such as

$$I = f(\eta) \int_{x_\ell}^{x_t} \ell og(\xi - x_c)^2 g(\xi,\eta) e^{-ik(x-\xi)} \left[1 + \frac{x-\xi}{\sqrt{(x-\xi)^2+\beta^2(y-\eta)^2}} \right] d\xi \qquad (37)$$

where x_c is a hingeline that lies within the integration interval.

The integration interval is divided into two parts

$$\int_{x_\ell}^{x_t} = \lim_{\varepsilon \to 0} \left[\int_{x_\ell}^{x_c-\varepsilon} + \int_{x_c+\varepsilon}^{x_t} \right]$$

and the same procedures are applied resulting in the expression for the spanwise derivative given as

$$\left.\frac{\partial I}{\partial \eta}\right|_{\eta=y} = \left.\frac{\partial f(\eta)}{\partial \eta}\right|_{\eta=y} 2 \int_{x_\ell}^{x} \ell og(\xi - x_c)^2 g(\xi,y) e^{-ik(x-\xi)} \, d\xi$$

$$+ f(y)\, 2 \int_{x_\ell}^{x} \ell og(\xi - x_c)^2 \left[\frac{\partial g(\xi,\eta)}{\partial \xi} \frac{\partial x_\ell}{\partial \eta} + \frac{\partial g(\xi,\eta)}{\partial \eta} \right]_{\eta=y} e^{-ik(x-\xi)} \, d\xi$$

$$+ f(y)\, 2ik \int_{x_\ell}^{x} \ell og(\xi - x_c)^2 g(\xi,y) e^{-ik(x-\xi)} \, d\xi$$

$$- f(y)\, 2 \frac{\partial x_\ell}{\partial \eta} \ell og(x - x_c)^2 \, g(x,y) \qquad (38)$$

Thus, the spanwise derivative of equation (32) may be evaluated for functions that have singular or non-singular characteristics and the downwash integral of equation (28) may be evaluated using integration quadrature functions that are appropriate to the functional characteristics of the integrand.

Lifting surface downwash distributions may be generated by evaluating equation (28) for any pressure expression that may be either continuous or non-continuous over the surface. Solutions for configurations having discontinuous downwash distributions require application of special techniques to minimize the solution sensitivity.

Solution Process for Discontinuous Downwash Distributions

No direct means is available to obtain a closed form solution of the downwash integral equation that satisfies the boundary conditions exactly everywhere on the surface. Approximate solutions are used in lieu of an exact solution process. The approximate solution process is one of generating a finite set of downwash sheets and constructing linear combinations of these sheets to satisfy the boundary conditions of a finite set of pre-selected control points on the surface.

The downwash sheets are obtained through an evaluation of the downwash integral using assumed pressure distributions that satisfy the required loading conditions on the planform edges. The assumption usually made is that if the boundary conditions are satisfied at a suitable number of control points distributed over the surface, then boundary conditions over the rest of the surface will be satisfied within small error limits.

This approximate procedure is equivalent to assuming that the downwash sheets may be represented by a series of polynomials that are continuous over the surface and may be combined to satisfy the surface boundary conditions at arbitrary control points.

This procedure provides reasonable results for analyses of configurations having continuous downwash distribution; however, it may fail to produce consistently accurate results when applied to analyses of wing-control surface configurations that have discontinuous downwash distributions.

The solution procedure used for analysis of continuous downwash configurations has been modified such that solutions may be obtained for configurations having discontinuous downwash distributions and is described in the matrix equation

$$|W(x,y)| - \left| \iint \Delta P(\xi,\eta)_{ae} \, K(\xi,\eta) \, d\xi d\eta \right| = \left[\iint \Delta P_i(\xi,\eta) \, K(\xi,\eta) \, d\xi d\eta \right] \times |a_i|$$

where

$|W(x,y)|$ is the kinematic downwash obtained from the motion of the lifting surface and containing discontinuities along the edges of a control surface.

$\iint \Delta P(\xi,\eta)_{ae} K(\xi,\eta) \, d\xi d\eta$ is the surface downwash distribution that is formulated having identical discontinuities along the control surface edges as defined for the kinematic distribution.

$\Delta P(\xi,\eta)_{ae}$ is the pressure distribution developed by the asymptotic expansion process that will provide the required change in boundary conditions across the control surface edges defined by the kinematic distribution.

$\iint \Delta P_i(\xi,\eta) \, K(\xi,\eta) d\xi d\eta$ is the standard lifting surface downwash distribution that is smooth and continuous and is calculated using smooth and continuous assumed pressure distributions $\Delta P_i(\xi,\eta)$

The solution process is a two step process. The first step is to calculate the "residual downwash distribution by performing the operation

$$\left| W(x,y)_{kinematic} \right| - \left| \iint \Delta P(\xi,\eta)_{ae} \, K(\xi,\eta) \, d\xi d\eta \right| \longrightarrow \left| W(x,y)_{residual} \right|$$

The residual distribution is to be smooth and continuous and is used as the boundary condition for the second step, which is the solution of

$$\left| W(x,y)_{residual} \right| = \left[\iint \Delta P_i(\xi,\eta) \, K(\xi,\eta) \, d\xi d\eta \right] \times \left| a_i \right|$$

The final pressure distribution is then the sum of the pressure components, i.e.

$$\Delta P(\xi,\eta) = P(\xi,\eta)_{ae} + \sum_i \Delta P_i(\xi,\eta) \, a_i$$

A schematic of the solution process is presented in figure 11 for a configuration having an oscillating trailing edge control surface.

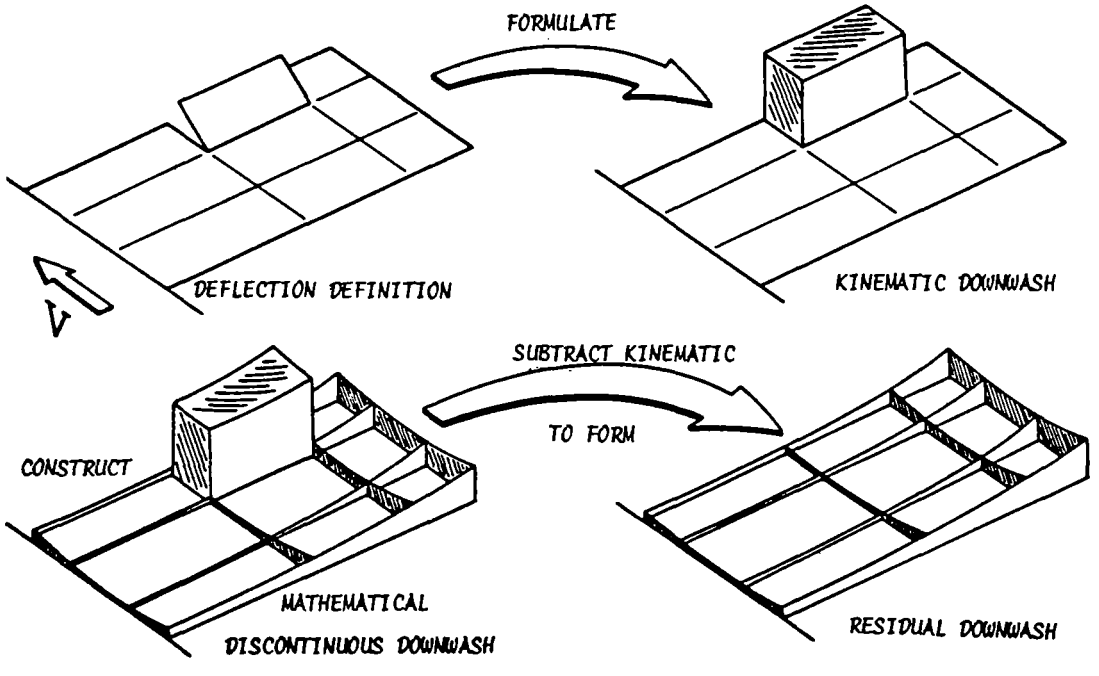

Figure 11. Solution Process for Trailing Edge Control Surfaces

The kinematic downwash distribution is developed from the surface motion definition and displays discontinuities along the boundaries of the control surface. A downwash distribution is calculated having identical discontinuity values that are contained in the kinematic distribution and is obtained by evaluating the downwash integral of equation (28) using an asymptotic pressure expression developed for a swept hingeline trailing edge control surface. The residual distribution is then formed by subtracting the kinematic distribution from the calculated distribution. The residual distribution must be smooth and continuous and is used as the new boundary condition definition for which solutions are obtained using standard lifting surface procedures.

A similar procedure is used to obtain solutions for motions of a small chord leading edge control surface as is shown in figure 12.

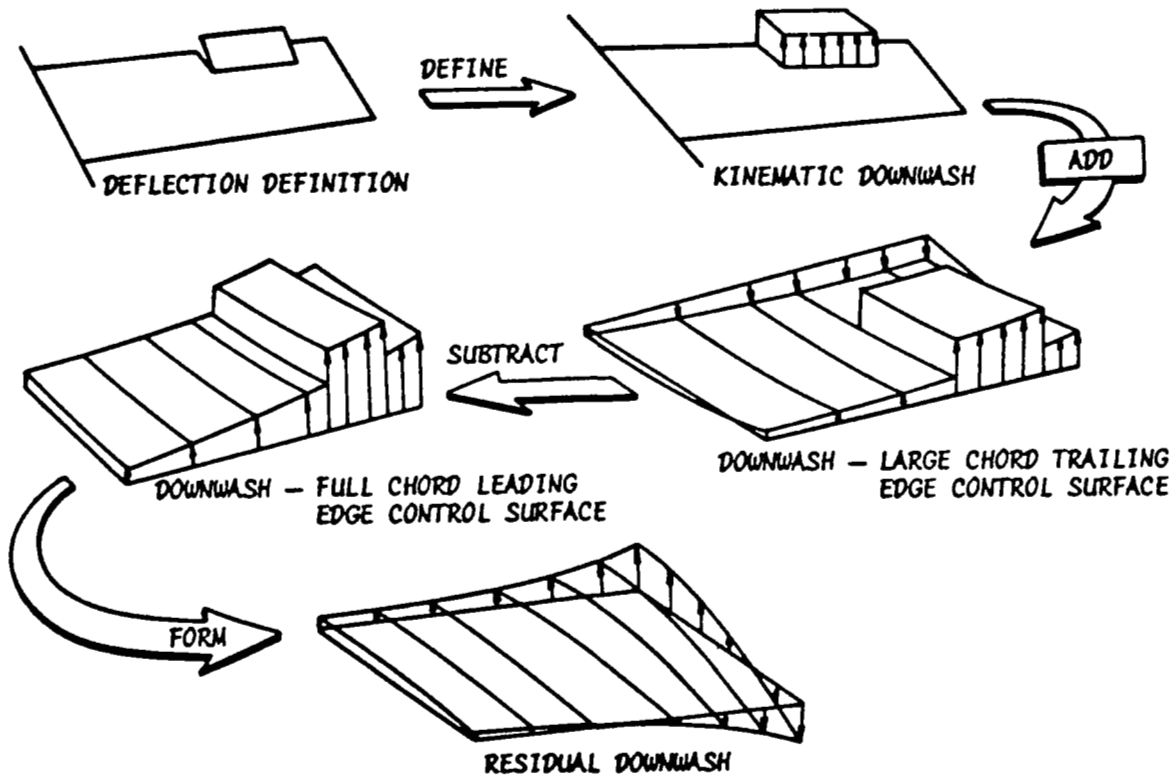

Figure 12. Solution Process for Leading Edge Control Surface

The residual distribution is formed by adding to the kinematic distribution a downwash distribution of a large chord trailing edge control surface that has a hingeline located at the same position as the small chord leading edge control surface and then subtracting out the downwash distribution generated for a full chord control surface.

The key to this solution process is the development of pressure distributions having coefficients of known strengths that will provide identical values of downwash discontinuities that are contained in the kinematic downwash distribution. Formulation of the analytical pressure distributions that provide the required discontinuities in boundary conditions are briefly discussed in the following section.

Pressure Functions

Use of the modified solution process requires two sets of pressure distributions to be defined over the lifting surface planform. One of the distributions is to provide identical values of downwash discontinuities as defined by the kinematic downwash distribution and the second pressure function is required to satisfy the smooth and continuous boundary conditions defined by the residual downwash description.

Incremental pressure expressions have been developed by Landahl[3] to satisfy the change in boundary conditions around the edges of a non-swept hingeline trailing edge control surface configuration that has its side edges inboard of the planform tip.

The solution of Landahl[3] was obtained using the asymptotic expansion process. The behavior of the pressure functions is readily obtained for regions in the immediate vicinity of the control surface leading edge and side edge since the effect of using asymptotic expansions is to magnify the singular region by stretching the coordinates by a small quantity ϵ .

The solution derived by Landahl[3] that will exactly satisfy the required change in boundary conditions near the corner of a non-swept hingeline trailing edge control surface is given as

$$\bar{P}(\xi,\eta,0) = -\frac{\Theta(\eta)}{\pi\beta}\left[1+2ik(\xi-\xi_c)\right] \ell og\left|\sqrt{(\xi-\xi_c)^2+\beta^2(\eta-y_s)^2} - \beta(\eta-y_s)\right| \quad (39)$$

$$-\frac{\Theta(\eta)}{\pi}\left[2ik-k^2(\xi-\xi_c)\right](\eta-y_s)\ell og\left|\sqrt{(\xi-\xi_c)^2+\beta^2(\eta-y_s)^2} - (\xi-\xi_c)\right|$$

where $\Theta(\eta)$ is the rotation angle of the control surface measured in a plane perpendicular to the y axis.

The expression contains the expected logarithmic singularity along the hingeline and the spanwise loading has slope singularity at the side edge of the control surface that is known to exist for lifting surface loadings on configurations having discontinuous downwash distributions.

Pressure functions have been formulated by Ashley[10] for a swept hingeline trailing edge control surface that extends to the tip of the planform. Application of asymptotic expansions along with use of Fourier transforms results in the following first order solution given in reference 10 and expressed in integral form as

$$C_p^{(0)}(\bar{x},\bar{y},0) = -\frac{\Theta(\eta)}{\pi\bar{\beta}}\sqrt{\sqrt{1+\frac{\tan^2\Lambda_c}{\beta^2}}+1}\int_0^{\beta\bar{y}/\bar{x}}\frac{\sqrt{\sqrt{1+\left(\frac{1}{q}-\frac{\tan\Lambda_c}{\beta}\right)}+1}}{\sqrt{q^2+\left(1-q\frac{\tan\Lambda_c}{\beta}\right)^2}}\,dq$$

$$+\frac{\Theta(\eta)}{\pi\bar{\beta}}\sqrt{\sqrt{1+\frac{\tan^2\Lambda_c}{\beta^2}}-1}\int_0^{\beta\bar{y}/\bar{x}}\frac{\sqrt{\sqrt{1+\left(\frac{1}{q}-\frac{\tan\Lambda_c}{\beta}\right)^2}-1}}{\sqrt{q^2+\left(1-q\frac{\tan\Lambda_c}{\beta}\right)^2}}\,dq \quad (40)$$

where the bar coordinates represent stretched coordinates measured from hingeline tip station, *i.e.*, $\bar{x} = (\xi-x_c)/\varepsilon$, $\bar{y} = (\eta-y_s)/\varepsilon$

The integrals may be expressed in a more easily handled integrable form by making the substitution

$$\frac{1}{q} - \frac{\tan\Lambda_c}{\beta} = \frac{1}{2}\left(\frac{1}{U^2} - U^2\right)$$

and performing the indicated integrations which result in the shortened expression

$$C_p^{(0)}(\bar{x},\bar{y},0) = -\frac{2\Theta(\eta)}{\pi\bar{\beta}} \ell og\left[\frac{\sqrt{\sqrt{d_1^2+1}+d_1}+\sqrt{\sqrt{d^2+1}-d}}{\sqrt{\sqrt{d_1^2+1}+d_1}-\sqrt{\sqrt{d^2+1}-d}}\right] \qquad (41)$$

where $\bar{\beta} = \sqrt{\beta^2+\tan^2\Lambda_c}$

$$d_1 = \frac{\tan\Lambda_c}{\beta}$$

$$d = \frac{\bar{x}}{\beta\bar{y}} - \frac{\tan\Lambda_c}{\beta} = \frac{\tilde{x}}{\beta\tilde{y}} = \frac{(\xi-\xi_{c_o})}{\beta(\eta-y_s)}$$

The above expression appears to be correct since $\bar{C}_p^{(0)}(\bar{x},\bar{y},0)$ approaches zero having a slope that is proportional to the square root of the distance from the wing-tip and also contains a term that is proportional to $\ell og(\xi-x_c)^2$ to provide the proper streamwise change in boundary conditions across the hingeline.

Pressure expressions developed in appendix 'A' satisfy the boundary conditions around the edges of a arbitrary configuration having a swept hingeline trailing edge control surface with side edges inboard of the planform tip. Asymptotic expansion procedures are used to reduce the very complicated boundary value problem to three simpler boundary value problems for which solutions are obtained by making a direct application of Green's Theorem. The resulting pressure expression obtained from the solution of the three boundary value problems is given as (with $\tilde{x} = \xi - x_{cs}$ and $\tilde{y} = \eta - y_s$)

$$\bar{P}(\tilde{x},\tilde{y},0) = C_1 \log\left[\sqrt{\tilde{x}^2+\beta^2\tilde{y}^2} - \left(\frac{\beta^2\tilde{y}+\tilde{x}\tan\Lambda}{\bar{\beta}}\right)\right] + C_2\,\tilde{y}\log\left[\sqrt{\tilde{x}^2+\beta^2\tilde{y}^2} - \tilde{x}\right] \quad (42)$$

where
$$C_1 = -\frac{\Theta_H}{\pi\bar{\beta}}\left\{1+2ik(\tilde{x}-\tilde{y}\tan\Lambda) - \frac{ikM^2\tan\Lambda}{\beta^2\,\bar{\beta}^2}(\tilde{x}\tan\Lambda+\tilde{y}\beta^2) - \frac{k^2M^2}{4\beta^2\bar{\beta}^2}(\tilde{x}-\tilde{y}\tan\Lambda)^2 + \frac{k^2M^2\tan^2\Lambda}{4\beta^2\bar{\beta}^4}\left[(\tilde{x}-\tilde{y}\tan\Lambda)^2 - 2\left(\frac{\tilde{x}\tan\Lambda}{\beta} + \beta\tilde{y}\right)^2\right] - \frac{2k^2M^2}{\beta^2}\left[\frac{\beta^2}{2\bar{\beta}^2}(\tilde{x}-\tilde{y}\tan\Lambda)^2 - (\tilde{x}^2-\tilde{x}\tilde{y}\tan\Lambda)\right] - \frac{k^2}{2}(\tilde{x}-\tilde{y}\tan\Lambda)^2\right\} e^{\left(\frac{ikM^2\tilde{x}}{\beta^2}\right)}$$

$$C_2 = \left\{-\frac{\Theta_H}{\pi}\left(2ik + \frac{2k^2M^2}{\beta^2} - k^2\right)\tilde{x} + \frac{k^2\tan\Lambda}{2}\,\tilde{y}\right\} e^{\left(\frac{ikM^2\tilde{x}}{\beta^2}\right)}$$

The expression for $\bar{P}(\tilde{x},\tilde{y},0)$ may be simplified by expanding the exponential, carrying out the indicated multiplication and collecting terms that are linear in $\tilde{x}$ and $\tilde{y}$ which results in the expression

$$\bar{P}(\tilde{x},\tilde{y},0) = -\frac{\Theta_H}{\pi\bar{\beta}}\left[1 + 2ik(\xi-\xi_c) + \frac{ikM^2}{\bar{\beta}^2}(\xi-\xi_c)\right]\log\left[\sqrt{\tilde{x}^2+\beta^2\tilde{y}^2} - \frac{\beta^2\tilde{y}+\tilde{x}\tan\Lambda}{\bar{\beta}}\right]$$

$$-\frac{\Theta_H}{\pi}\left[2ik - k^2(\xi-\xi_c)\right]\,\tilde{y}\log\left[\sqrt{\tilde{x}^2+\beta^2\tilde{y}^2} - \tilde{x}\right] \quad (43)$$

The limiting value of this expression for $\Lambda=0$ is equivalent to the expression developed by Landahl[3] for the rectangular non-swept control surface. The above expression for $\Lambda=0$ is

$$\bar{P}(\tilde{x},\tilde{y},0) = -\frac{\Theta_H}{\pi\beta}\left[1 + 2ik(\xi-\xi_c) + \frac{ikM^2(\xi-\xi_c)}{\beta^2}\right]\log\left[\sqrt{(\xi-\xi_c)^2+\beta^2\tilde{y}^2} - \beta\tilde{y}\right]$$

$$-\frac{\Theta}{\pi}\left[2ik-k^2(\xi-\xi_c)\right]\,\tilde{y}\log\left[\sqrt{(\xi-\xi_c)^2+\beta^2\tilde{y}^2} - (\xi-\xi_c)\right] \quad (44)$$

and is identical to Landahl's zero sweep expression. The expression developed for the arbitrary sweep angle case does exactly satisfy the change in boundary conditions across the hingeline and side edge of a swept hingeline trail-

ing edge control surface and should provide smooth and continuous residual downwashes for which solutions may be obtained that are relatively insensitive to the number of collocation stations placed on the lifting surface.

Pressure expressions have also been developed in Appendix "B" that satisfy the change in boundary conditions across the side edge of a full chord swept leading edge control surface.

The zero-th order solution is given in terms of an inverse square root function that is multiplied by a coefficient whose value can only be determined after performing a global integration. The inverse square root function is continuous in the spanwise direction, that is, it does not exhibit any spanwise singularities that could contribute to the change in downwash across the side edge. Consequently, the zero-th order boundary value problem solution is not included within the incremental pressure expression necessary to satisfy the change in boundary conditions across the control surface side edge.

The pressure expressions obtained as solutions of the first order and second order boundary value problems are given as follows:

First order solution is:

$$\bar{p}^{(1)}(\bar{x},y,0) = \frac{\lambda}{\pi}\left\{\frac{2\sqrt{2}}{\bar{\beta}_{\ell}^{\,2}}\left(\frac{1}{\sqrt{\bar{x}-y\tan\Lambda_{\ell}}} + \frac{ik}{\beta^2}\sqrt{\bar{x}-y\tan\Lambda_{\ell}}\right)\chi\right.$$

$$\left(\beta\, sgn(y)\sqrt{\sqrt{\bar{x}^2+\beta^2y^2}-\bar{x}} + \tan\Lambda_{\ell}\sqrt{\sqrt{\bar{x}^2+\beta^2y^2}+\bar{x}}\right)$$

$$\left. + \frac{ik}{\beta^2}\, y\, \ell og\left[\frac{\sqrt{\bar{x}^2+\beta^2y^2}+\bar{x}-y\tan\Lambda_{\ell}+\sqrt{2}\sqrt{\bar{x}-y\tan\Lambda_{\ell}}\sqrt{\sqrt{\bar{x}^2+\beta^2y^2}+\bar{x}}}{\sqrt{\bar{x}^2+\beta^2y^2}+\bar{x}-y\tan\Lambda_{\ell}-\sqrt{2}\sqrt{\bar{x}-y\tan\Lambda_{\ell}}\sqrt{\sqrt{\bar{x}^2+\beta^2y^2}+\bar{x}}}\right]\chi\right\}$$

$$e^{ikM^2\bar{x}/\beta^2} \qquad (45)$$

The second order solution is:

$$\bar{p}^{(2)}(\bar{x},y,0) = \frac{C_2}{\pi}\left\{\frac{2\sqrt{2}\sqrt{\bar{x}-y\tan\Lambda_\ell}}{\beta\bar{\beta}_\ell^{\,2}}\left[\tan\Lambda_\ell+\left(\frac{ik}{\beta^2}\right)\left(\frac{2\bar{x}\tan\Lambda_\ell-(3\tan^2\Lambda_\ell+\beta^2)y}{4}\right)\right]\sqrt{\sqrt{\bar{x}^2+\beta^2y^2}+x}\right.$$

$$+\quad 2\sqrt{2}\left[1+\left(\frac{ik}{\beta^2}\right)\frac{(\bar{x}-y\tan\Lambda_\ell)}{2}\right]\sqrt{\bar{x}-y\tan\Lambda_\ell}\;sgn(y)\sqrt{\sqrt{\bar{x}^2+\beta^2y^2}-\bar{x}}$$

$$+\left(\frac{ik}{\beta^2}\right)\frac{y^2}{2}sgn(y)\tan^{-1}\left[\frac{\sqrt{2}\sqrt{\sqrt{\bar{x}^2+\beta^2y^2}-\bar{x}}\;\sqrt{\bar{x}-y\tan\Lambda_\ell}}{\sqrt{\bar{x}^2+\beta^2y^2}-(\bar{x}-y\tan\Lambda_\ell)}\right]$$

$$+\frac{1}{\beta}\left[1+\left(\frac{ik}{\beta^2}\right)\left(x-\frac{3y\tan\Lambda_\ell}{4}\right)\right]\chi$$

$$\left.y\;\ell og\left[\frac{\sqrt{\bar{x}^2+\beta^2y^2}+\bar{x}-y\tan\Lambda_\ell+\sqrt{2}\sqrt{\bar{x}-y\tan\Lambda_\ell}\sqrt{\sqrt{\bar{x}^2+\beta^2y^2}+\bar{x}}}{\sqrt{\bar{x}^2+\beta^2y^2}+\bar{x}-y\tan\Lambda_\ell-\sqrt{2}\sqrt{\bar{x}-y\tan\Lambda_\ell}\sqrt{\sqrt{\bar{x}^2+\beta^2y^2}+\bar{x}}}\right]\right\}\cdot e^{ikM^2\bar{x}/\beta^2} \qquad (46)$$

where $C_2 = \nu - \frac{ikM^2\lambda}{\beta}$; $\nu = \theta_H(ik\beta)$; $\lambda = \theta_H(1-ikx_c)$

$\bar{x} = \xi - x_{\ell s}$; $y = \eta - y_s$

(note: $\bar{x}$,y used here is not to be confused with the downwash coordinate x,y)

Pressure distributions obtained by the above described asymptotic expansion process are valid only in localized regions of the planform since the distributions of the outer regions have not been defined nor matched with the inner region solutions. However, the essential part of the pressure distribution that provides the discontinuities in downwash along the control

surface edge is defined by the inner region solution. The distribution in the outer regions may take on any convenient form that satisfies the required loading condition along the edges of the planform since a unique distribution is not being determined at this stage of the solution process. Consequently, the surface pressure loading functions that provide the downwash discontinuities are obtained by extending the applicable range of the inner solution and modifying these distributions to meet the condition of having the pressure vanish in proportion to the square root of the distance from the edges.

The functions used to modify the asymptotic pressure expressions are usually artfully devised and are not unique expressions. However, there are certain characteristics that are required to be satisfied by these functions such that the resulting residual downwash sheet will contain a minimum amount of distortion. Some of the required functional characteristics are established in the following section.

Pressure Modification Functions

Pressure loading functions are developed using the asymptotic pressure expressions and extending their applicable range from localized regions to cover the entire planform.

For the case of a trailing edge control surface, the asymptotic pressure expressions that are valid only for small regions around the discontinuity region may be written as

$$C_p(\xi,\eta,0) = -\frac{\theta_H}{\pi\bar{\beta}_h}\bar{C}_1 \log\left[\sqrt{(\xi-x_{cs})^2+\beta^2(\eta-y_s)^2} - \frac{\beta^2(\eta-y_s)+(\xi-x_{cs})\tan\Lambda_c}{\bar{\beta}_h}\right]$$

$$-\frac{\theta_H}{\pi}\bar{C}_2 \log\left[\sqrt{(\xi-x_{cs})^2+\beta^2(\eta-y_s)^2} - (\xi-x_{cs})\right] \qquad (47)$$

where $\bar{C}_1 = C_1/(-\theta_H/\pi\beta)$, $\bar{C}_2 = C_2/(-\theta_H/\pi)$; C_1, C_2 are defined in equation (42)

$C_p(x,y,0)$ is related to the change in pressure loading across the surface by

$$\Delta C_p = +\,2\,C_{p_\ell}$$

$$\frac{\Delta P}{\frac{1}{2}\rho V^2} = +\,2\,C_{p_\ell}$$

$$\Delta P = +\,C_{p_\ell} \times \rho V^2$$

where C_{p_ℓ} is given by the above equation (47)

Then

$$\Delta P(\xi,\eta) = \rho V^2 \left\{ -\frac{\theta_H}{\pi\bar{\beta}_h}\bar{C}_1 \log\left[\sqrt{(\xi-x_{cs})^2+\beta^2(\eta-y_s)^2} - \frac{\beta^2(\eta-y_s)+(\xi-x_{cs})\tan\Lambda_c}{\bar{\beta}_h}\right]\right.$$

$$\left. -\frac{\theta_H}{\pi}\bar{C}_2 \log\left[\sqrt{(\xi-x_{cs})^2+\beta^2(\eta-y_s)^2} - (\xi-x_{cs})\right]\right\} \qquad (48)$$

A characteristic of the first logarithmic term is that it is singular only along the hingeline and the coefficient value of the singularity must be maintained along the hingeline such that the unit change in downwash is obtained for all points on the control surface. Thus, to distribute this function over the entire lifting surface a pressure modifying function is devised to multiply this term such that the coefficient value is maintained along the hingeline and approaches zero at the planform edges in proportion to the square root of the distance from the planform edges.

The modifying function is made up as a product of two functions such that the streamwise and spanwise boundary conditions may be satisfied independently.

The spanwise modifying function, $H(\eta)$, is defined as

$$H(\eta) = \begin{cases} \sqrt{1-\hat{C}}\ (1. + .5\hat{C} + .375\hat{C}^2) & |\eta| \geq y_o \\ 1.0 & |\eta| < y_o \end{cases} \tag{49}$$

where $$\hat{C} = \frac{(|\eta|-y_o)}{(s-y_o)}$$

y_o = the spanwise coordinate of outboard side edge of the control surface.

$H(\eta)$ has a value of 1.0 and a slope of zero at the control surface outboard side edge and then diminishes to zero in proportion to the square root of the distance from the planform tip.

The chordwise modification function, E_1, must be devised such that E_1 = 1.0 at the chordwise hingeline station to maintain the singularity strength and must approach zero in proportion to the square root of the distance from the leading and trailing edges.

However, there is an additional condition required of E_1 such that smooth and continuous residual downwash are developed. The additional condition imposed on E_1 is that E_1 must have a zero slope in the streamwise direction at the hingeline station. The requirement of having a zero slope may be illustrated by examining the results of a numerical investigation that was accomplished to identify the essential properties of E_1 such that reasonable distributions of residual downwashes would result.

Downwash distributions were obtained at the four downwash chords shown in figure 13 by applying the zero sweep loading function given as follows:

$$\Delta P(\xi,\eta) = 4\rho V^2\, f(\eta) \sqrt{s^2-\eta^2}\, H(\eta)\, E_1\, Log\left[\sqrt{(\xi-\xi_c)^2+\beta^2(\eta-y_s)^2} - \beta(\eta-y_s)\right] \tag{50}$$

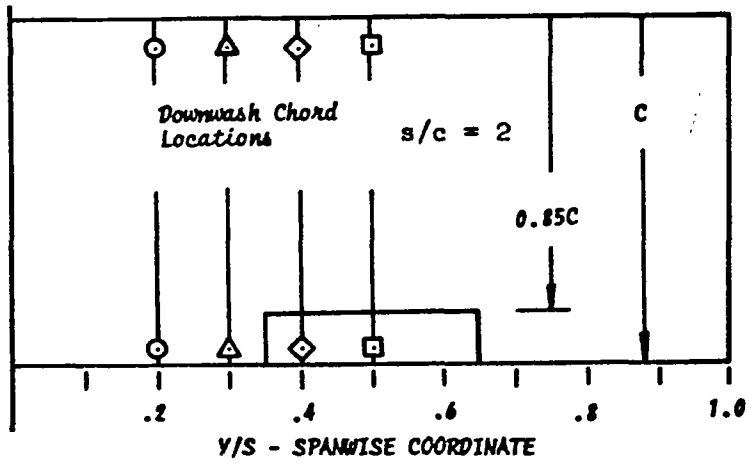

Figure 13. Analysis Planform Used to Evaluate E_1 Characteristics

One of the many modifying functions investigated is the function suggested by Landahl[3] which has a value of 1.0 at the hingeline and approaches zero in proportion to the square root of the distance from the leading and trailing edges as shown in figure 14.

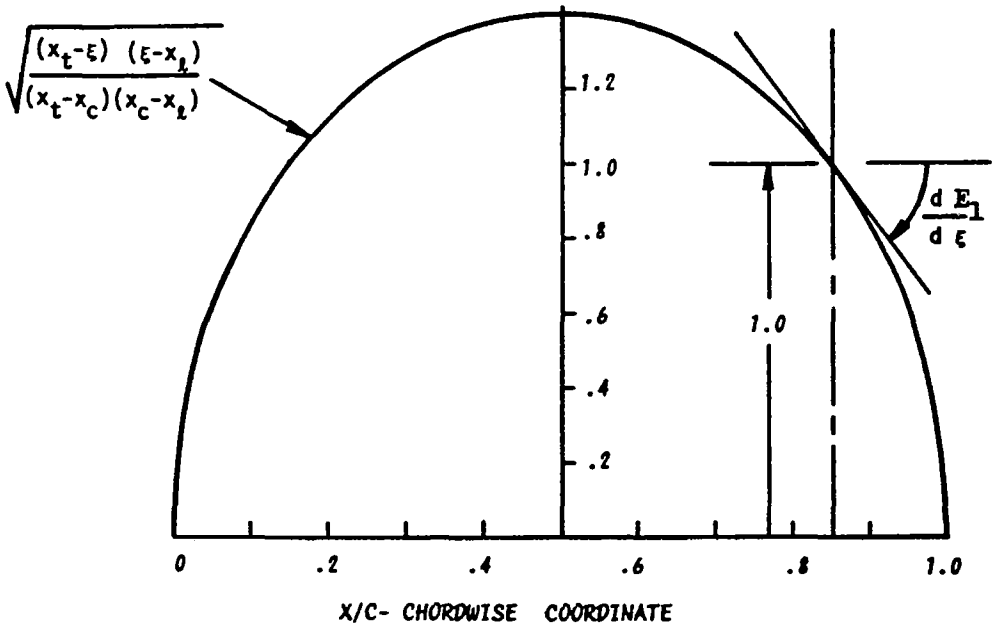

Figure 14. Functional Characteristics of $E_1(\xi)$

The residual downwashes that result using the $E_1(\xi)$ function of figure 14 are shown in figure 15 and represent the distributions on the aft portion of the wing-control surface regions. The residual downwashes are smooth and continuous for downwash chords that are inboard of the control surface side edge. However, for spanwise downwash stations located on the control surface, the distributions contain a slope discontinuity that may not be easily satisfied by the downwashes generated by the remaining portion of the solution process.

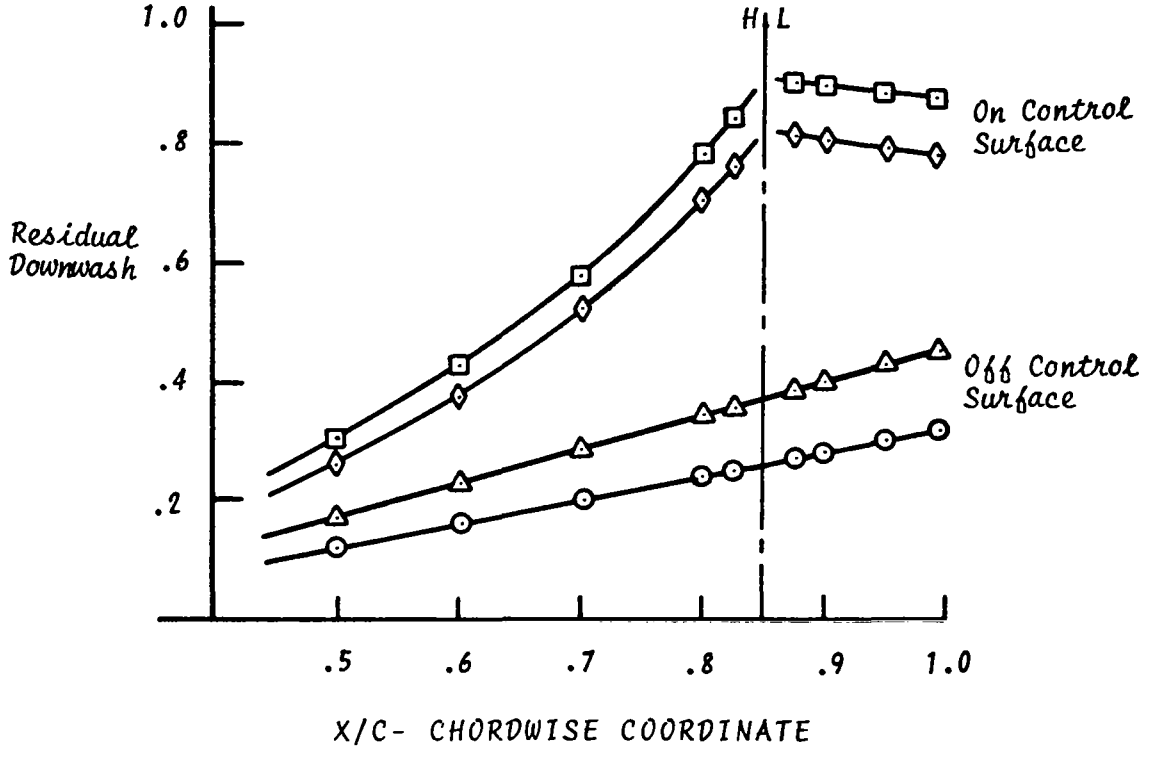

Figure 15. Residual Downwash Distributions Resulting from Using the $E_1(\xi)$ Function of Figure 14.

This slope discontinuity could have been anticipated by noting that the logarithmic term of the loading function may be written as

$$\log(\xi-\xi_c)^2 - \log\left[\sqrt{(\xi-\xi_c)^2+\beta^2(\eta-y_s)^2} + \beta(\eta-y_s)\right] \qquad (51)$$

and coupling this with the $E_1(\xi)$ function represented as a Taylor series expansion about the hingeline in the form of

$$E_1(\xi) = 1 + (\xi-\xi_c)\left.\frac{dE_1}{d\xi}\right|_{\xi=\xi_c} + \frac{(\xi-\xi_c)^2}{2}\left.\frac{d^2E_1}{d\xi^2}\right|_{\xi=\xi_c} + \cdots \quad (52)$$

then insertion of these terms into downwash equations provides a series of downwash integrals having the properties presented in figure 16.

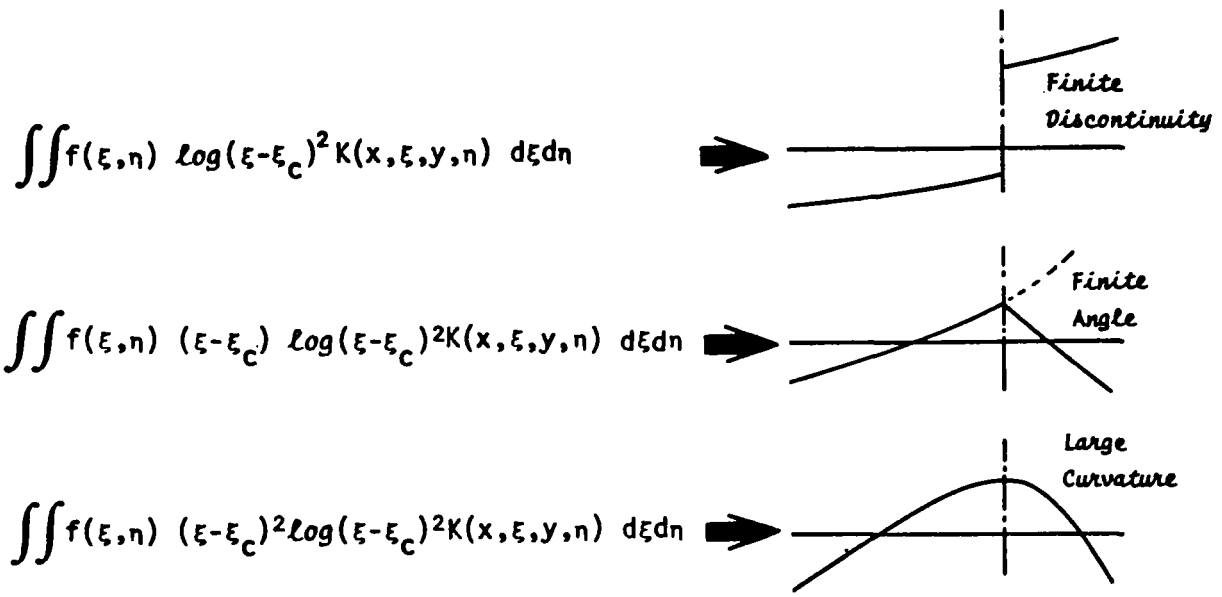

Figure 16. Chordwise Downwash Variations Caused by Singularity Multiplier Functions

It is apparent that the finite angle slope discontinuity displayed in figure 15 is due to the non-zero slope at the hingeline contained in the definition of $E_1(\xi)$ shown in figure 14. Also, it may be noted that large curvatures in downwashes may be minimized by devising a function that contains only a small amount of curvature in the vicinity of the hingeline.

After extensive numerical evaluations of various $E_1(\xi)$ functions, the function shown in figure 17 represents the final form of $E_1(\xi)$ that has been selected to modify the chordwise loading expressions.

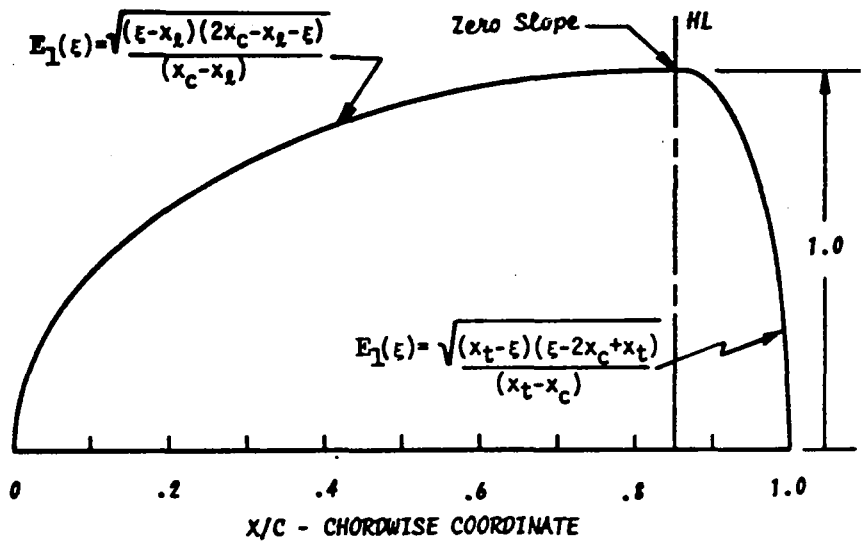

Figure 17- Final Form of Chordwise Modification Function

Residual downwash distributions of figure 18 were obtained using the $E_1(\xi)$ function of figure 17. It appears that this function does provide slope continuity across the hingeline as well as developing minimum waviness over the rest of the chord. Solutions using this modification function should then be relatively insensitive to the distribution of downwash collocation stations.

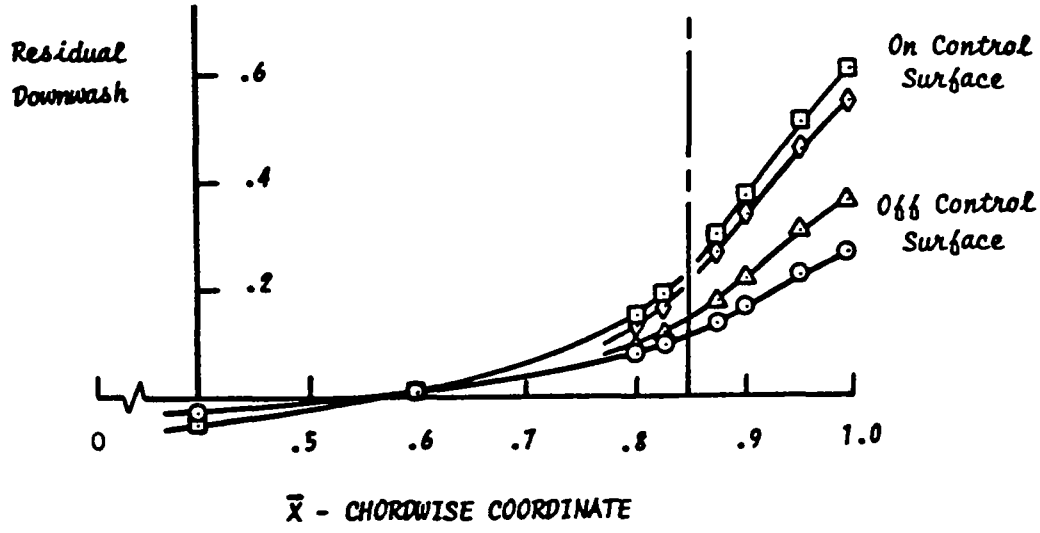

Figure 18- Residual Downwashes Obtained Using $E_1(\xi)$ of Figure 17

The second logarithmic term of equation (42) contains a singularity of the type $(n-y_s)\log(n-y_s)$ that is to be applied along the side edge of the control surface. The strength of this singularity is to be maintained along the length of the side edge to provide the proper downwash discontinuity along the side edge for the unsteady flow condition.

A function (suggested by Landahl[3]) that may be used as a pressure modification function to maintain the singularity strength along the side edge as well as forcing the pressures to zero in proportion to the square root of the distance from the trailing edge is given by the following equation and also presented in figure 19.

$$E_2(\xi,\eta) = \left[\frac{(x_t-\xi)^2}{(x_t-\xi)^2+\beta^2(\eta-y_s)^2}\right]^{1/4}$$

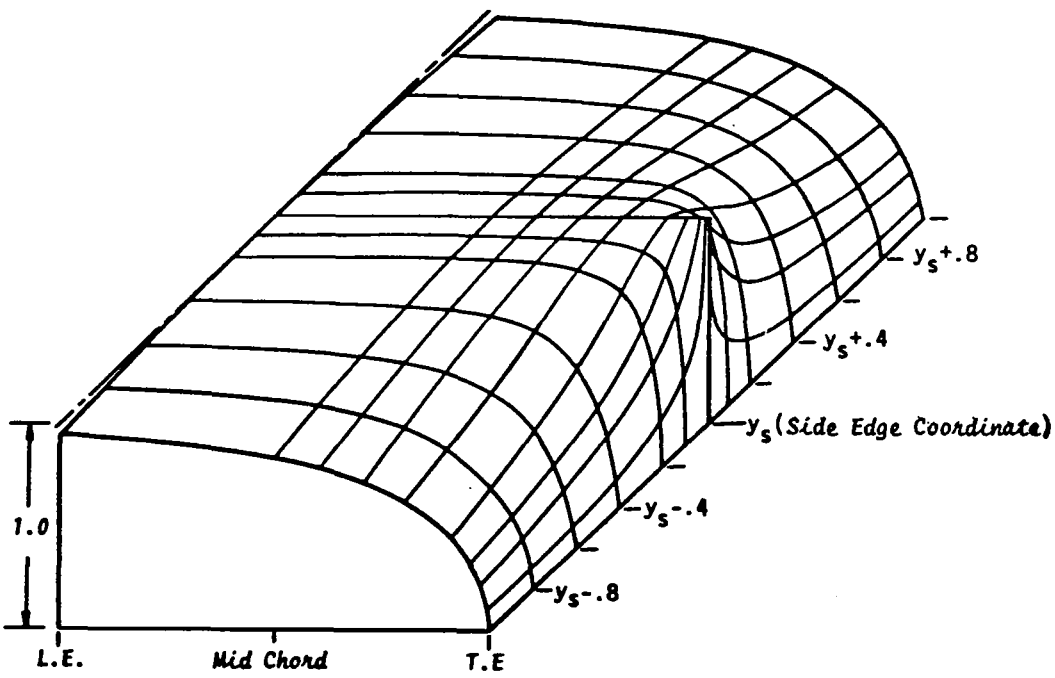

Figure 19. Schematic of $E_2(\xi,\eta)$, Pressure Modification Function

The side edge modification function given by equation (53) has been investigated using numerical procedures to determine its range of validity in maintaining the side edge singularity strengths. Results of the investigation indicate that the function requires a modification to reduce its spanwise gradients in the region of the side edge-trailing edge junction. It appears that in applying equation (53) to the side edge pressures that the singularity strengths near the trailing edge are being modified to such an extent that the spanwise integration quadrature functions are unable to detect the infinite slope of the pressure function which results in an error in predicting the spanwise downwash discontinuity.

Equation (53) has been modified to provide a proper evaluation of the side edge downwash discontinuity and is given in the following form for use in a full chord control surface analysis.

$$E_2(\xi,\eta) = \left[\frac{(x_t-\xi)^2}{(x_t-x_\ell)^2}\left[\frac{(x_t-x_\ell)^2+\bar{C}(\eta-y_s)^2}{(x_t-\xi)^2+\bar{C}(\eta-y_s)^2}\right]\right]^{1/4} \qquad \bar{C} = 0.1 \tag{54}$$

Equation (54) has a value of 1.0 along the side edge and leading edge and also forces the pressures to approach zero in proportion to the square root of the distance from the trailing edge.

The side edge modification function used for a trailing edge control surface configuration is given as

$$E_2(\xi,\eta) = \left[\frac{(\xi-x_\ell)^2}{(\xi-x_\ell)^2+\bar{C}(\eta-y_s)^2}\right]^{1/4} \cdot \left[\frac{(x_t-\xi)^2}{(x_t-\xi)^2+\bar{C}(\eta-y_s)^2}\right]^{1/4} \tag{55}$$

In this case, the pressures are forced to zero in proportion to the square root of the distance from both the leading and trailing edges.

Loading Functions for an Inboard Partial Span Control Surface

Pressure loading functions formulated for a trailing edge partial span control surface having side edges inboard of the planform tip are devised from the trailing edge control surface pressure expansion of equation (42) as follows:

$$\Delta P(\xi,\eta) = 4\rho V^2 \sqrt{s^2-\eta^2}\; f(\eta)\; g(\xi,\eta) \tag{56}$$

where $f(\eta) = \theta_H/(4\pi \sqrt{s^2-\eta^2})$

$$g(\xi,\eta) = \left[g_1^R(\xi,\eta) + g_2^R(\xi,\eta) \right] + SF\left[g_1^L(\xi,\eta) + g_2^L(\xi,\eta) \right]$$

θ_H is the control surface rotation angle relative to the wing rotation angle and measured in a plane perpendicular to the y axis.

SF is the symmetrical sign factor that has a value of SF = 1.0 for symmetrical loadings and SF = - 1.0 for antisymmetrical loadings.

The $g_1^R(\xi,\eta)$ loading functions are the loading functions that are due to the right-hand semispan control surface deflection. The functions are formulated such that the hingeline singularity is turned on at the inboard side edge and maintained at full strength along the hingeline and then turned off at the outboard side edge.

The $g_1^R(\xi,\eta)$loading functions are non-singular for spanwise stations that are outside of the spanwise control surface location. Consequently, the loadings are extended over the rest of the surface to the planform tips where the loadings are forced to zero in proportion to the square root of the distance from the tips.

$$g_1^R(\xi,\eta) = E_1\, H(\eta)\, C_1 \left\{ \log\left[\bar{\beta}\sqrt{(\xi-x_{ci})^2 + \beta^2(\eta-y_i)^2} - (\beta^2(\eta-y_i) + (\xi-x_{ci})\tan\Lambda_c) \right] \right.$$

$$\left. - \log\left[\bar{\beta}\sqrt{(\xi-x_{co})^2 + \beta^2(\eta-y_o)^2} - (\beta^2(\eta-y_o) + (\xi-x_{co})\tan\Lambda_c) \right] \right\} \qquad (57)$$

The subscripts i and o represent the inboard and outboard side edges respectively. The parameters x_i, y_i and x_o, y_o represent the coordinates of the hingeline at the inboard and outboard side edge stations of the control surface.

The E_1 function forces the loadings to go to zero in proportion to the square root of the distance from the leading and trailing edges and also has a value of $E_1 = 1.0$ and zero streamwise slope at the hingeline.

The expression for E_1 for stations ahead of the hingeline is given by

$$E_1 = \frac{\sqrt{(\xi-x_\ell)(2x_c-x_\ell-\xi)}}{(x_c-x_\ell)} \qquad (58)$$

for stations aft of the hingeline,

$$E_1 = \frac{\sqrt{(x_t-\xi)(\xi-2x_c+x_t)}}{(x_t-x_c)} \qquad (59)$$

The $H(\eta)$ function is the spanwise pressure modification function having a value of $H(\eta) = 1.0$ for spanwise stations located between the left hand outboard and right hand outboard control surface side edges. For stations outboard of the outboard side edges, the $H(\eta)$ function goes to zero in proportion to the distance from the planform tip station:

$$H(\eta) = \begin{cases} \sqrt{1. - \hat{C}}\,(1 + .5\hat{C} + .375\hat{C}^2) & |\eta| \geq y_o \\ 1. & |\eta| < y_o \end{cases} \qquad (60)$$

$$\text{where} \quad \hat{C} = \frac{(|\eta| - y_o)}{(s - y_o)}$$

The C_1 function represents the coefficient multipliers obtained in deriving the pressure expressions by means of asymptotic expansions. The C_1 expression of equation (42) has been shortened by expanding the exponential function and performing the indicated multiplication that results in the expression

$$C_1 = -\frac{1}{\bar{\beta}}\left[1 + 2ik(\xi - \xi_c) + \frac{ikM^2}{\bar{\beta}^2}(\xi - \xi_c) - (\xi - \xi_c)^2\left(\frac{k^2M^4}{4\beta^2\,\bar{\beta}^2} + \frac{k^2M^2}{\beta^2} + \frac{k^2}{2}\right)\right] \qquad (61)$$

$$\text{where} \quad \bar{\beta} = \sqrt{\beta^2 + \tan^2\Lambda_c}$$

The loading functions that are due to motions of the left hand side control surface are obtained from the above expression by replacing y_o, y_i, and $\tan\Lambda_c$ by $-y_o$, $-y_i$ and $-\tan\Lambda_c$, respectively.

The second part of the pressure function defined in equation (42) is formulated into loading functions $g_2^R(\xi,\eta)$ and $g_2^L(\xi,\eta)$ by applying other pressure modification functions. The loading function due to the singularity developed for the right hand side control surface motion is given as

$$g_2^R(\xi,\eta) = H(\eta)\Big[E_2(y_i)\,C_2(y_i)\,(\eta - y_i)\,\log\left[\sqrt{(\xi - x_{ci})^2 + \beta^2(\eta - y_i)^2} - (\xi - x_{ci})\right] \qquad (62)$$

$$- E_2(y_o)\,C_2(y_o)\,(\eta - y_o)\,\log\left[\sqrt{(\xi - x_{co})^2 + \beta^2(\eta - y_o)^2} - (\xi - x_{co})\right]\Big]$$

The subscripts i and o pertain to the inboard and outboard side edges respectively. The (x_i, y_i), (x_o, y_o) parameters are the hingeline coordinates at the inboard and outboard side edges respectively.

The logarithmic function is singular only along the side edge which requires that the strength of the singularity be maintained only along the side edge and then may take on any other desired form away from the side edge. The $E_2(y_s)$ function is devised in such a manner as to have a value of $E_2(y_s) = 1.0$ along the side edge to maintain the singularity strength and is also devised to have a characteristic of reducing the pressures to zero in proportion to the square root of the distance from the leading and trailing edges.

Using y_s to represent either y_i for inboard or y_o for outboard side edges results in the following chordwise pressure modification function.

$$E_2(y_s) = \left[\frac{(x_t-\xi)^2}{(x_t-\xi)^2 + \bar{C}(\eta-y_s)^2}\right]^{\frac{1}{4}} \left[\frac{(\xi-x_\ell)^2}{(\xi-x_\ell)^2 + \bar{C}(\eta-y_s)^2}\right]^{\frac{1}{4}} \qquad (63)$$

where $\bar{C} = 0.10$

The spanwise modification function $H(\eta)$ is the same function previously described and is given by equation (60).

The $C_2(y_s)$ terms are obtained from equation (42) by expanding the exponential function and performing the indicated multiplication that results in the expression:

$$C_2(y_s) = \left[-2ik + k^2(\xi-\xi_c) + \frac{k^2}{2}(\eta-y_s)\tan\Lambda_c \right] \qquad (64)$$

The loading functions developed for motions of the left hand side control surface are obtained from the right hand side terms by replacing y_2, y_o, and $\tan\Lambda_c$ by $-y_2$, $-y_o$, and $-\tan\Lambda_c$, respectively.

Loading Functions for a Full Chord Control Surface

Loading functions for a full chord control surface are formulated in a similar manner using the pressure expressions of equation (45) and equation (46).

Loading functions developed from equation (45) for the inboard side edge of the right hand side control surface are given in localized coordinates of $\hat{x} = \xi - x_{\ell i}$ and $\hat{y} = \eta - y_i$.

$$
\begin{aligned}
g_i^R(\xi,\eta) = e^{ikM^2\hat{x}/\beta^2} H(\eta,y_i) \Bigg[& E_3 C_3 \frac{1}{\sqrt{\hat{x} - \hat{y}\tan\Lambda_\ell}} \chi \\
& \chi \left[\frac{\beta\hat{y}}{|\hat{y}|} \left[\sqrt{\hat{x}^2 + \beta^2\hat{y}^2} - \hat{x} \right]^{\frac{1}{2}} + \tan\Lambda_\ell \left[\sqrt{\hat{x}^2 + \beta^2\hat{y}^2} + \hat{x} \right]^{\frac{1}{2}} \right] \\
& + E_3 C_4 \sqrt{\hat{x} - \hat{y}\tan\Lambda_\ell} \left[\frac{\beta\hat{y}}{|\hat{y}|} \left[\sqrt{\hat{x}^2 + \beta^2\hat{y}^2} - \hat{x} \right]^{\frac{1}{2}} + \tan\Lambda_\ell \left[\sqrt{\hat{x}^2 + \beta^2\hat{y}^2} + \hat{x} \right]^{\frac{1}{2}} \right] \\
& + E_2 \left[(C_5 + C_8) \hat{y} \right] \chi \\
& \chi \, \ell og \left[\frac{\sqrt{\hat{x}^2 + \beta^2\hat{y}^2} + \hat{x} - \hat{y}\tan\Lambda_\ell + \sqrt{2(\hat{x} - \hat{y}\tan\Lambda_\ell)} \left[\sqrt{\hat{x}^2 + \beta^2\hat{y}^2} + \hat{x} \right]^{\frac{1}{2}}}{\sqrt{\hat{x}^2 + \beta^2\hat{y}^2} + \hat{x} - \hat{y}\tan\Lambda_\ell - \sqrt{2(\hat{x} - \hat{y}\tan\Lambda_\ell)} \left[\sqrt{\hat{x}^2 + \beta^2\hat{y}^2} + \hat{x} \right]^{\frac{1}{2}}} \right] \\
& + E_3 \sqrt{\hat{x} - \hat{y}\tan\Lambda_\ell} \left[C_6 \left[\sqrt{\hat{x}^2 + \beta^2\hat{y}^2} + \hat{x} \right]^{\frac{1}{2}} + \frac{\beta\hat{y}}{|\hat{y}|} C_7 \left[\sqrt{\hat{x}^2 + \beta^2\hat{y}^2} + \hat{x} \right]^{\frac{1}{2}} \right] \\
& + E_2 C_9 \frac{\beta\hat{y}}{|\hat{y}|} \frac{\hat{y}^2}{2} \tan^{-1} \left[\frac{\sqrt{2(\hat{x} - \hat{y}\tan\Lambda_\ell)} \left[\sqrt{\hat{x}^2 + \beta^2\hat{y}^2} + \hat{x} \right]^{\frac{1}{2}}}{\sqrt{\hat{x}^2 + \beta^2\hat{y}^2} - \hat{x} + \hat{y}\tan\Lambda_\ell} \right] \Bigg]
\end{aligned}
\tag{65}
$$

The spanwise modification function $H(\eta,y_i)$ is defined as having a value of 1.0 with a zero slope in the spanwise direction at the control surface side edge and then diminishes to zero in proportion to the square root of the distance from either planform tip and is given by the following expression:

$$H(\eta,y_s) = \sqrt{1 - \hat{C}}\left[1 + .5\hat{C} + .375\hat{C}^2\right] \tag{66}$$

where $$\hat{C} = \begin{cases} -(\eta - y_s)/(|y_s| + s) & \text{if } \eta < y_s \\ (\eta - y_s)/(s - |y_s|) & \text{if } \eta > y_s \end{cases}$$

The modification function E_2 has a value of 1.0 along the side edge and diminishes to zero in proportion to the square root of the distance from the trailing edge and is defined as

$$E_2 = \left[\frac{(x_t - \xi)^2\left[(x_t - x_\ell)^2 + .1(\eta - y_s)^2\right]}{(x_t - x_\ell)^2\left[(x_t - \xi)^2 + .1(\eta - y_s)^2\right]}\right]^{1/4} \tag{67}$$

The E_3 modification function has a value of 1.0 along the leading edge and approaches zero in proportion to the square root of the distance from the trailing edge and is given by

$$E_3 = \left[\sqrt{3 - 2\underline{\xi} - \underline{\xi}^2}\right]/2 \tag{68}$$

where $\underline{\xi}$ is defined within the expression of

$$\xi = (\xi_t + \xi_\ell)/2 + \left[(\xi_t - \xi_\ell)/2\right]\underline{\xi}$$

The pressure coefficients C_3 through C_9 are obtained from the expressions of equations (45) and (46), and are given as follows:

$$C_3 = 2\sqrt{2}\left[1 - ik(x_{cs} - x_{\ell s})\right] / \bar{\beta}_\ell^2$$

$$C_4 = 2\sqrt{2}\left[1 - ik(x_{cs} - x_{\ell s})\right](ik/\beta^2)(1/\bar{\beta}_\ell^2)$$

$$C_5 = ik\left[1 - ik(x_{cs} - x_{\ell s})\right] / \bar{\beta}_\ell^2$$

$$C_6 = 2\sqrt{2}\, k\left[\frac{-kM^2(x_{cs} - x_{\ell s}) + i(\beta^2 - M^2)}{\beta^2}\right] X$$

$$X\left[\tan\Lambda_\ell + (ik/\beta^2)\frac{\left[2\hat{x}\tan\Lambda_\ell - (3\tan^2\Lambda_\ell - \beta^2)\hat{y}\right]}{4}\right]$$

$$C_7 = 2\sqrt{2}\, k\left[\frac{-kM^2(x_{cs} - x_{\ell s}) + i(\beta^2 - M^2)}{\beta^2}\right]\left[1 + (ik/\beta^2)(\hat{x} - \hat{y}\tan\Lambda_\ell)/2\right]$$

$$C_8 = k\left[\frac{-k^2M^2(x_{cs} - x_{\ell s}) + i(\beta^2 - M^2)}{\beta^2}\right]\left[1 + (ik/\beta^2)(\hat{x} - .75\hat{y}\tan\Lambda_\ell)\right]$$

$$C_9 = (ik^2/2\beta^2)\left[\frac{-k^2M^2(x_{cs} - x_{\ell s}) + i(\beta^2 - M^2)}{\beta^2}\right]$$

The loading function described in equation (65) is formulated using pressure expressions that exactly satisfy the boundary conditions at the inboard side edge of the full chord control surface located within the right hand semi-span region. Loading functions due to downwash discontinuities at other side edges are obtained from equation (65) by inserting new definitions of $\hat{x}$ and $\hat{y}$ into the equation such that the equation is transformed into local coordinates of individual side edge stations.

Loading Functions Used in Solution of Residual Downwash Distribution

The loading functions used to obtain solutions of the residual downwash distribution are defined as follows:

$$\Delta P(\xi,\eta) = 4\rho V^2 \frac{\sqrt{s^2 - \eta^2}}{s} \sum_{n=1}^{\bar{N}} \sum_{m=1}^{\bar{M}} a_{nm}\, f^{(n)}(\eta)\, g^{(m)}(\xi,\eta) \qquad (69)$$

where a_{nm} are the unknown coefficient multipliers

$$f^{(n)}(\eta) = \frac{\sin(\bar{n}\phi)}{\sin\phi}$$

$$\bar{n} = \begin{cases} 1,3,5,\text{-- } 2n\text{-}1 \text{ -- } 2\bar{N}\text{-}1 & \text{symmetrical} \\ 2,4,6,\text{-- } 2n \text{ ---- } 2\bar{N} & \text{antisymmetrical} \end{cases}$$

$n = 1,2,3,\text{----------}\bar{N}$

$\bar{N}$ is the number of downwash chords on a semispan

$\phi = \cos^{-1}(\eta/s)$

$$g^{(m)}(\xi,\eta) = \begin{cases} \cot\frac{\theta}{2} & m = 1 \\ \sin(m-1)\theta & m = 2,3,4, \text{ --- } \bar{M} \end{cases}$$

$\bar{M}$ is the number of downwash stations on a downwash chord

The chordwise coordinate θ is not to be confused with the control surface rotation angle $\theta_H(\eta)$.

The loading functions $g(\xi,\eta)$ have been described only in terms of a particular side edge deflection to indicate how the asymptotic pressures have

been modified and extended to the planform boundaries. The complete set of expressions are provided in the computer program and are well annotated for each of the control surface configurations and need not be repeated in this section.

Output of the solution portion of the program using the above described loading functions results in generalized forces described in the following section.

Generalized Forces

Generalized forces are formulated using two sets of pressure distributions that result from the solution of lifting surfaces having discontinuous downwash distributions.

Generalized forces are defined as follows:

$$Q_{ij} = \iint_{surface} \Delta P_j(\xi,\eta)\, H_i(\xi,\eta)\, d(b_0\xi)\, d(b_0\eta) \tag{70}$$

where the limits of integration are the physical boundaries of the half span configuration.

$H_i(\xi,\eta)$ is *ith* deflection mode shape.

$\Delta P_j(\xi,\eta)$ is the sum of the singular (asymptotic pressures) and regular pressures obtained as a solution of the residual downwash distributions.

$$\Delta P_j(\xi,\eta) = \Delta P_j(\xi,\eta)_r + \Delta P_j(\xi,\eta)_{ae} \tag{71}$$

The dimensions of $\Delta P_j(\xi,\eta)$ are: (force/area)(per unit q_j)

The regular pressure distribution $\Delta P_j(\xi,\eta)_r$ is given as

$$\Delta P_j(\xi,\eta)_r = 4\rho V^2 \frac{\sqrt{s^2 - \eta^2}}{s} \sum_{n=1}^{\bar{N}} \sum_{m=1}^{\bar{M}} a_{nm}^{(j)} f^{(n)}(\eta) \; g^{(m)}(\xi,\eta) \qquad (72)$$

where $a_{nm}^{(j)}$ are the coefficient multipliers obtained from the integral equation solution using the residual downwash distributions as boundary conditions for the j*th* mode.

$f^{(n)}(\eta)$ represents the assumed form of the spanwise pressure variation defined in equation (69).

$g^{(m)}(\xi,\eta)$ is the assumed form of the chordwise pressure variation defined in equation (69).

The singular asymptotic pressure distribution is given as

$$\Delta P_j(\xi,\eta)_{ae} = 4\rho V^2 \sqrt{s^2 - \eta^2} \sum_{\underline{k}=1}^{4} A_{\underline{k}-1}^{(j)} f(\eta) \; g(\xi,\eta) \qquad (73)$$

where $f(\eta) = 1/\left[4\pi\sqrt{s^2 - \eta^2}\right]$

$g(\xi,\eta)$ = are the loading functions that are formulated using the asymptotic pressure expressions and the pressure modification functions given in equation (56) or equation (65) depending upon the configuration being evaluated.

$A_{\underline{k}-1}^{(j)}$ are four coefficients of a cubic polynomial used to define the spanwise twist distribution of $\theta_H(\eta)$.

The program output of pressure is lifting pressure coefficient per unit generalized coordinate q_j , and its units are: per unit generalized coordinate q_j . Its numerical values are proportional to the modal-displacement input. The program output of pressures is given as follows:

$$\frac{\Delta P_j(\xi,\eta)}{\frac{1}{2}\rho V^2} = \text{PROGRAM OUTPUT} \tag{74}$$

where $\text{PROGRAM OUTPUT} = 8\frac{\sqrt{s^2-\eta^2}}{s}\chi$

$$\left[\sum_{n=1}^{\bar{N}}\sum_{m=1}^{\bar{M}} a_{nm}^{(j)} f^{(n)}(\eta)\, g^{(m)}(\xi,\eta) + \sum_{k=1}^{4} A_{k-1}^{(j)} f(\eta)\, g(\xi,\eta)\right]$$

Sectional generalized forces may be obtained for any number of arbitrary locations along the semispan and are defined as:

$$Q_{ij}^{s} = \frac{1}{2}\rho V^2 \int_{b_0 x_\ell}^{b_0 x_t} \left[\frac{\Delta P_j(\xi,\eta)}{\frac{1}{2}\rho V^2}\right] H_i(\xi,\eta)\, d(b_0\xi) \tag{75}$$

The section generalized forces Q_{ij}^{s} have the units: (force per unit planform dimension per unit q_j)×(units of modal-displacement input).

The program output of section generalized forces has the units: (planform length units)×(modal-displacement units) per unit q_j , and the program output is proportional to the modal displacement squared and to planform length.

The program output of section generalized forces is given by

$$\frac{Q^{s}_{ij}}{\frac{1}{2}\rho V^2} = \text{PROGRAM OUTPUT} \tag{76}$$

where PROGRAM OUTPUT = $8\,\frac{\sqrt{s^2 - \eta^2}}{s}\,\chi$

$$\int_{b_0 x_\ell}^{b_0 x_t} \left[\sum_{n=1}^{\bar{N}} \sum_{m=1}^{\bar{M}} a^{(j)}_{nm}\, f^{(n)}(\eta)\, g^{(m)}(\xi,\eta) + \sum_{k=1}^{4} A^{(j)}_{k-1}\, f(\eta)\, g(\xi,\eta) \right] H_i(\xi,\eta)\, d(b_0\xi)$$

Total generalized forces are formulated using the definition of equation (70) and the generalized force elements Q_{ij} have the units:

(force per unit q_j)×(units of modal-displacement input)

The program output of total generalized forces is given by

$$\frac{Q_{ij}}{\frac{1}{2}\rho V^2} = \text{PROGRAM OUTPUT} = 8 \int_0^{b_0 s} \int_{b_0 x_\ell}^{b_0 x_t} H_i(\xi,\eta)\, \frac{\sqrt{s^2 - \eta^2}}{s}\, \chi$$

$$\left[\sum_{n=1}^{\bar{N}} \sum_{m=1}^{\bar{M}} a^{(j)}_{nm}\, f^{(n)}(\eta)\, g^{(m)}(\xi,\eta) + \sum_{k=1}^{4} A^{(j)}_{k-1}\, f(\eta)\, g(\xi,\eta) \right] d(b_0\xi)\, d(b_0\eta) \tag{77}$$

The program output has the units: (planform area units)×(modal displacement units) per unit q_j , and the program output is proportional to the modal displacement squared and to planform area.

It should be noted that the sectional generalized forces of equation (75) are used to obtain information on the spanwise loadings. There is no restriction on the number of stations where sectional generalized forces may be obtained and is limited only by user option.

The spanwise locations where the sectional generalized forces are calculated do not coincide with the spanwise quadrature stations where chordwise integrals of equation (77) are evaluated. The chordwise integrals of equation (77) are calculated at particular spanwise stations depending upon the quadrature distribution being used for a particular configuration and are not printed as output from the program.

PROGRAM CAPABILITIES AND LIMITATIONS

The computer program developed around the preferred solution process may be used for a vast array of analysis configurations and has capabilities and limitations listed below:

1. Trailing edge control surface configurations may be composed of a full span, inboard partial-span, outboard tip partial-span, or up to six individual control surfaces including side-by-side common edge control surfaces, and nested controls.

2. For reasons of detail accuracy, leading edge control surfaces are recommended to be limited to control surfaces having side edges inboard of the planform tip station.

3. All hinge lines of trailing edge control surfaces are assumed to be located at the leading edge of the control surfaces. All hinge lines of leading edge control surfaces are assumed to be located at the trailing edge of the control surface. Control surface hinge lines may have individual definitions; however, each hinge line is assumed to be defined by a linear equation.

4. All control surface hinge lines and inboard side edges are assumed to be represented by a sealed gap condition.

5. All control surface side edges are assumed to be parallel to the remote stream direction.

6. Spanwise elastic twist distribution of the control surface hinge line is approximated by a cubic polynomial to allow a spanwise variation of the hinge line rotation $\Theta_H(\eta)$.

7. Control surface camber bending is treated within the regular lifting surface solution.

8. Lifting surface solutions of planforms not having control surfaces may be obtained upon user option.

9. Spanwise symmetrical or antisymmetrical analysis may be accomplished upon user option.

10. Planform definition is assumed to consist of linear segments defined by input data. (See Appendix C on effect of locating downwash chords near junctions of linear segments of planform definition.)

11. Downwash boundary conditions may be modified to include local streamwise velocity variations due to airfoil thickness effects. (See Appendix C.) (See reference 4 for limitations.)

12. Input mode shapes may be defined at many points on the surface (such as obtained from a finite element structural analysis).

13. Multiple k value and Mach number analyses may be made in a single machine run (see reference 4, section 3.7.2 LIMITATIONS).

14. The printed output of the program, obtained on user option, consists of a definition of kinematic downwash matrix, mathematically discontinuous downwash matrix, residual downwash matrix, pressure series coefficients, chordwise array of pressures at prescribed spanwise stations, sectional generalized forces, and total generalized forces.

15. Intermediate and/or final results may be optionally saved on tapes for economy of reuse.

VALIDATION STUDIES OF ASYMPTOTIC PRESSURE EXPRESSIONS

Numerical investigations have been conducted to determine the validity of using any of the various asymptotic pressure expressions that have been proposed[3,7,8] for analysis of configurations having swept hingeline trailing edge controls.

The criteria used to judge the correctness of the asymptotic pressure expressions is that the residual downwashes are required to be smooth and continuous over the lifting surface including the region of the control surface edges. Since the asymptotic pressure expressions are developed to satisfy the basic flow equation and the change in boundary conditions across the edges of the control surface, then the subtraction of the kinematic downwash distribution from the distribution having identical discontinuity values must result in a residual distribution that is smooth and continuous. Otherwise, it must be presumed that the expressions are functionally insufficient to satisfy the original boundary value problem.

Initial studies to determine the characteristics of the residual downwashes were conducted on a zero sweep planform having a 30% chord control surface. The analysis was conducted for several spanwise length control surfaces. The pressure expression used in the analysis is the expression developed by Landahl[3] for the zero sweep rectangular control surface and for the steady flow case of k=0, the expression is given as

$$C_p = -\frac{\theta_H}{\pi\beta} \log\left[\sqrt{(\xi-\xi_c)^2 + \beta^2(\eta-y_s)^2} - \beta(\eta-y_s)\right] \tag{78}$$

Analysis results obtained for all of the control surface configurations indicate that the residual downwashes are smooth and continuous over the entire planform and the final solutions provide generalized force values that are almost invariant with the number of collocation stations used in the

analyses. Chordwise pressure distributions obtained for spanwise stations located at large distances from the control surface side edges decrease in value montonically from the leading edge to the trailing edge without displaying any chordwise waviness in any of the study configurations including solutions for very small span control surface configurations.

It appears that solutions obtained for the zero sweep control surface case using the pressure expression of equation (78) will be almost variant with the number of collocation stations used in the solution process.

Solution sensitivities were then obtained for the swept hingeline case using another loading function as suggested by Ashley[11] and as applied in computer programs developed by Darras and Dat[12] and by Zwaan[13].

The form of the k=0 asymptotic pressure expression is given as

$$C_p = -\frac{\theta_H}{\pi\bar{\beta}} \log\left[\sqrt{(\xi-\xi_c)^2 + \beta^2(\eta-y_s)^2} - \beta(\eta-y_s)\right] \qquad (79)$$

where

$$\bar{\beta} = \sqrt{(1-M^2\cos^2\Lambda_c)/\cos^2\Lambda_c} = \sqrt{\beta^2 + \tan^2\Lambda_c}$$

It should be noted that the only difference between this expression for swept hingelines and Landahl's expression for non-swept hingelines is the factor $\bar{\beta}$ as contained in the multiplying coefficient. Unsteady lifting surface pressure distributions were obtained using the constant chord 25° sweep planform of reference 17 shown in figure 20 for which experimental lifting surface data are available. Motion of the configuration is composed of an oscillating outboard flap with all other components maintained in a stationary position.

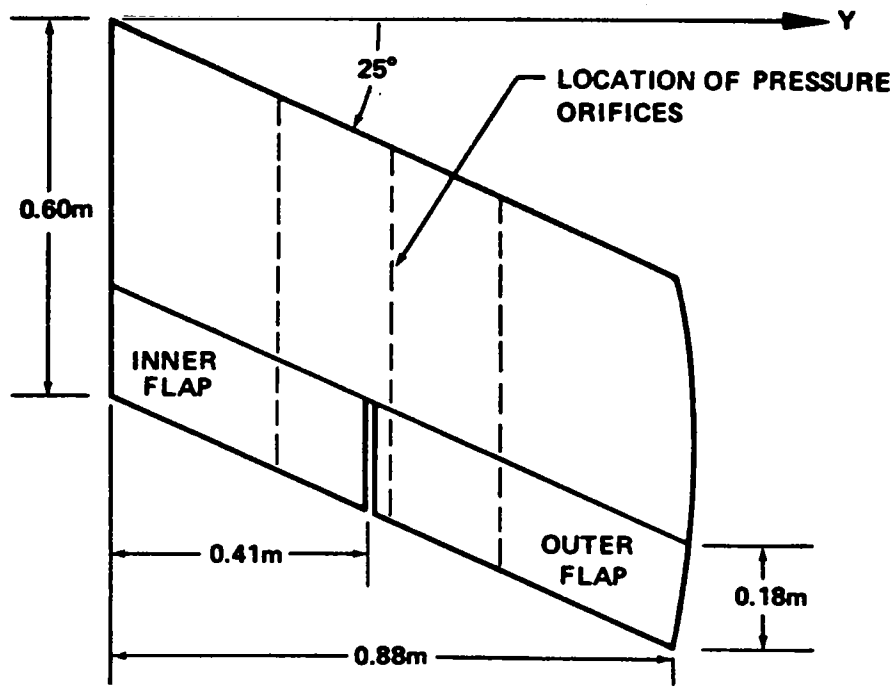

Figure 20 - Experimental Planform of Reference 17 Showing the Side-by-Side Control Surface Arrangement. (dimensions in meters)

Figure 21 represents the chordwise variation of the in-phase pressure component (ΔC_preal) for a spanwise station that is located at a large distance away from the control surface side edge. Experimental values are represented by the open symbols and two theoretical curves are given that represent the solution results using two distinctly different distributions of collocation stations. The theoretical results for the (4,6) solution represent the results obtained using 4 collocation stations on 6 downwash chords. The downwash chords are located at relatively large distances away from the control surface side edge. Theoretical prediction using the (4,6) distribution follows the trends of the experimental values, except in the region of the hingeline gap where the gap is affecting the experimental results. Whereas, the solution results of (7,9) distribution contain a chordwise waviness near the trailing edge that is thought to be due to having the downwash chords located very near the control surface side edge. The presence of small pressure wave lengths of the (7,9) distribution results, in

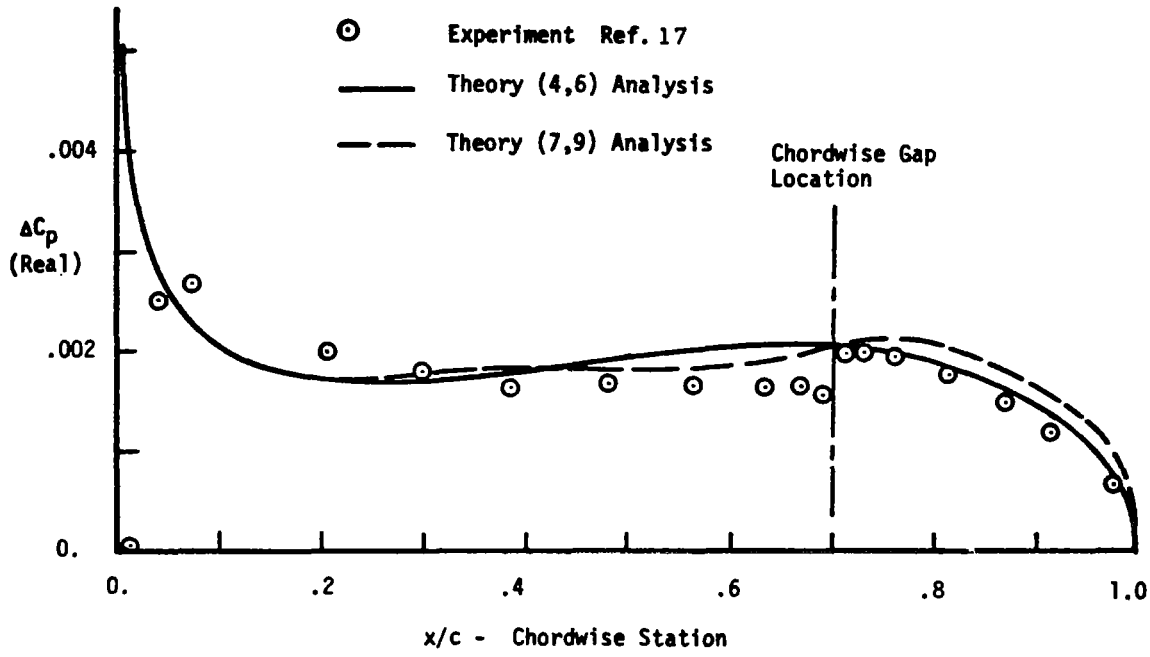

Figure 21 - Comparison of Theoretical and Experimental In-phase Pressures.

comparison with the (4,6) distribution results, indicates that the residual downwash distribution may not be smooth and continuous across the control surface side edge with the result that some of the low wave length assumed pressure modes are required to satisfy irregular boundary conditions being generated by the asymptotic pressure function of equation (79).

Numerical investigation has been conducted to determine the characteristics of the residual downwashes being generated using the pressure expression of equation (79) applied to the analysis planform of figure 22. Effect of the large hingeline sweep angle on residual downwashes should be well identified in using this configuration since $\tan\Lambda$ becomes equal to the same order of magnitude as β^2.

The spanwise variations of the residual downwashes obtained from the investigation for $k=0$ and $M=0$ are shown in figure 23. The spanwise variation of residual downwash for stations ahead of the hingeline is smooth

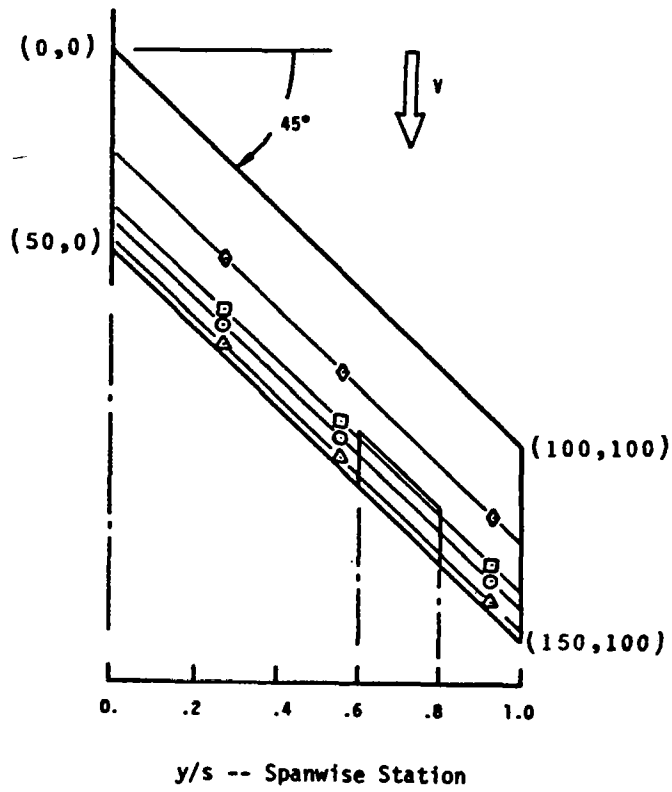

Figure 22. Planform Used to Evaluate Residual Downwash Characteristics.

and continuous. However, for stations aft of the hingeline, there is a finite discontinuity as well as a slope discontinuity at the side edges of the control surface. This side edge discontinuity may be analytically predicted, since it can be shown that the pressure expression will satisfy the boundary condition discontinuity across the hingeline, but will not satisfy the side edge discontinuity condition. Consequently, use of the pressure expression of equation (79) should be limited to configurations having zero sweep angles and large span length control surfaces with the restriction that the collocation stations are spaced well away from the control surface side edges.

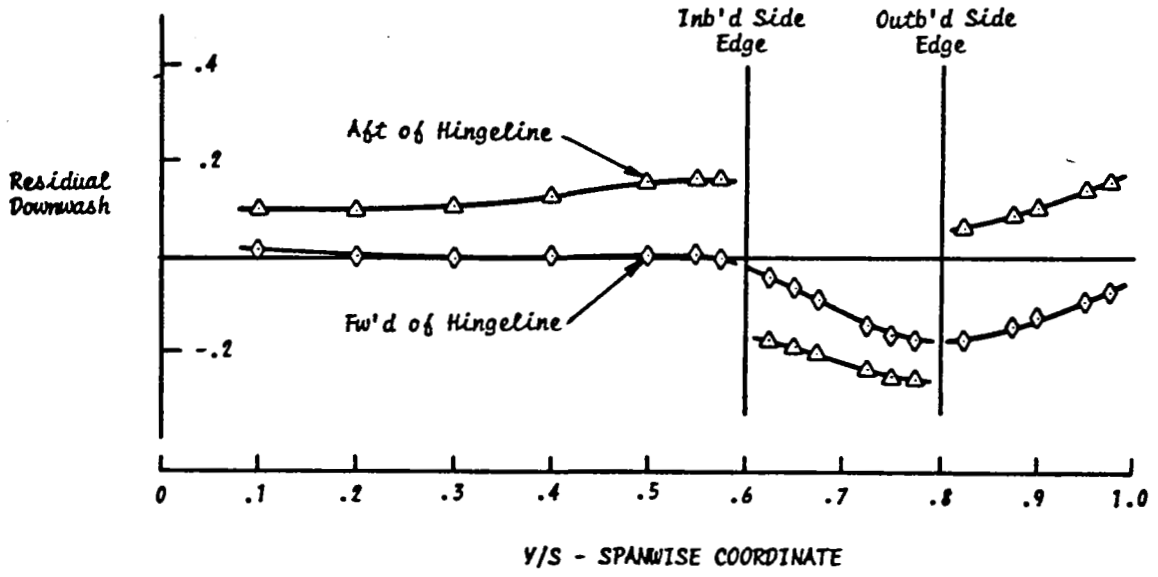

Figure 23 - Spanwise Residual Downwash Distributions Along Spars Forward and Aft of Hingeline Using Pressure Expression of Equation 79.

Residual downwashes have also been obtained using the configuration of figure 22 and applying another pressure expression that has been used in computer programs developed by Rowe[14], Medan[15], and Hewitt[16]. The pressure expression contained in these references for k=0 is

$$C_p = -\frac{\Theta_H}{\pi\bar{\beta}} \log\left[\sqrt{(\xi-\xi_c)^2 + \bar{\beta}^2(\eta-y_s)} - \bar{\beta}(\eta-y_s)\right] \qquad (80)$$

This expression differs from equation (79) by having $\bar{\beta}$ included within the logarithmic function as well as appearing in the multiplying coefficient.

The residual downwashes shown in figure 24 indicate that for chordwise stations ahead of the hingeline the residual distribution are smooth and continuous across the side edge. However, the distributions have a slope discontinuity across the side edges for stations aft of the hingeline.

It was also noted that for small control surface span lengths the magnitude of the distributions remained the same and the discontinuity peaks were spaced closer together which produces a highly localized oscillatory distribution in

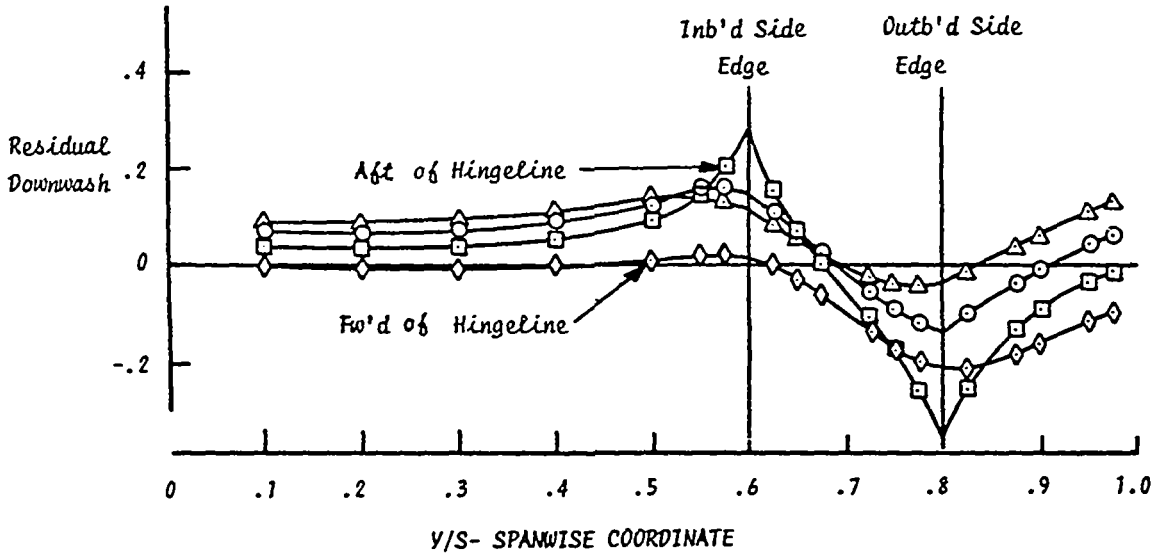

Figure 24 - Spanwise Residual Downwash Distributions Along Spars Forward and Aft of Hingeline Using Pressure Expression of Equation 80.

the residual downwashes. This localized distribution in residual downwashes is identified as being the major contributing factor that may produce questionable results for small span length control surface analyses.

In order to alleviate the solution sensitivities caused by irregular residual downwashes new pressure expressions were obtained by reformulating the asymptotic expansion process following the procedures suggested by Landahl[3]. The step-by-step procedure is presented in appendix 'A'. The k=0 pressure expression obtained from the new formulation is given as

$$C_p = -\frac{\Theta_H}{\pi\bar{\beta}} \log\left[\sqrt{\tilde{x}^2 + \beta^2(\eta-y_s)^2} - \left[\beta^2(\eta-y_s) + \tilde{x}\tan\Lambda\right]/\bar{\beta}\right] \qquad (81)$$

where $\tilde{x} = \xi - x_{cs}$

and the resulting residual downwash distributions are shown in figure 25 for the analysis configuration of figure 22. It should be noted that the residual distributions are now smooth and continuous for all stations either ahead or behind the hingeline. The chordwise pressure distributions at large spanwise distances away from the control surface were found to be montonically decreasing in value from the leading edge to the trailing edge. Furthermore, the final lifting surface pressure distributions remain almost invariant with the distribution and number of collocation stations used in the analyses.

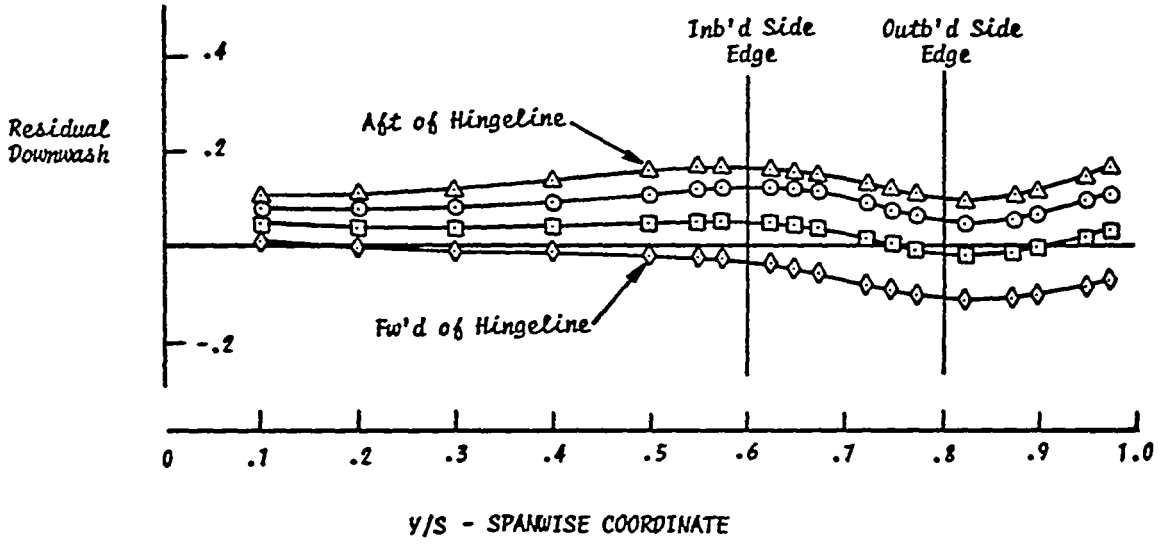

Figure 25. Spanwise Variation of Residual Downwash Distribution Using Pressure Expression of Equation 81.

Numerical investigations have also been conducted to determine the validity of the equations developed to satisfy the change in boundary conditions across the side edge of an oscillating full chord control surface.

Loading functions developed for the full chord control surface given by equation (65) have been used to evaluate the residual downwash distribution.

The analysis configuration is a constant chord 45° swept planform having a full chord control surface with side edges located at 60% and 80% of the semispan length. The residual downwash distribution is shown in figure 26 and indicates that the residual downwashes are smooth and continuous across the side edges.

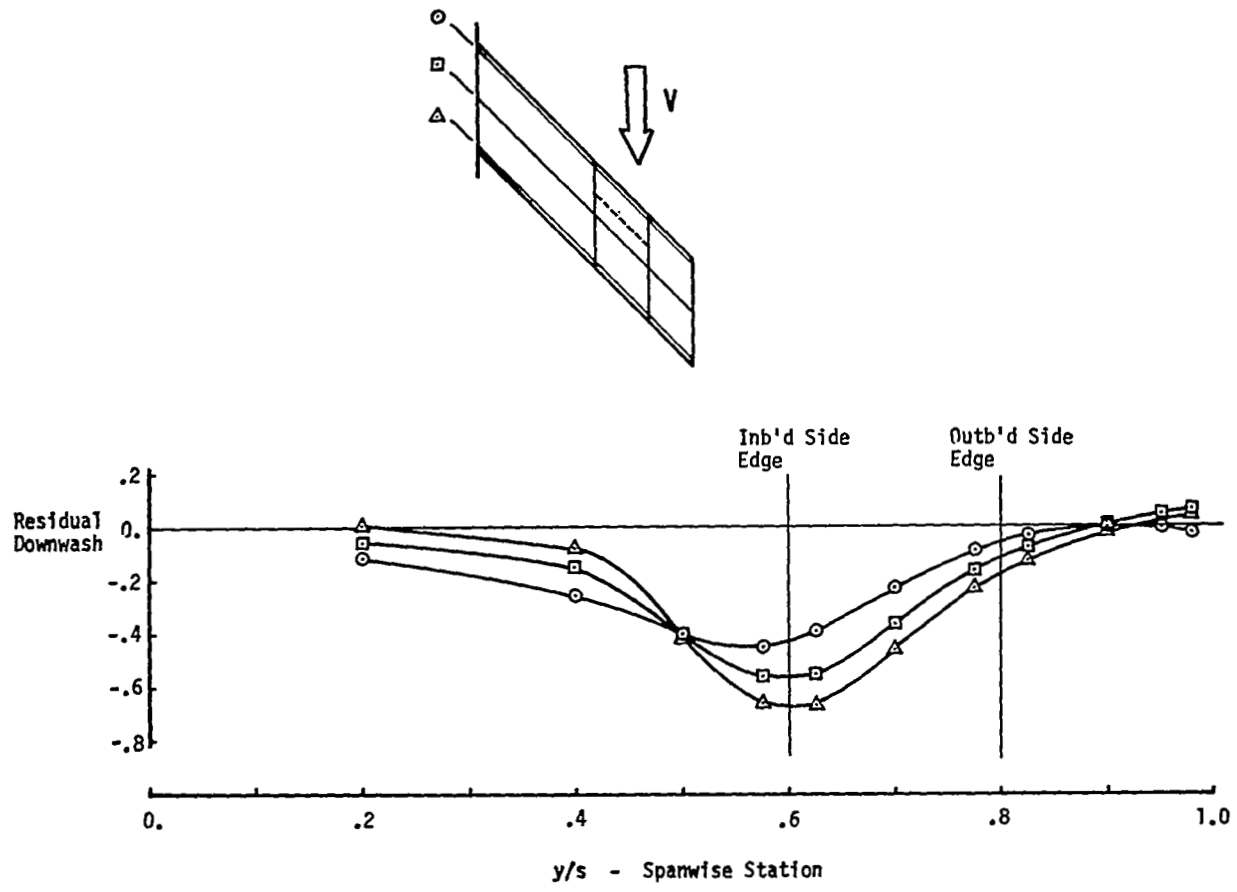

Figure 26. Spanwise Residual Downwash Distributions for a Full Chord Control Surface Hinged at 30 Percent Chord.

It appears that the asymptotic pressure expressions developed for the swept hinge line trailing edge control surface and for the swept leading edge control surface does provide the proper downwash discontinuities and may be combined to provide analysis capability for the partial chord leading edge control surface.

RESULTS, COMPARISONS AND DISCUSSION

This section contains an illustration of the downwash subtraction procedure and also provides pressure distributions and generalized forces resulting from analysis of five wing-control surface configurations for which experimental data are available. The experimental configurations consist of (1) the swept-wing with a non-oscillating full span flap of reference 18, (2) a swept-wing having an inboard partial span control surface of reference 19 for which non-pscillatory pressures are available, (3) a rectangular wing having an oscillating full span flap (reference 20), (4) a swept wing having oscillating side-by-side control surfaces (reference 17), and (5), a highly swept delta wing having leading and trailing edge controls (reference 23).

Description of Downwash Subtraction Process

The configuration of reference 17, shown in figure 27, is used to illustrate the downwash subtraction process.

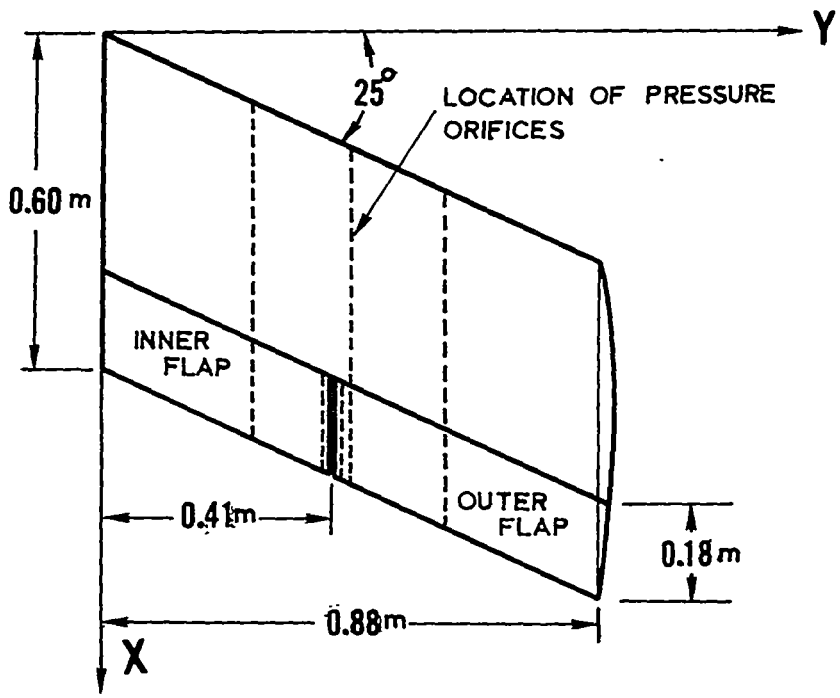

Figure 27.- Experimental Planform of Reference 17 Showing the Side-by-Side Control Surface Arrangement (dimensions in meters)

The inboard control surface is assumed to be oscillating about its hingeline at a reduced frequency of k = 0.372 and at a Mach number of M = 0. The rotation angle is assumed to be constant across the span of the control surface having a value of one radian measued in a plane perpendicular to the y axis. The remaining portion of the lifting surface is assumed to be at rest.

The in-phase part of the kinematic downwash distribution obtained from the motion definition is shown in figure 28 for nine chords equally spaced across the semispan. The downwash has a uniform value of $\frac{w}{V}$ = 1.0 over the control surface and is zero everywhere else.

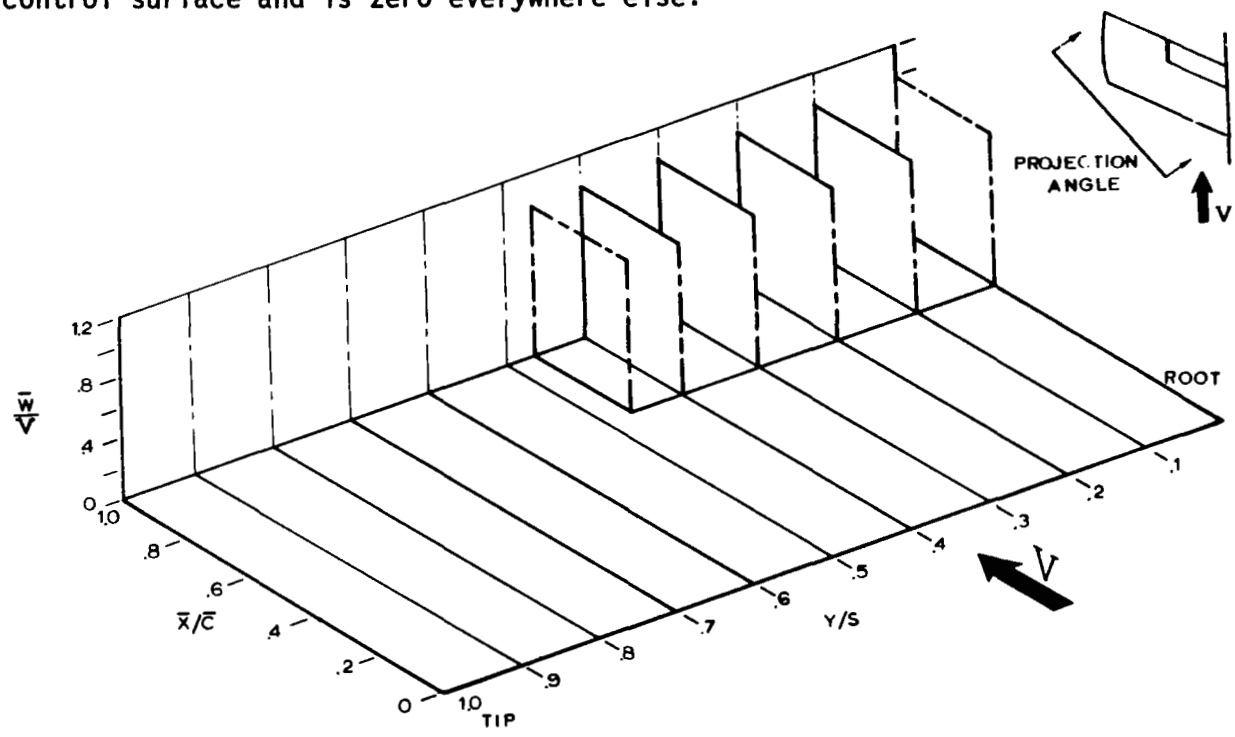

Figure 28. Kinematic Downwash Distribution Derived from Motions of Inboard Flap

Downwash distribution resulting from the integral evaluation using the loading functions defined by equation (56) is shown in figure 29. The distributions are smooth in regions outside of the control surface and a unit change in downwash across the hingeline is obtained for the chords that lie on the control surface.

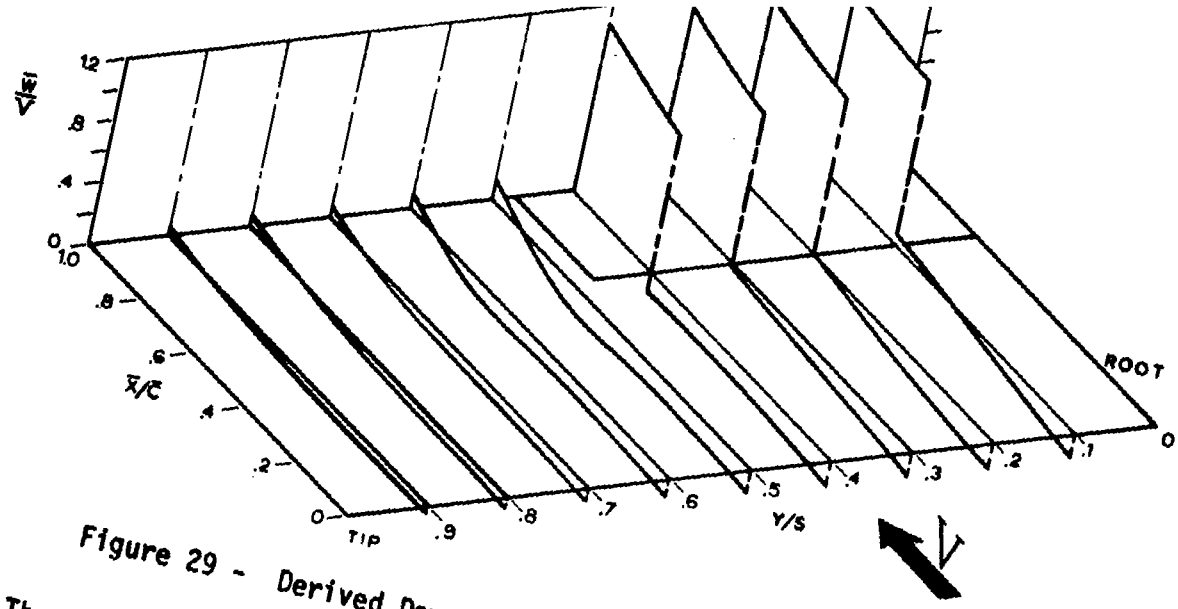

Figure 29 - Derived Downwash Distribution

The distribution of figure 29 is subtracted from that of figure 28 which results in the modified distribution of figure 30.

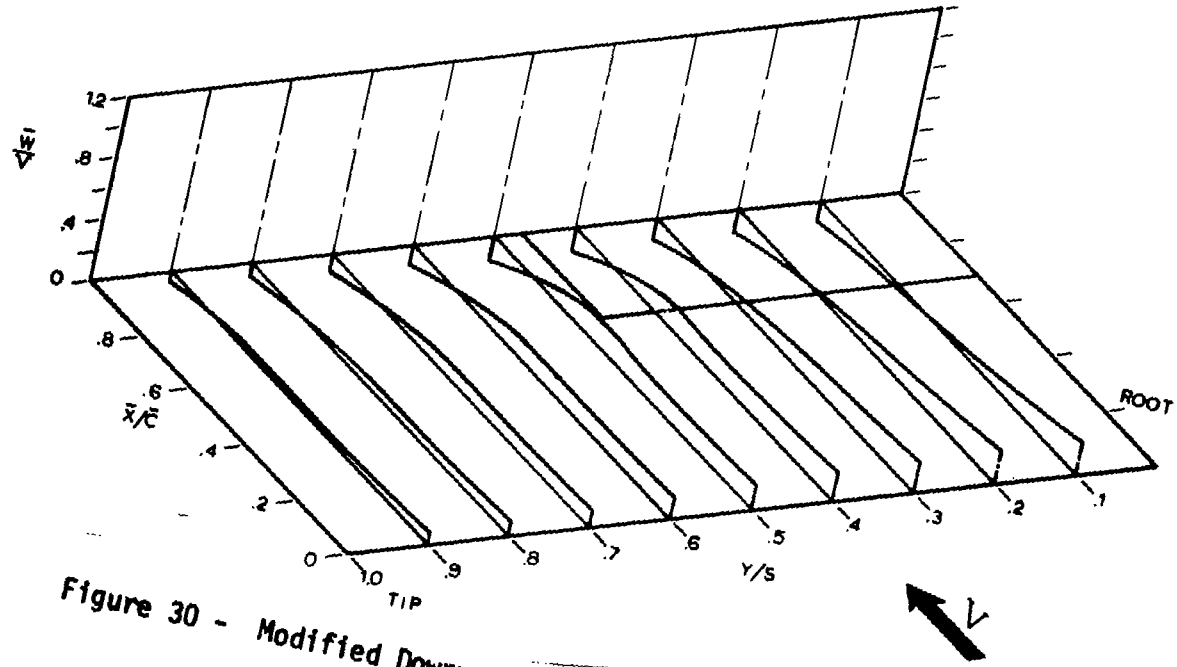

Figure 30 - Modified Downwash Distribution

Since the modified distribution is smooth and does not contain any discontinuities, it appears that the pressure loading functions (equation (56)) that were developed from the asymptotic expansion process of reference 3 provide the proper description of surface loadings to be used in obtaining solutions for configurations having discontinuous downwash distributions.

Steady-State Results for Full-Span Flap Configuration

The full-span flap configuration of reference 18 is shown in figure 31 for which experimental pressures were obtained for various combinations of flap deflections and wing angles of attack. The flap deflection and wing angle of attack were maintained at constant values for each experimental run.

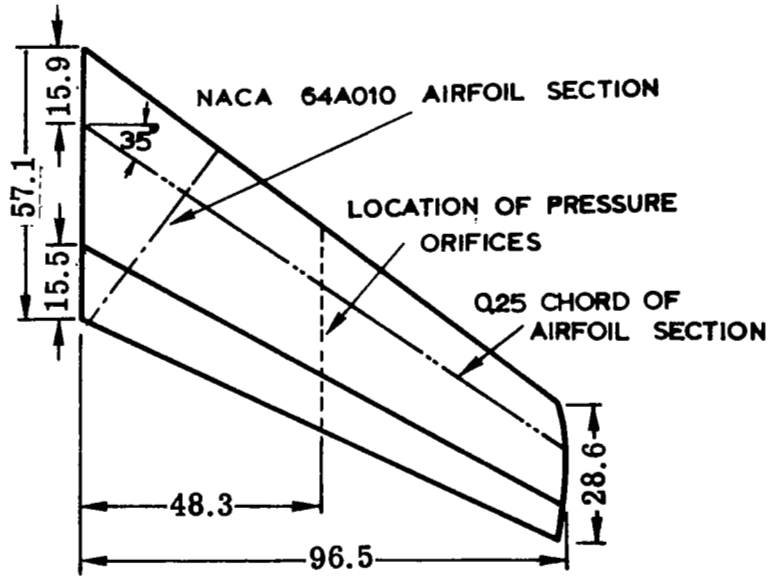

Figure 31.- Experimental Full-Span Flap Configuration NACA RM A9G13 (dimensions in cm)

Experimental pressures were obtained along a streamwise section located at the 50% semispan station. The longitudinal junction between the wing and flap was sealed to prevent flow leakage between the lower and upper surfaces at the hingeline.

The theoretical pressure distributions are obtained using a modification on the boundary conditions (described in Appendix C) that include local streamwise velocity variations due to airfoil thickness effects. A comparison of the experimental and theoretical results are shown in figure 32.

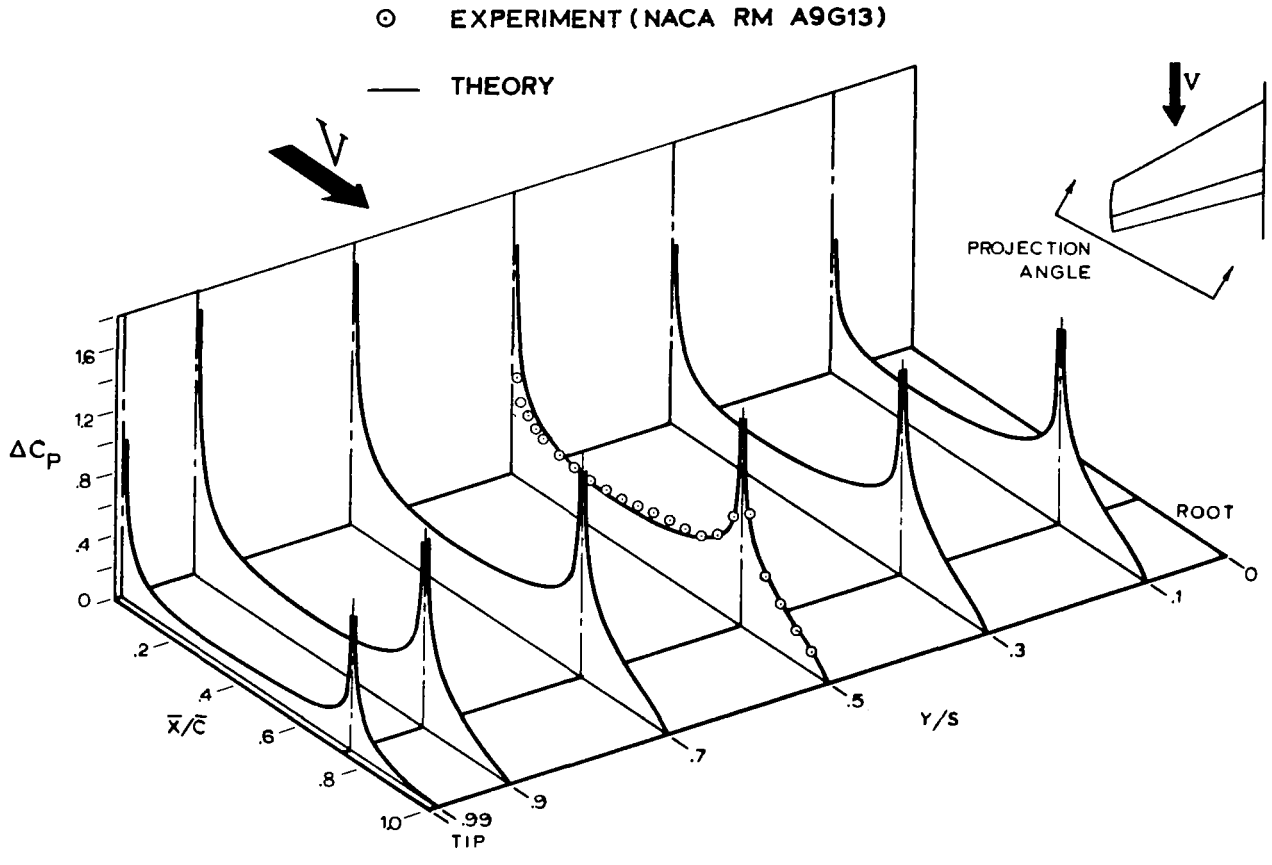

Figure 32.- Theoretical and Experimental Chordwise Pressure Distributions for a Full-Span Flap Deflected by $\delta = 10°$, $\alpha = 0.0°$ at $M = 0.21$ and $k = 0$

The experimental sealed gap condition at the hingeline satisfies the theoretical assumptions (reference 3) and provides a one-to-one basis for evaluating the accuracy of the theoretical prediction method.

The comparison indicates that the experimental values are theoretically predicted within very close tolerances over the entire length of the chord even in the vicinity of the hingeline.

Steady-State Results for a Partial-Span Flap Configuration

The partial-span control surface configuration shown in figure 33 represents the experimental planform of reference 19 to obtain chordwise pressure distributions due to a steady flap deflection. Pressures were obtained along a streamwise chord located at the 46% semispan station. The hingeline gap was sealed providing a one-to-one basis for comparing theoretical and experimental results.

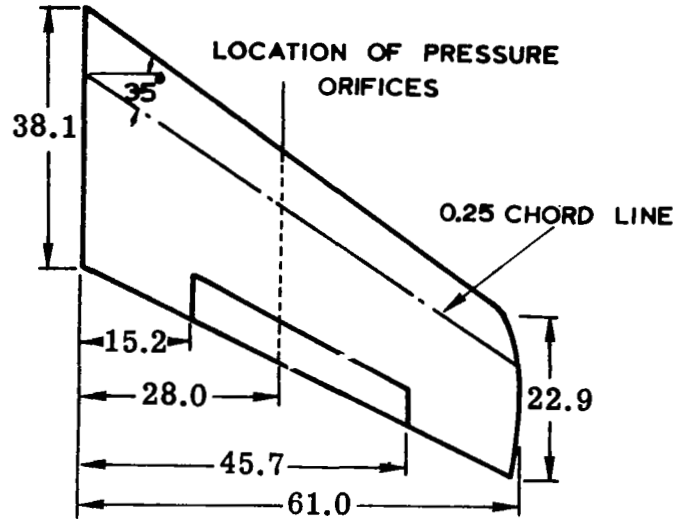

Figure 33.- Experimental Planform of a Partial-Span Flap Configuration of NACA RM L53C23 (dimensions in cm)

Theoretical pressures were obtained along various streamwise chords spaced over the semispan and are shown in figure 34. The comparison indicates that the experimental pressures are accurately predicted by the theoretical technique over the length of the chordwise strip forward of the hingeline. The theoretical distribution over the control surface are only slightly larger than the experimental values. Consequently, it appears that the lifts and hinge moments may be predicted within reasonable accuracy limits for configurations having a sealed gap at the wing-control surface junction.

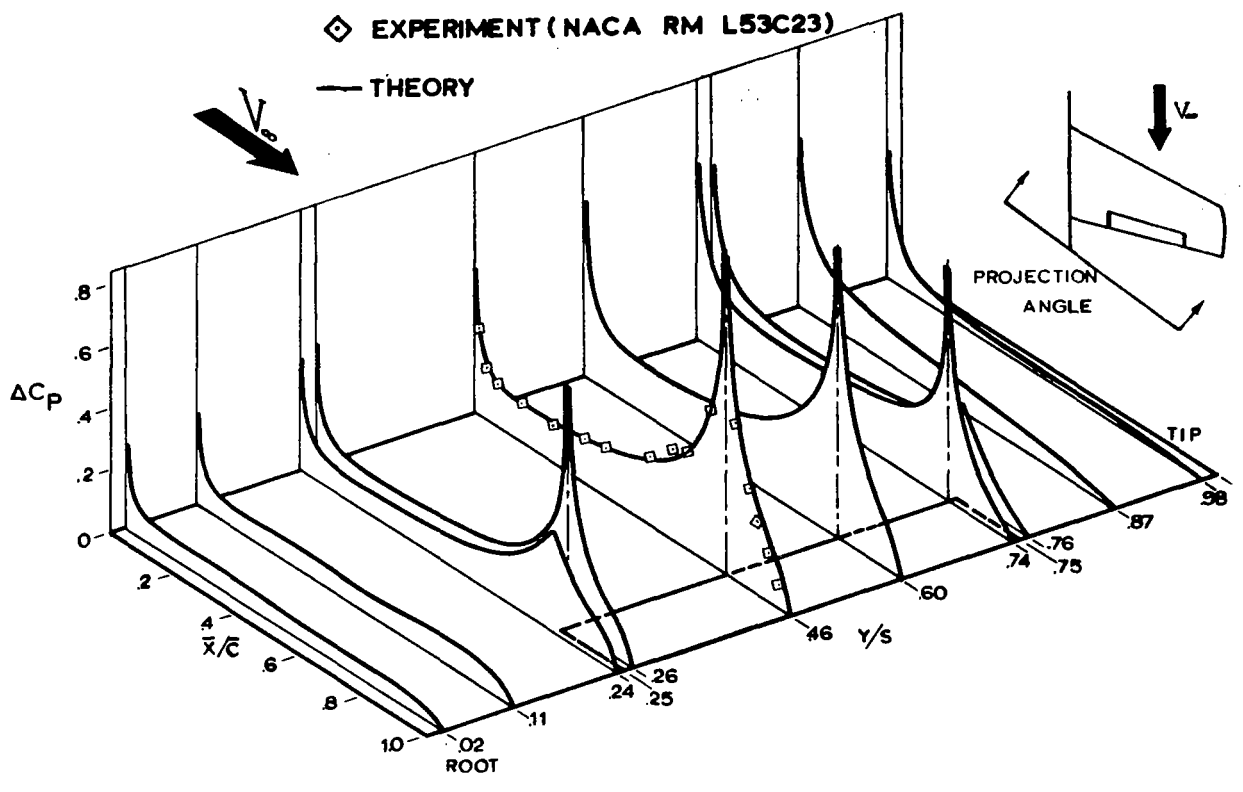

Figure 34. Theoretical and Experimental Pressure Distributions for Partial-Span Flap Deflected by $\delta = 10°$, $\alpha = 0°$, at $M = 0.60$ and $k = 0$

Rectangular Planforms Having Full-Span Control Surfaces

Two rectangular planforms having aspect ratios of 1.0 and 2.0 were tested in combination with a 40% chord flap for various values of reduced frequencies to obtain hinge moments and lifts due to the control surface motions. The experimental data are reported in reference 20. Each planform had a small gap along its hingeline that may have a small influence on the pressure distributions in regions near the hingeline.

Experimental and theoretical values of hinge moments and phase angles as a function of reduced frequency are presented in figure 35 for the aspect ratio 2.0 planform. The theoretical hinge moments appear to agree with the experimental values; however, there is a discrepancy in the predicted phase angles that may be due to the open gap at the hingeline.

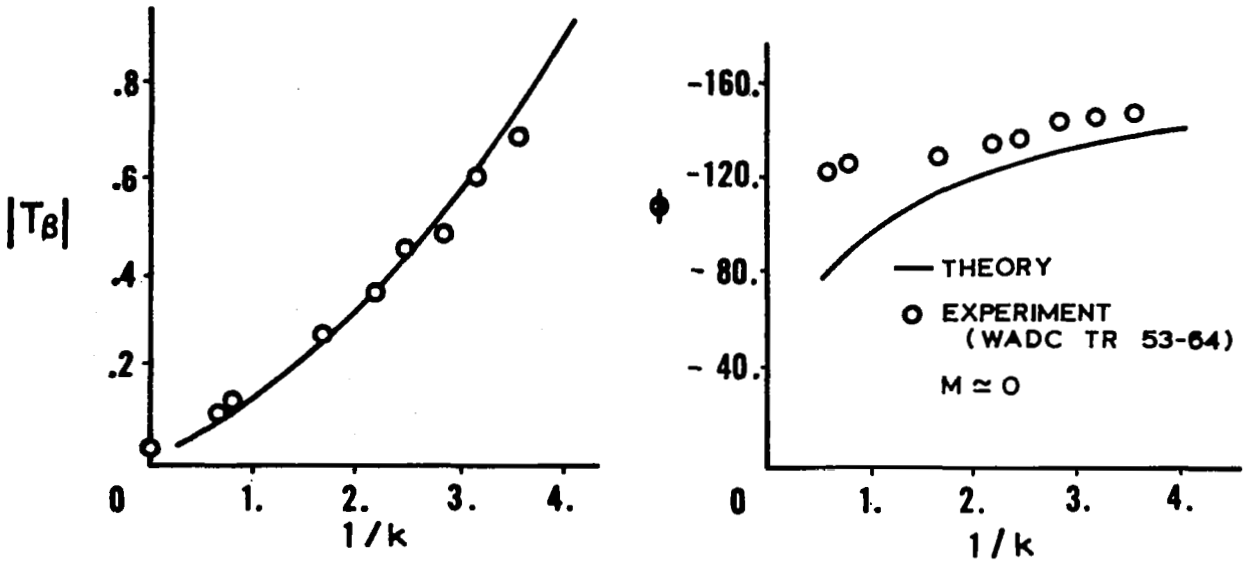

Figure 35.- Theoretical and Experimental Hinge Moments and Phase Angles for an Oscillating Full-Span Flap AR = 2.0 Configuration of WADC TR 53-64

Comparison of wing lifts and phase angles are shown in figure 36. There is good agreement between the theoretical and experimental results over the entire range of reduced frequencies used in the tests. Consequently, it appears that wing lift is not greatly affected by open gaps at the hingeline.

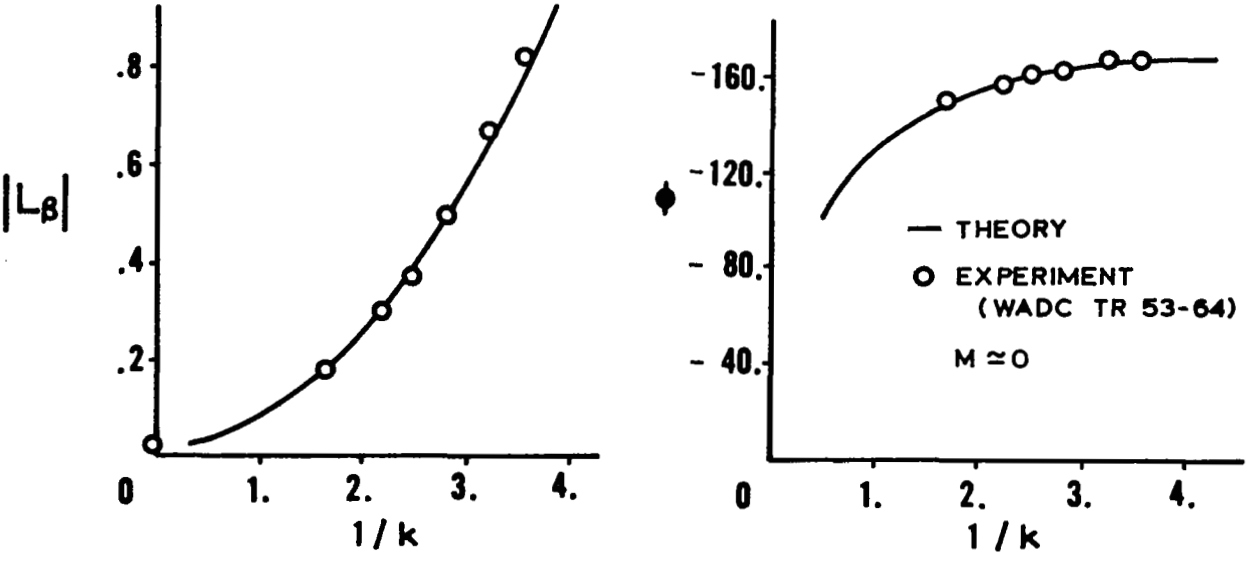

Figure 36.- Theoretical and Experimental Lifts and Phase Angles for an Oscillating Full-Span Flap AR = 2.0 Configuration of WADC TR 53-64

Experimental and theoretical results for the full span control surface configuration of aspect ratio 1.0 are shown in figure 37 and figure 38. Again, the theoretical method appears to predict reasonable values of hinge moments and total lifts; however, the predicted hinge moment phase angles deviate from the experimental values and the discrepancy may be due to the open gap at the hingeline.

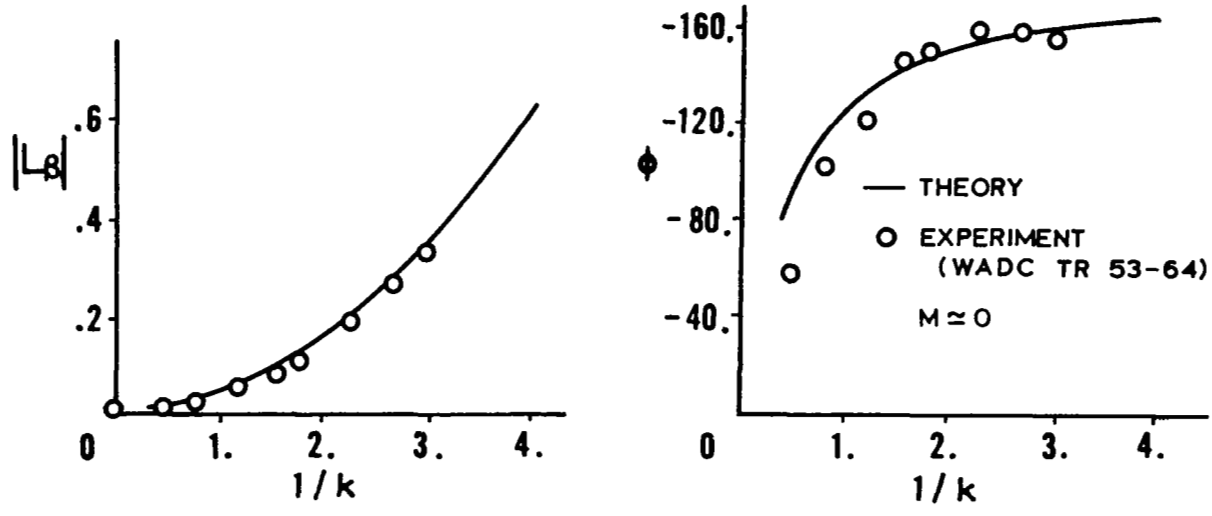

Figure 37.- Theoretical and Experimental Lifts and Phase Angles for an Oscillating Full-Span Flap AR = 1.0 Configuration of WADC TR 53-64

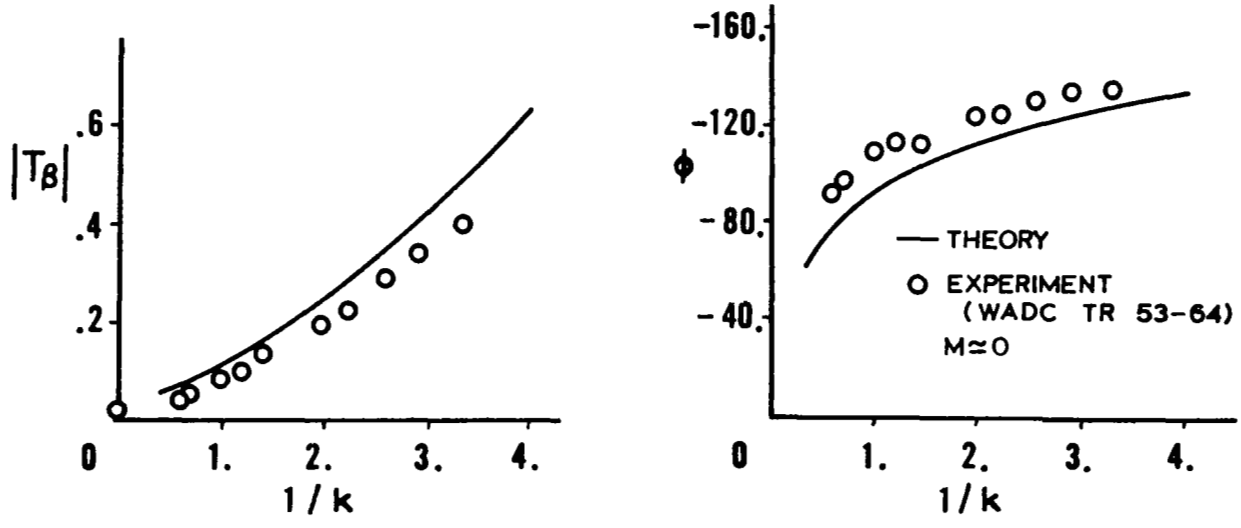

Figure 38.- Theoretical and Experimental Hinge Moments and Phase Angles for an Oscillating Full-Span Flap AR = 1.0 Configuration of WADC TR 53-64

The difference may also be caused by trailing edge flow separation that could have been experienced during the test since there is a very large adverse pressure gradient at the trailing edge that might not have been maintained during the experiment. (see page 315 of reference 24 for the pressure gradient plot of the NACA 0010 airfoil section used in the experiment.)

Effect of Hingeline Gaps on Chordwise Loadings

A theoretical study has been made (reference 21) to investigate the effect of hingeline gaps on chordwise pressure distribution, and the results are shown in figure 39.

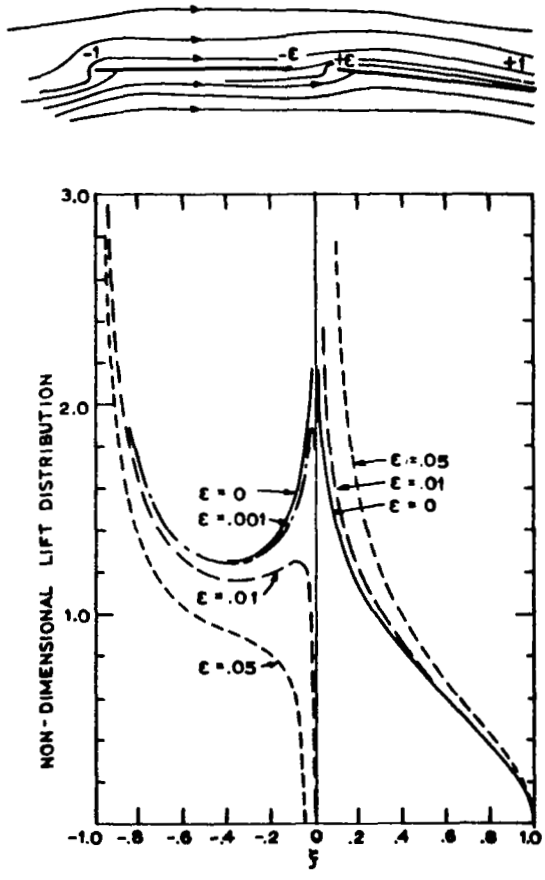

Figure 39.- Non-Dimensional Lift Distribution (reproduced from reference 21)

The study configuration is composed of a pair of two-dimensional equal chord lifting surfaces that are placed in a coplanar arrangement. The leading surface is at a zero angle of attack and the trailing surface is given an angle of attack by rotating the surface about its leading edge. Chordwise pressures are obtained for various separation spacings in steady flow.

For a zero gap spacing, the loadings produced at the junction of the two surfaces exhibit the typical symmetrical logarithmic singularity identified for a discontinuous downwash distributions of a two-dimensional wing-control surface combination. As separation begins, the loadings on the wing near the wing trailing edge change from a singularity characteristic to a loading that becomes equal to zero. However, the loadings near the leading edge of the control surface change from a logarithmic characteristic to that of having an inverse square root singularity that causes a higher loading to exist on the control surface for the open gap condition than for the zero gap condition.

Large separation distances between the surfaces result in loadings that are vastly different from the zero separation case. However, small separations affect the pressure distributions only in localized regions near the hingeline. It appears that the zero gap theoretical method will provide reasonable predictions of total lifts and moments for configurations having small hingeline gaps.

Side-by-Side Control Surface Configuration

The side-by-side control surface configuration is shown in figure 27 for which unsteady pressures are obtained for various combinations of flap deflections. The experimental model had small open gaps at the hingelines and at the side edges. Reference 17 provides no information to define the exact dimensions between the control surface side edges and the pressure measuring stations located in the vicinity of the side edges. The spanwise location of the experimental pressure chords were established by measuring the pressure chord locations off the planform drawing.

Figures 40 and 41 present comparisons of theoretical and experimental results for a mode shape in which both flaps are oscillating with the same phase and amplitude and the wing is maintained in a stationary position. There is good agreement between the theoretical and experimental results in all areas except in localized regions near the hingelines. The experimental values are less than the theoretical values forward of the hingeline and slightly greater than the predicted values aft of the hingeline. The variations near the hingeline are attributed to the open gaps at the hingelines. Even though the comparisons deteriorate in regions near the hingeline, it appears that the total lifts and moments may be estimated within reasonable bounds for configurations that have small open gaps at the hingelines.

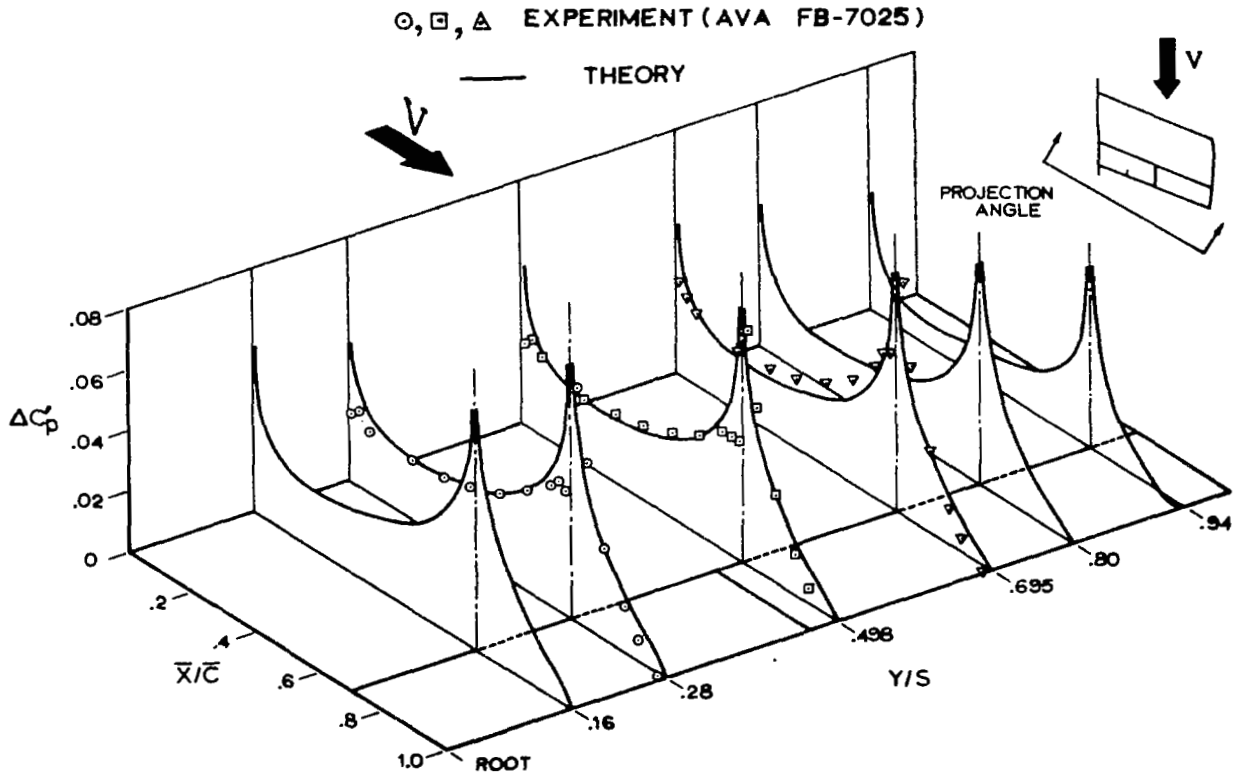

Figure 40. In-Phase Pressure Distributions for Both Flaps Oscillating with the Same Phase and Amplitude. $A_{i.f.} = 0.82°$, $A_{o.f.} = 0.82°$, $A_W = 0°$, $k = 0.372$, and $M \approx 0$

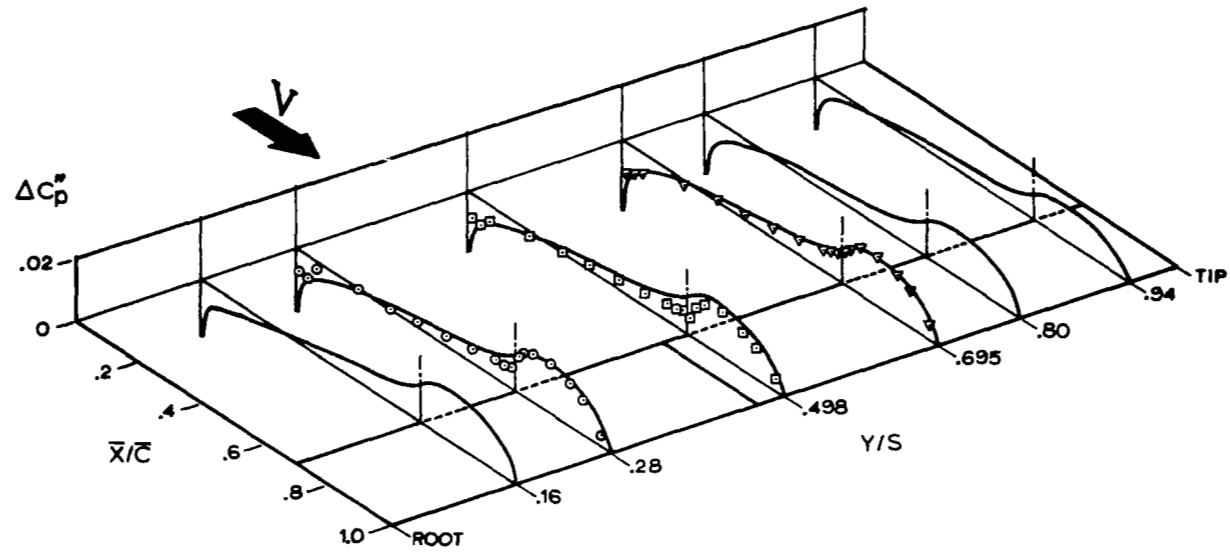

Figure 41. Out-of-Phase Pressure Distributions for Both Flaps Oscillating

Figures 42 and 43 present comparisons of theoretical and experimental pressure distributions for a mode shape in which the outer flap is oscillating and the inner flap and wing are maintained in a stationary position.

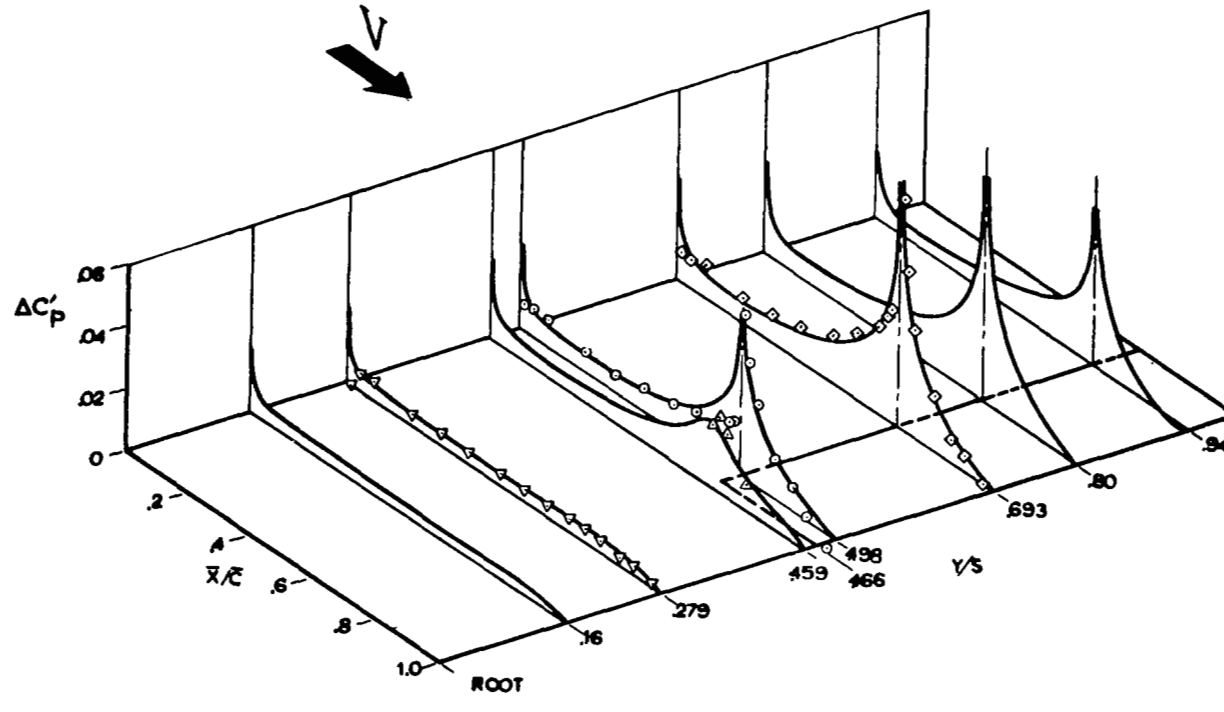

Figure 42. In-Phase Pressure Distributions Resulting from Motions of Outer Flap. $A_{i.f.} = 0°$, $A_{o.f.} = 0.66°$, $A_w = 0°$, $k = 0.372$, and $M = 0$

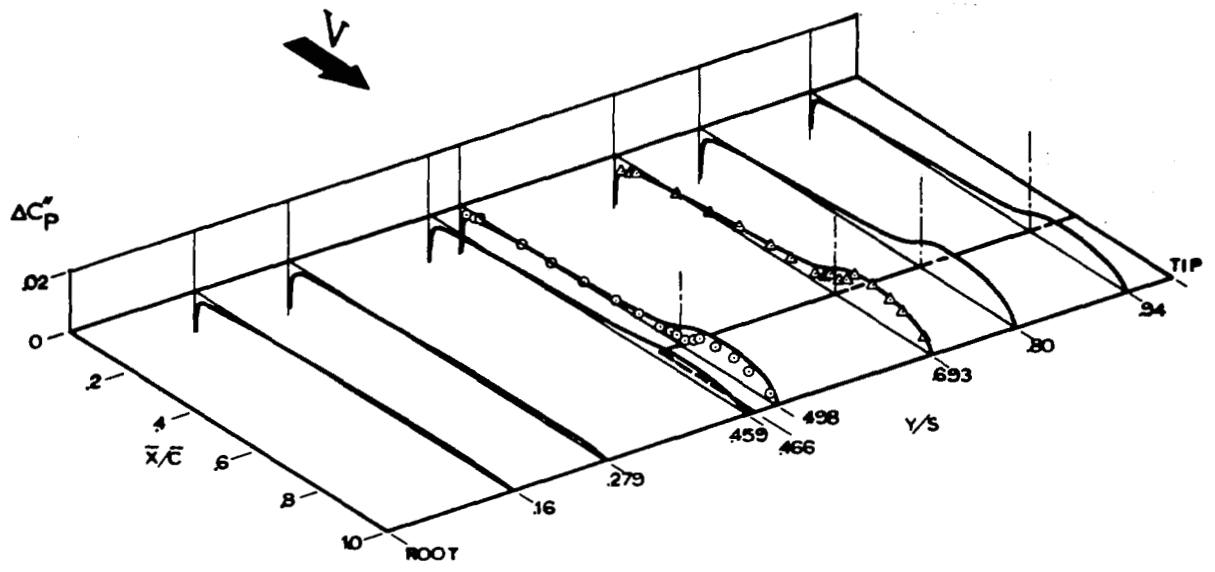

Figure 43.- Out-of-Phase Chordwise Pressure Distributions Resulting from Motions of Outer Flap. $A_{i.f.} = 0°$, $A_{o.f.} = 0.66°$, $A_w = 0°$, $k = 0.372$, and $M \simeq 0$

Again, the only area where the comparisons deteriorate is within the hingeline region and is probably due to open gap effects at the hingeline.

Swept Delta Wing with Leading and Trailing Edge Controls

The planform configuration shown in figure 44 represents the experimental planform of reference 22 where experimental studies were accomplished to investigate use of active controls to suppress flutter. Steady state hinge moments obtained within this investigation were reported within reference 23 and are reproduced in figure 45.

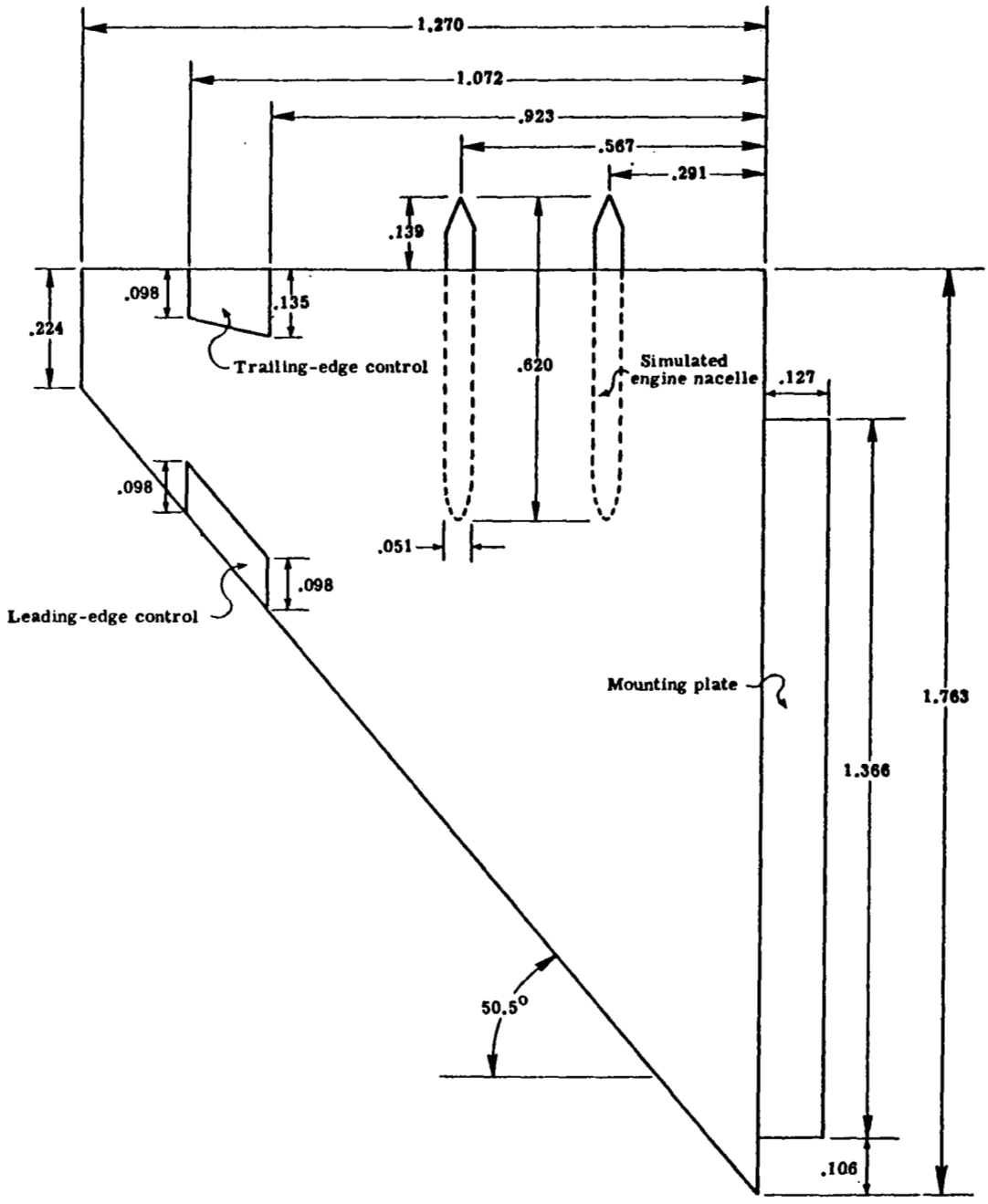

Figure 44- Experimental Delta-wing Model of NASA TM X-2909
(all linear dimensions in meters)

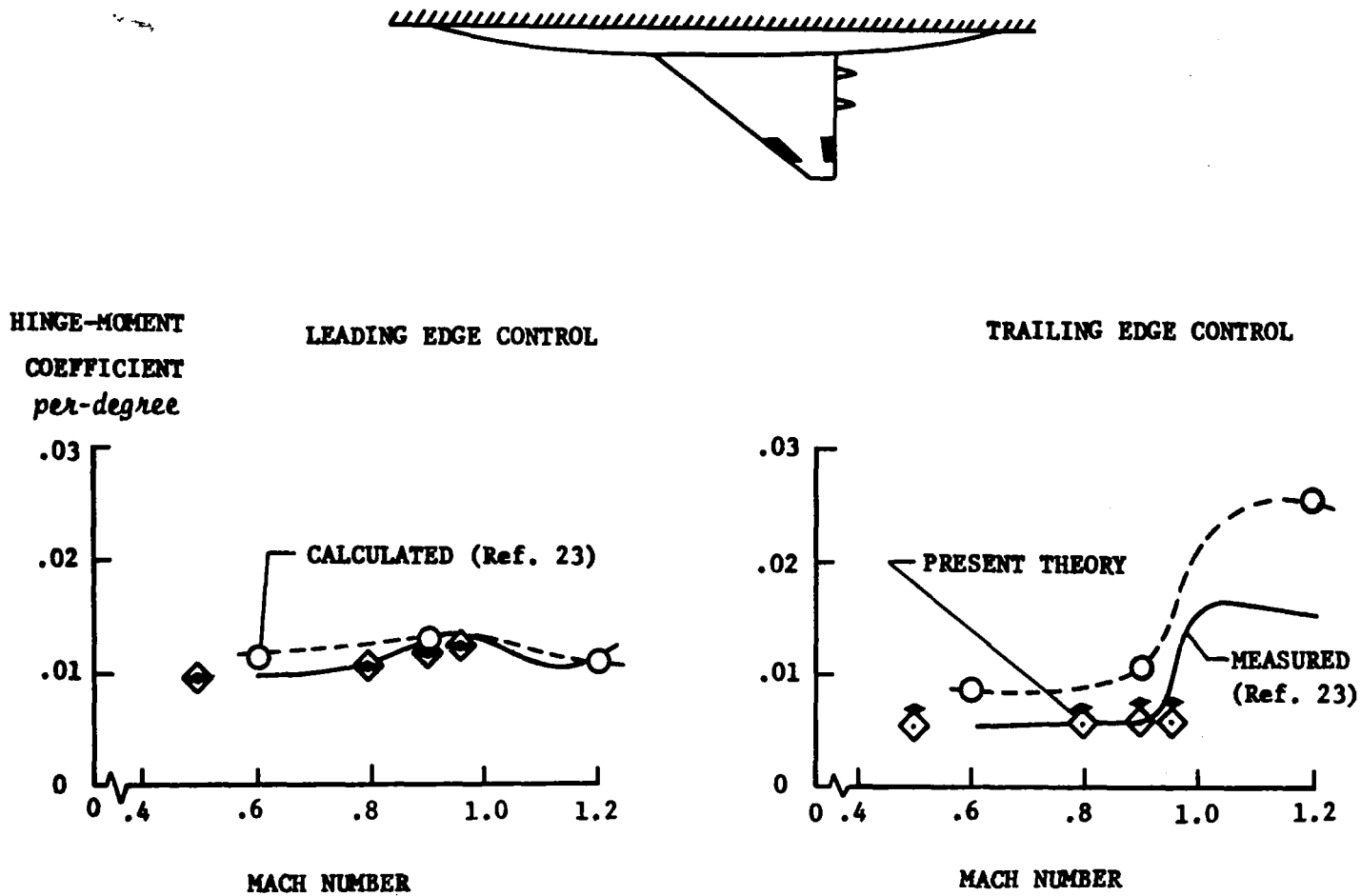

Figure 45. Comparison of Measured and Calculated Static Hinge Moment Coefficients

Two sets of analysis results obtained from the present procedure are superimposed on the test results of figure 45. The set of results denoted by the symbol ◆ represent the solutions obtained using standard flat plate boundary conditions. The set of results denoted by the symbol ◈ represent the solutions obtained using local linearization of boundary conditions to include effects of incremental velocities due to thickness distribution as described in Appendix C.

It appears that the application of local linearization of boundary conditions does affect the hinge-moments of the trailing edge control surface. However, there is only a slight change in hinge-moments of the leading edge control surface due to local linearization effects.

The analytical results appear to correlate well with the experimental data for the Mach range of interest. The comparison tends to deteriorate as the Mach number approaches 1.0 which may be due to shock effects that may be caused by the control surface deflection.

CONCLUSION

A theoretical analysis and computer program has been developed for the prediction of unsteady lifting surface loadings caused by motions of leading edge and trailing edge control surfaces having sealed gaps. The program has been developed around a systematic solution process where the discontinuities in the downwash distributions are separated (and handled separately) prior to applying standard lifting-surface solution techniques.

Theoretical results are presented to demonstrate the versatility of the program capabilities. Comparisons of theoretical and experimental data are presented for five wing-control surface configurations. Two of the experimental configurations had sealed gaps at the hingelines, and two configurations had small open gaps.

The comparisons indicate that reasonable pressure distributions are obtained for the sealed gap cases, but there are moderate differences near the hingelines for the open gap cases.

Pressure distributions and hinge moment coefficients obtained for all trailing edge control surface configurations appear to approximate the experimental values within close tolerances.

Hinge-moment coefficients obtained for the one leading edge control surface configuration does not appear to be sensitive to the use of local linearization of boundary conditions. Analysis results correlate well with experimental data for most of the Mach number range except for Mach numbers in the close vicinity of 1.0.

APPENDIX A

DEVELOPMENT OF PRESSURE EXPRESSIONS THAT SATISFY THE BOUNDARY CONDITIONS ON A TRAILING EDGE CONTROL SURFACE HAVING A SWEPT HINGELINE

Pressure expressions are formulated such that the boundary conditions are exactly satisfied and the residual downwashes that remain after subtracting the downwash discontinuities are smooth and continuous across the side edge of the control surface. The analytical procedure used to obtain the expressions is the asymptotic expansion process suggested by Landahl in reference 3 . Solutions of the boundary value problem obtained by application of Green's theorem provides the required change in boundary conditions across the hingeline and side edges such that subtraction of the discontinuous kinematic downwash distribution result in residual distributions that are smooth and continuous for which standard lifting surface solutions may be readily applied.

The analysis coordinate system is shown in figure 46 where the $\tilde{x},\tilde{y}$ coordinates are referenced to the inboard side edge of the hingeline.

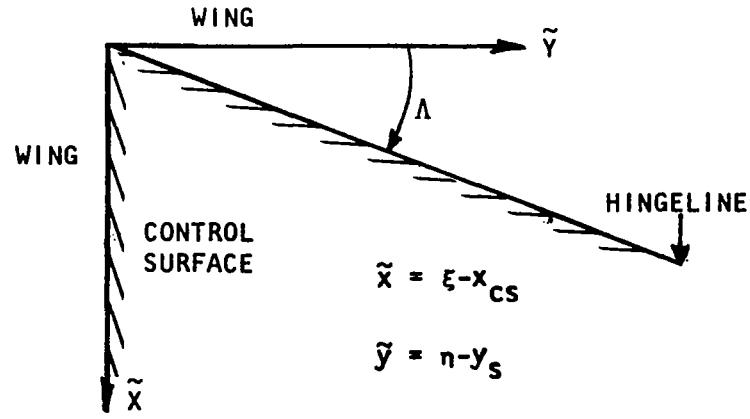

Figure 46 : Analysis Coordinate System

The Linearized boundary value problem is developed in terms of the pressure perturbation $C_p = \bar{P}\, e^{ikt}$ where the pressure magnitude satisfies the equation of flow

$$\beta^2 \bar{P}_{\tilde{x}\tilde{x}} + \bar{P}_{\tilde{y}\tilde{y}} + \bar{P}_{\tilde{z}\tilde{z}} - 2ikM^2 P_{\tilde{x}} + k^2 M^2 \bar{P} = 0 \qquad \text{(A1)}$$

and boundary conditions on the surface of

$$\bar{P}_z = \begin{cases} -2\Theta_H \left[\delta(\tilde{x}-x_c) + 2ik - k^2(\tilde{x}-x_c)\ U(\tilde{y})\right] & \text{for } \tilde{x} \geq x_c \\ 0 \quad - - - - - - - - - - - - - - - - - & \text{for } \tilde{x} < x_c \end{cases} \qquad \text{(A2)}$$

Scaling the $\tilde{x}$ coordinate to remove the β^2 factor we let

$$x_o = \frac{\tilde{x}}{\beta} \qquad y_o = \tilde{y} \qquad z_o = \tilde{z}$$

$$\frac{\partial}{\partial \tilde{x}} = \frac{1}{\beta}\frac{\partial}{\partial x_o}\ ; \quad \frac{\partial^2}{\partial \tilde{x}^2} = \frac{1}{\beta^2}\frac{\partial^2}{\partial x_o^2} \qquad \text{(A3)}$$

and the equation of flow becomes

$$\bar{P}_{x_o x_o} + \bar{P}_{y_o y_o} + \bar{P}_{z_o z_o} - 2\frac{ikM^2}{\beta}\bar{P}_{x_o} + k^2 M^2 \bar{P} = 0 \qquad \text{(A4)}$$

The terms of the boundary condition are modified by letting

$$\begin{aligned} x - x_c &= \tilde{x} - \tilde{y} \tan \Lambda \\ &= \beta(x_o - y_o \tan \Lambda/\beta) \\ &= \beta(x_o - y_o \tan \Lambda_1) \end{aligned}$$

and noting that

$$\delta(ax) = \frac{1}{a}\delta(x)$$

Thus the boundary conditions are given as

$$\bar{P}_{z_o} = \begin{cases} -2\Theta_H\left[\frac{1}{\beta}\delta(x_o - y_o\tan\Lambda_1) + 2ik - k^2\beta(x_o - y_o\tan\Lambda_1)\right] & x_o \geq x_{c_o} \\ 0 \quad - & \text{for } x_o < x_{c_o} \end{cases} \tag{A5}$$

The first derivative term of (A4) is now removed by defining a variable ψ defined as

$$\bar{P} = \exp\left(\frac{ikM^2x_o}{\beta}\right)\psi \tag{A6}$$

which will change the flow equation into the form

$$\psi_{x_ox_o} + \psi_{y_oy_o} + \psi_{z_oz_o} + \frac{k^2M^2\psi}{\beta^2} = 0 \tag{A7}$$

and provide a boundary condition definition of

$$\frac{\partial\psi}{\partial z_o} = \begin{cases} -2\Theta_H\left[\frac{1}{\beta}\delta(x_o - y_o\tan\Lambda_1) + 2ik - k^2\beta^2(x_o - y_o\tan\Lambda_1)\right] e^{-ikM^2x_o/\beta} & y_o \geq 0 \\ 0 \quad - & y_o < 0 \end{cases} \tag{A8}$$

To study the lifting surface problem in the vicinity of the corners all coordinates are scaled by ε

$$\bar{x} = \frac{x_o}{\varepsilon} \; ; \quad \bar{y} = \frac{y_o}{\varepsilon} \; ; \quad \bar{z} = \frac{z_o}{\varepsilon}$$

that modifies the differential equation into the form of

$$\psi_{\bar{x}\bar{x}} + \psi_{\bar{y}\bar{y}} + \psi_{\bar{z}\bar{z}} + \varepsilon^2\frac{k^2M^2}{\beta^2}\psi = 0 \tag{A9}$$

and provides a boundary condition definition of

$$\varepsilon\frac{\partial\psi}{\partial\bar{z}} = \begin{cases} -2\Theta_H\left[\frac{1}{\varepsilon\beta}\delta(\bar{x} - \bar{y}\tan\Lambda_1) + 2ik - k^2\varepsilon\beta(\bar{x} - \bar{y}\tan\Lambda_1)\right] e^{-ikM^2\varepsilon\bar{x}/\beta} & y \geq 0 \\ 0 \quad - & y < 0 \end{cases} \tag{A10}$$

We now seek solutions of the form

$$\psi = \psi_0 \, \varepsilon^0 + \psi_1 \, \varepsilon + \psi_2 \, \varepsilon^2 + \ldots . \tag{A11}$$

and expand the exponential in the boundary condition and set to zero the collected terms of equal powers in ε. We finally arrive at the following boundary value problems whose sum of solutions will satisfy the original boundary value problem.

$$\begin{cases} \nabla^2 \psi_0 = 0 \\ \dfrac{\partial \psi_0}{\partial \bar{z}} = \begin{cases} -2\Theta_H \left[\dfrac{1}{\beta} \, \delta \, (\bar{x} - \bar{y} \tan \Lambda_1) \right] & \bar{y} \geq 0 \\ 0 & \bar{y} < 0 \end{cases} \end{cases} \tag{A12}$$

$$\begin{cases} \nabla^2 \psi_1 = 0 \\ \dfrac{\partial \psi_1}{\partial \bar{z}} = \begin{cases} -2\Theta_H \left[2 \, ik - \dfrac{ik \, M^2 \bar{x}}{\beta^2} \, \delta \, (\bar{x} - \bar{y} \tan \Lambda_1) \right] & \bar{y} \geq 0 \\ 0 & \bar{y} < 0 \end{cases} \end{cases} \tag{A13}$$

$$\begin{cases} \nabla^2 \psi_2 = - \dfrac{k^2 M^2}{\beta^2} \psi_0 \\ \dfrac{\partial \psi_2}{\partial \bar{z}} = \begin{cases} -2\Theta_H \left[\dfrac{2 \, k^2 \, M^2 \, \bar{x}}{\beta} - k^2 \beta (\bar{x} - \bar{y} \tan \Lambda_1) - \dfrac{k^2 M^4 \bar{x}^2}{2 \, \beta^3} \delta (\bar{x} - \bar{y} \tan \Lambda_1) \right] & \bar{y} \geq 0 \\ 0 & \bar{y} < 0 \end{cases} \end{cases} \tag{A14}$$

Since the boundary value problems contain (or can be made to contain) a Laplace equation $\nabla^2 \psi = 0$ then use of Green's theorem may be readily applied to obtain solutions of the form

$$\psi(x,y,z) = -\frac{1}{2\pi}\int_{-\infty}^{\infty}\int_{-\infty}^{\infty}\left.\frac{\partial\psi(\bar{x},\bar{y},0)}{\partial\bar{z}}\right|_{\bar{z}=0}\frac{d\bar{x}d\bar{y}}{\left((x-\bar{x})^2+(y-\bar{y})^2+z^2\right)^{1/2}} \qquad \text{(A15)}$$

where

$$\left.\frac{\partial\psi(\bar{x},\bar{y},0)}{\partial\bar{x}}\right|_{\bar{z}=0}$$

represents the surface boundary conditions on the $\bar{z}=0$ plane and the Green's function (developed from the method of images)

$$v = \frac{1}{\left((x-\bar{x})^2+(y-\bar{y})^2+(z+\bar{z})^2\right)^{1/2}} + \frac{1}{\left((x-\bar{x})^2+(y-\bar{y})^2+(z-\bar{z})^2\right)^{1/2}}$$

v satisfies the conditions of

$$\frac{\partial v}{\partial\bar{z}} = 0 \qquad \text{on} \qquad \bar{z} = 0$$

$$\nabla^2 v = -4\pi\delta(x-\bar{x},y-\bar{y},z-\bar{z})$$

Integration of (A15) is accomplished in rectangular coordinate system that have coordinates defined within figure , and the coordinate subscripts and bars are removed with the understanding that these are scaled coordinates and that the solution will be finalized in physical coordinates at the end of this section.

Solution of the Zeroth Order Problem

The zeroth order boundary value problem is given as

$$\text{P.D.E.} \quad \nabla^2\psi_0 = 0$$

$$\text{B.C.} \quad \frac{\partial\psi_0(\tilde{x},\tilde{y},0)}{\partial z} = -\frac{2\Theta_H}{\beta}\,\delta(\tilde{x}-\tilde{y}\tan\Lambda_1)\,U(\tilde{y})$$

Substituting the boundary conditions into equation (A15) gives

$$\psi_0(x,y,z) = \frac{\Theta_H}{\pi\beta} \int_{-\infty}^{\infty}\int_{-\infty}^{\infty} \frac{\delta(x-y'\tan\Lambda_1)U(y')dx'dy'}{\left((x-x')^2+(x-y')^2+z^2\right)^{1/2}} \tag{A16}$$

Changing the lower integration limit of y' $\left(\text{due to } U(y')\right)$ and the x' integration produces the expression

$$\psi_0(x,y,z) = \frac{\Theta_H}{\pi\beta} \int_0^{\infty} \frac{dy'}{\left((x-y'\tan\Lambda_1)^2 + (y-y')^2 + z^2\right)^{1/2}} \tag{A17}$$

substituting $x=x-x_c+y\tan\Lambda_1$ in (A17) yields

$$\psi_0(x,y,z) = \frac{\Theta_H}{\pi\beta} \int_0^{\infty} \frac{dy'}{\left(\left((x-x_c) + (y-y')\tan\Lambda_1\right)^2 + (y-y')^2 + z^2\right)^{1/2}}$$

Expanding the terms in the radical provides

$$\psi_0(x,y,z) = \frac{\Theta_H}{\pi\beta} \int_0^{\infty} \frac{dy'}{\left((1+\tan^2\Lambda_1)(y'-y)^2-2(x-x_c)\tan\Lambda_1(y'-y)+(x-x_c)^2+z^2\right)^{1/2}}$$

that is integrated to yield the function

$$\psi_0(x,y,z) = + \frac{\Theta_H}{\pi\beta} \frac{1}{(a)^{1/2}} \ell n\left[(a)^{1/2}(a\eta^2 + 2b\eta + c)^{1/2} + a\eta + b\right]\Big|_{-y}^{\infty} + \psi_0(\text{Regular}) \tag{A18}$$

where

$$a = (1 + \tan^2 \Lambda_1)$$

$$b = -(x-x_c) \tan \Lambda_1$$

$$c = (x-x_c)^2 + z^2$$

The divergent upper limit is handled in the manner of Landhal and the expression is reduced to the form of

$$\psi_o(x,y,z) = \frac{-\Theta_H}{\pi\beta} \frac{1}{(a)^{\frac{1}{2}}} \ell n \left[(a)^{\frac{1}{2}} (x^2+y^2+z^2)^{\frac{1}{2}} - (y+x\tan\Lambda_1) \right] + \psi_o(\text{Regular}) \qquad \text{(A19)}$$

where x,y,z are scaled coordinates. A check may now be made on whether the boundary conditions are satisfied. The boundary conditions on the $z=0$ plane are evaluated as follows

$$\frac{\partial \psi_o}{\partial z} = \frac{-\Theta_H}{\pi\beta} \frac{1}{(a)^{\frac{1}{2}}} \left\{ \frac{(a)^{\frac{1}{2}} (x^2+y^2+z^2)^{\frac{1}{2}} + (y+x\tan\Lambda_1)}{a(x^2+y^2+z^2) - (y^2+2xy\tan\Lambda_1+x^2\tan^2\Lambda_1)} \right\} \frac{(a)^{\frac{1}{2}} z}{(x^2+y^2+z^2)^{\frac{1}{2}}}$$

reorganizing this expression by inserting $a=(1+\tan^2\Lambda_1)$ into the denominator of the bracketed term we obtain

$$\frac{\partial \psi_o}{\partial z} = \frac{-\Theta_H}{\pi\beta} \frac{1}{(a)^{\frac{1}{2}}} \left\{ (a)^{\frac{1}{2}} + \frac{(y+x\tan\Lambda_1)}{(x^2+y^2+z^2)^{\frac{1}{2}}} \right\} \frac{(a)^{\frac{1}{2}} z}{(x-y\tan\Lambda_1)^2+az^2}$$

and noting that $\lim_{x\to 0} \frac{u}{x^2+u^2} = \pi\delta(x)$ then

$$\left.\frac{\partial \psi_o}{\partial z}\right|_{z\to 0} = \frac{-\Theta_H}{\pi\beta} \frac{1}{(a)^{\frac{1}{2}}} \left[(a)^{\frac{1}{2}} + \frac{y(1+\tan^2\Lambda_1)}{|y| \left((1+\tan^2\Lambda_1)\right)^{\frac{1}{2}}} \right] \pi\delta(x-y\tan\Lambda_1)$$

$$\left.\frac{\partial \psi_0}{\partial \tilde{z}}\right|_{\tilde{z}\to 0} = -\frac{2\Theta_H}{\beta}\,\delta(\tilde{x}-\tilde{y}\tan\Lambda_1)\;U(\tilde{y}) \qquad \text{(A20)}$$

which is identical to the scaled boundary conditions of equation (12-A) and thus the function of equation (A19) is a valid solution of the zeroth order boundary value problem.

Scaled coordinates are used in equation (A19) and the expression may be returned to physical coordinates by replacing

x by $\frac{\tilde{x}}{\beta\varepsilon}$; y by $\frac{\tilde{y}}{\varepsilon}$; and z by $\frac{\tilde{z}}{\varepsilon}$

$\tan\Lambda_1 = \frac{\tan\Lambda}{\beta}$; $a^{1/2} = \frac{\bar{\beta}}{\beta}$; $\bar{\beta}^2 = \beta^2 + \tan^2\Lambda$

to provide the zeroth order pressure expression on $z=0$ of

$$\psi_0 = \frac{-\Theta_H}{\pi\bar{\beta}}\,\ell n\left[(\tilde{x}^2+\beta^2\tilde{y}^2)^{1/2} - \frac{(\beta^2\tilde{y}+\tilde{x}\tan\Lambda)}{\bar{\beta}}\right] + \psi_0(\text{Regular}) \qquad \text{(A21)}$$

Solution of First Order Problem

The first order boundary value problem in scaled coordinates is defined by

$$\left[\begin{array}{l} \nabla^2\psi_1 = 0 \\ \\ \dfrac{\partial \psi_1}{\partial z} = \begin{cases} -2\Theta_H\left[2ik - \dfrac{ikM^2\tilde{x}}{\beta^2}\,\delta(\tilde{x}-\tilde{y}\tan\Lambda_1)\right] & y \geq 0 \\ 0 \quad - - - - - - - - - - - - - - - - - - & y < 0 \end{cases} \end{array}\right. \qquad \text{(A22)}$$

and is divided into two separate problems corresponding to the two terms within the boundary condition statement. The first part of the first order problem is defined as

$$\nabla^2 \psi_{1_A} = 0$$

$$\left.\frac{\partial \psi_{1_A}}{\partial z}\right|_{z=0} = -2\Theta_H [2ik]\, U(\tilde{x}-\tilde{y}\tan\Lambda_1)\, U(\tilde{y})$$

Inserting the boundary conditions into equation (A15) and changing limits due to the unit functions provides the expression

$$\psi_{1_A}(\tilde{x},\tilde{y},\tilde{z}) = +\frac{2\Theta_H ik}{\pi} \int_0^{\infty} \int_{y'\tan\Lambda_1}^{\infty} \frac{dx'dy'}{\left((\tilde{x}-x')^2+(\tilde{y}-y')^2+\tilde{z}^2\right)^{1/2}} \qquad \text{(A23)}$$

A straight forward integration of this equation followed by a transformation of the coordinates into physical coordinates $\tilde{z}=0$ yields the solution

$$\varepsilon\psi_{1_A}(\tilde{x},\tilde{y},\tilde{z}) = -\frac{\Theta_H 2ik}{\pi}\left\{\tilde{y}\, \ell n\left[(\tilde{x}^2+\beta^2\tilde{y}^2)^{1/2} - \tilde{x}\right] + \frac{(\tilde{x}-\tilde{x}_c)}{\bar{\beta}}\, \ell n\left[(\tilde{x}^2+\beta^2\tilde{y}^2)^{1/2} - \left(\frac{\beta^2\tilde{y}+\tilde{x}\tan\Lambda_1}{\bar{\beta}}\right)\right]\right\} \qquad \text{(A24)}$$

The second part of the first order problem is given as

$$\left[\begin{array}{l} \nabla^2 \psi_{1_B} = 0 \\ \left.\dfrac{\partial \psi_{1_B}}{\partial z}\right|_{z\to 0} = \dfrac{2\Theta_H ikM^2}{\beta^2}\, \delta(\tilde{x}-\tilde{y}\tan\Lambda_1)\, U(\tilde{y}) \end{array}\right.$$

Again inserting the boundary condition into equation (A15) and performing the indicated integration yields the expression for the pressure term in physical coordinates on $z=0$ plane given as

$$\varepsilon\psi_{1_B} = \frac{\Theta_H ikM^2 \tan\Lambda}{\pi\beta^2\bar{\beta}^3} (\tilde{x}\tan\Lambda+\tilde{y}\beta^2) \ln\left[(\tilde{x}^2+\beta^2\tilde{y}^2)^{1/2} - \left(\frac{\beta^2\tilde{y}+\tilde{x}\tan\Lambda}{\bar{\beta}}\right)\right] \tag{A25}$$

The above solutions of the first order boundary value problem have been obtained using the same techniques of Landahl in the evaluation of the integral at the divergent upper limit.

Solution of the Second Order Problem

The definition of the second order boundary value problem given in scaled coordinates is

$$\begin{cases} \nabla^2\psi_2 = -\frac{k^2M^2}{\beta^2}\psi_o \\ \left.\frac{\partial\psi_2}{\partial z}\right|_{z=0} = 2\Theta_H \left\{ \frac{k^2M^4\tilde{x}^2}{2\beta^3}\delta(\tilde{x}-\tilde{y}\tan\Lambda_1) - 2\frac{k^2M^2\tilde{x}}{\beta}U(\tilde{x}-\tilde{y}\tan\Lambda_1) \right. \\ \qquad \left. + k^2\beta(\tilde{x}-\tilde{y}\tan\Lambda_1)\,U(\tilde{x}-\tilde{y}\tan\Lambda_1) \right\} U(\tilde{y}) \end{cases} \tag{A26}$$

The differential equation is a Poisson equation whose solution requires some added manipulations over the procedures used in obtaining the preceding boundary value problem solutions. The technique applied here to obtain solutions of the second order problem is one of redefining the boundary value problem into separate parts and obtaining individual solutions whose sum will satisfy the original boundary value problem.

We first seek solutions that satisfy the following boundary value problems

$$\begin{cases} \nabla^2\psi_2^{PL} = -\frac{k^2M^2}{\beta^2}\psi_o \\ \left.\frac{\partial\psi_2^{PL}}{\partial z}\right|_{z=0} = 0 \end{cases} \tag{A27}$$

$$\nabla^2 \psi_2^{\,A} = 0$$

$$\left.\frac{\partial \psi_2^{\,A}}{\partial \tilde{z}}\right|_{\tilde{z}=0} = \frac{\Theta_H k^2 M^4 \tilde{x}^2}{\beta^3}\, \delta(\tilde{x}-\tilde{y}\tan\Lambda_1)\, U(\tilde{y}) \qquad \text{(A28)}$$

$$\nabla^2 \psi_2^{\,B} = 0$$

$$\left.\frac{\partial \psi_2^{\,B}}{\partial \tilde{z}}\right|_{\tilde{z}=0} = -\,4\Theta_H\, \frac{k^2 M^2 \tilde{x}}{\beta}\, U(\tilde{x}-\tilde{y}\tan\Lambda_1)\, U(\tilde{y}) \qquad \text{(A29)}$$

$$\nabla^2 \psi_2^{\,C} = 0$$

$$\left.\frac{\partial \psi_2^{\,C}}{\partial \tilde{z}}\right|_{\tilde{z}=0} = 2\Theta_H\, k^2 \beta (\tilde{x}-\tilde{y}\tan\Lambda_1)\, U(\tilde{x}-\tilde{y}\tan\Lambda_1)\, U(\tilde{y}) \qquad \text{(A30)}$$

Solutions of the last three boundary value problems may be obtained in the same manner that was used to obtain the solution of the zeroth order boundary value problem. Insertion of the boundary conditions into equation (A15) and performing the straight forward integration will result in the desired solutions which will be summarized at the end of this development.

Solution of the Poisson equation and its associated boundary condition is obtained by seeking a solution of the form

$$\psi_2^{\,Pq} = \psi_2^{\,P} + \psi_2^{\,q}$$

such that $\psi_2^{\,P}$ is a solution of

$$\nabla^2 \psi_2^{\,P} = -\,\frac{k^2 M^2}{\beta^2}\, \psi_o$$

Once ψ_2^P is obtained then the boundary conditions developed by ψ_2^P are determined by evaluating the function $\lim_{\tilde{z}\to 0} \left(\partial\psi_2^P / \partial\tilde{z} \right)$.

Then a new boundary value problem is formulated such that ψ_2^q will satisfy

$$\begin{cases} \nabla^2\psi_2^q = 0 \\ \left.\dfrac{\partial\psi_2^q}{\partial\tilde{z}}\right|_{\tilde{z}\to 0} = -\lim\limits_{\tilde{z}\to 0} \dfrac{\partial\psi_2^P}{\partial\tilde{z}} \end{cases}$$

Thus the sum of ψ_2^P and ψ_2^q will then satisfy the differential equation

$$\nabla^2\psi_2^{Pq} = -\frac{k^2M^2}{\beta^2}\psi_o$$

having boundary conditions

$$\left.\frac{\partial\psi_2^{Pq}}{\partial\tilde{z}}\right|_{\tilde{z}\to 0} = 0$$

In order to simplify the expressions a coordinate transformation is made such that new coordinates are defined along and perpendicular to the hinge line as shown in figure 47 .

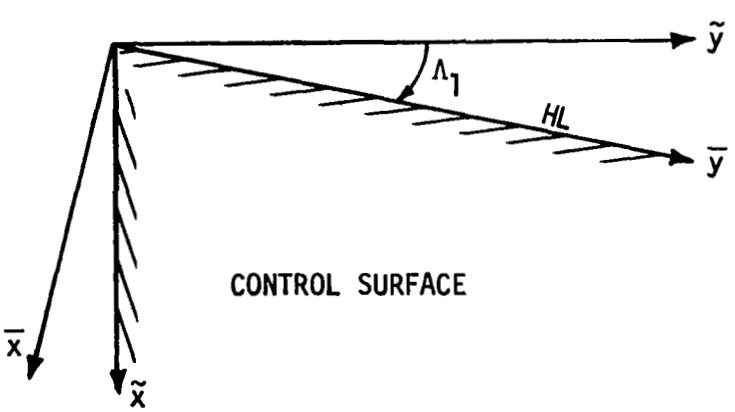

Figure 47 : Rigid Rotation Coordinate Transformation

$$\left[\begin{array}{l} \bar{x} = \tilde{x}\cos\Lambda_1 - \tilde{y}\sin\Lambda_1 \\ \bar{y} = \tilde{x}\sin\Lambda_1 + \tilde{y}\cos\Lambda_1 \\ \bar{z} = \tilde{z} \end{array}\right] \quad \text{or} \quad \left[\begin{array}{l} \tilde{x} = \bar{x}\cos\Lambda_1 + \bar{y}\sin\Lambda_1 \\ \tilde{y} = -\bar{x}\sin\Lambda_1 + \bar{y}\cos\Lambda_1 \\ \tilde{z} = \bar{z} \end{array}\right] \tag{A31}$$

Using the above relationships it can be shown that

$$\nabla^2(\tilde{x},\tilde{y},\tilde{z}) \equiv \nabla^2(\bar{x},\bar{y},\bar{z})$$

$$(\tilde{x}^2+\tilde{y}^2+\tilde{z}^2)^{1/2} \equiv (\bar{x}^2+\bar{y}^2+\bar{x}^2)^{1/2} \equiv R$$

and that the solution of the zeroth order problem may be expressed as

$$\psi_0(\bar{x},\bar{y},\bar{z}) = -\frac{\Theta_H\cos\Lambda_1}{\pi\beta}\,\ell n\,[R - \bar{y}] \tag{A32}$$

We now seek a solution of Poisson's equation by developing an expression having all the required characteristics that remain after performing the three coordinate second derivative operation. One such expression that may fulfill these requirements is

$$\psi_2^P = AR^2\,\ell n\,(R - \bar{y}) + BR^2 \tag{A33}$$

where A and B are to be determined such that

$$\nabla^2\psi_2^P = C\;\ell n\;(R - \bar{y})$$

where $C = \left(\frac{k^2M^2}{\beta^2}\right)\frac{\Theta_H\cos\Lambda_1}{\pi\beta}$

now

$$\nabla^2\psi_2^P = A\,\nabla^2\left(R^2\ell n(R - \bar{y})\right) + B\nabla^2R^2 \tag{A34}$$

and noting that for a general function (uv)

$$\nabla^2 uv = u\nabla^2 v + 2(\overline{\nabla} u) \cdot (\nabla u) + v \cdot \nabla^2 u$$

then

$$\nabla^2 \psi_2^P = A\left[R^2\nabla^2 \ell n(R-\bar{y}) + 2(\nabla R^2) \cdot \left(\nabla \ell n(R-\bar{y})\right) + \ell n(R-\bar{y})\nabla^2 R^2\right] + B\nabla^2 R^2$$

now $\nabla^2 \ell n(R-\bar{y})=0$ since this is a solution to the zeroth order problem, also $\nabla^2 R^2=6$ and $2(\nabla R^2)\cdot\left(\nabla \ell n(R-\bar{y})\right)= 4$. Therefore, the expression becomes

$$\nabla^2 \psi_2^P = A\left[4 + 6\ \ell n\ (R-\bar{y})\right] + 6B$$
$$= 6A\ \ell n\ (R-\bar{y}) + (4A+6B)$$

and constants must take on value of

$$A = \frac{C}{6}\ ; \quad B = -\frac{C}{9}$$

to satisfy the differential equation. Finally, the pressure expression that satisfies the Poisson equation is given as

$$\psi_2^P = \left(\frac{k^2M^2}{\beta^2}\right)\frac{\Theta_H \cos\Lambda_1}{\pi\beta}\left[\frac{R^2}{6}\ \ell n\ (R-\bar{y}) - \frac{R^2}{9}\right] \qquad \text{(A35)}$$

or

$$\psi_2^P = \frac{CR^2}{18}\left[3\ell n(R-\bar{y}) - 2\right] \qquad C = \left(\frac{k^2M^2}{\beta^2}\right)\frac{\Theta_H \cos\Lambda_1}{\pi\beta}$$

The boundary conditions generated by ψ_2^P are now determined by performing the differentiation of ψ_2^P with respect to z and evaluating the limiting functional value as $z \to 0$.

$$\frac{\partial \psi_2^P}{\partial z} = \frac{C}{18}\left\{2\bar{z}\left[3\ell n(R-\bar{y}) - 2\right] + 3R^2\left[\frac{1}{(R-\bar{y})}\ \frac{\bar{z}}{R}\right]\right\}$$

$$= \frac{C}{18}\left\{6\bar{z}\ell n(R-\bar{y}) - 4\bar{z} + \frac{3R\bar{z}}{(R-\bar{y})}\right\} \qquad \text{(A36)}$$

The limiting value of the first two terms as $z \to 0$ are identically equal to zero and we are left with the limiting value of the last term.

$$\lim_{\bar{z}\to 0} \frac{\partial \psi_2^P}{\partial \bar{z}} = \lim_{\bar{z}\to 0} \frac{C}{6}\left(\frac{\bar{z}\ R}{R-\bar{y}}\right) = \frac{C}{6}\lim_{\bar{z}\to 0} \frac{\bar{z}\ R}{(R-\bar{y})}\ \frac{(R+\bar{y})}{(R+\bar{y})} = \frac{C}{6}\lim_{\bar{z}\to 0}\left(\frac{\bar{z}}{\bar{x}^2+\bar{y}^2}\right)R(R+y)$$

$$= \frac{C}{6}\pi\delta(\bar{x})(\bar{x}^2+\bar{y}^2)^{1/2}\left[(\bar{x}^2+\bar{y}^2)^{1/2} + \bar{y}\right]$$

$$= \frac{C}{6}\pi\delta(\bar{x})|\bar{y}|\ [\ |\bar{y}| + \bar{y}\ ] = \begin{cases} 0 & \text{- - - - - - - -}\ \ \bar{y} < 0 \\ 2\delta(\bar{x})|\bar{y}|^2 & \text{- - - -}\ \ \bar{y} > 0 \end{cases}$$

$$\lim_{\bar{z}\to 0} \frac{\partial \psi_2^P}{\partial \bar{z}} = \frac{C}{3}\pi\delta(\bar{x})\bar{y}^2 U(\bar{y}) \qquad \text{(A37)}$$

In summary, the function

$$\psi_2^P = \frac{CR^2}{18}\left[3\ell n(R-\bar{y}) - 2\right]$$

is a solution of

$$\nabla^2\psi_2^P = C\ell n(R-\bar{y})$$

and produces the boundary condition given as

$$\lim_{z\to 0} \frac{\partial \psi_2^P}{\partial \bar{z}} = C\frac{\pi}{3}\delta(\bar{x})\bar{y}^2 U(\bar{y}) \qquad \text{where} \quad C = \left(\frac{k^2M^2}{\beta^2}\right)\frac{\Theta_H \cos\Lambda_1}{\pi\beta}$$

The next step is to find a function ψ_2^q such that it satisfies the boundary value problem

$$\begin{cases} \nabla^2\psi_2^q = 0 \\ \left.\dfrac{\partial\psi_2^q}{\partial z}\right|_{z=0} = -\dfrac{C\pi}{3}\delta(\bar{x})\bar{y}^2U(\bar{y}) \end{cases} \tag{A38}$$

Following the same procedure that was used to solve the zeroth order problem results in the expression for ψ_2^p given as

$$\psi_2^q = -\frac{C}{6}\left\{\frac{3}{2}\bar{y}R - \left[\frac{R^2}{2} - \frac{3}{2}\bar{y}^2\right]\ell n(R-\bar{y}) + \bar{y}^2\right\} \tag{A39}$$

Finally, the solution of the Poisson equation

$$\nabla^2\bar{\psi}_2 = -\frac{k^2M^2}{\beta^2}\psi_o$$

having zero boundary conditions

$$\left.\frac{\partial\bar{\psi}_2}{\partial\bar{z}}\right|_{\bar{z}=0} = 0$$

is given by the sum of solutions

$$\bar{\psi}_2 = \psi_2^p + \psi_2^q$$

$$\bar{\psi}_2 = \frac{C}{4}(R^2-\bar{y}^2)\ell n(R-\bar{y}) - \frac{C}{36}(4R^2 + 9\bar{y}R + 6\bar{y}^2) \tag{A40}$$

where

$$C = \left(\frac{k^2M^2}{\beta^2}\right)\frac{\Theta_H\cos\Lambda_1}{\pi\beta}$$

The expression for $\bar{\psi}_2$ is separated into singular and regular expressions that are functions of the scaled and transformed coordinates

$$\bar{\psi}_2 = \frac{C}{4}(R^2-\bar{y}^2)\ell n(R-\bar{y}) + \bar{\psi}_2(\text{Regular}) \tag{A41}$$

The expression given in physical coordinates is obtained by first rotating the coordinate system back into the scaled coordinate system (where 'o' subscripts are used to denote scaled coordinates) then transform from scaled coordinates to physical coordinates.

$$R \equiv (\bar{x}^2+\bar{y}^2+\bar{z}^2)^{1/2} = (x_o^2+y_o^2+z_o^2)^{1/2}$$

$$\bar{y} = x_o\sin\Lambda_1+y_o\cos\Lambda_1$$

The singular part given in scaled coordinates is

$$\bar{\psi}_2(x_o,y_o,z_o)=\frac{C}{4}\left([x_o^2+y_o^2+z_o^2]-[x_o\sin\Lambda_1+y_o\cos\Lambda_1]^2\right)\ell n\left[[x_o^2+y_o^2+z_o^2]^{1/2}-[x_o\sin\Lambda_1+y_o\cos\Lambda_1]\right] \tag{A42}$$

The expression in physical coordinates is finally developed by applying the scaling transformations

$$x_o = \frac{\tilde{x}}{\beta\varepsilon}\ ; \quad y_o = \frac{\tilde{y}}{\varepsilon}\ ; \quad z_o = \frac{\tilde{z}}{\varepsilon} \equiv 0\ ; \ \tan\Lambda_1 = \frac{\tan\Lambda}{\beta}$$

Thus, the singular part of the pressure expression obtained from the solution of the Poisson boundary value problem is given as

$$\varepsilon^2\bar{\psi}_2(\tilde{x},\tilde{y},0) = \frac{\Theta_H k^2M^2}{4\pi\beta^2\bar{\beta}^3}(\tilde{x}-\tilde{y}\tan\Lambda)^2\ell n\left[(\tilde{x}^2+\beta^2\tilde{y}^2)^{1/2} - \left(\frac{\beta^2\tilde{y}+\tilde{x}\tan\Lambda}{\bar{\beta}}\right)\right] \tag{A43}$$

The rest of the solutions required to satisfy the remaining second order boundary value problems defined by equations (A28) , (A29) , and (A30) may be obtained by inserting the boundary conditions into equation (A15) and performing the indicated integration. The solutions obtained and expressed in physical coordinates are summarized as follows:

$$\left[\begin{array}{l} \nabla^2\psi_2^{\,A} = 0 \\ \left.\dfrac{\partial\psi_2^{\,A}}{\partial z_o}\right|_{z_o=0} = \dfrac{\Theta_H k^2 M^4 x_o^{\,2}}{\beta^3}\,\delta(x_o - y_o\tan\Lambda_1)U(y_o) \end{array}\right. \qquad \begin{array}{l}\text{BOUNDARY VALUE PROBLEM}\\ \text{IN SCALED COORDINATES.}\end{array} \qquad \text{(A44)}$$

Solution given in physical coordinates is

$$\varepsilon^2\psi_2^{\,A} = -\frac{\Theta_H k^2 M^2 \tan^2\Lambda}{4\pi\beta^2\overline{\beta}^5}\left[(\tilde{x}-\tilde{y}\tan\Lambda)^2 - 2\left(\frac{\tilde{x}\tan\Lambda}{\beta}+\tilde{y}\beta\right)^2\right] \ell n[R_2-\tilde{y}_2] \qquad \text{(A45)}$$

where

$$R_2 = (\tilde{x}^2+\beta^2\tilde{y}^2)^{1/2}\ ;\quad y_2 = \frac{\beta^2+\tilde{x}\tan\Lambda}{\overline{\beta}}$$

$$\left[\begin{array}{l} \nabla^2\psi_2^{\,B} = 0 \\ \left.\dfrac{\partial\psi_2^{\,B}}{\partial z_o}\right|_{z_o=0} = -\,4\Theta_H\dfrac{k^2M^2}{\beta}\,x_o U(x_o - y_o\tan\Lambda_1)U(y_o) \end{array}\right. \qquad \begin{array}{l}\text{BOUNDARY VALUE PROBLEM}\\ \text{IN SCALED COORDINATES.}\end{array} \qquad \text{(A46)}$$

Solution in physical coordinates is

$$\varepsilon^2\psi_2^{\,B} = \frac{2\Theta_H k^2M^2}{\pi\beta^2}\left[\frac{\beta^2}{2\overline{\beta}^3}(\tilde{x}-\tilde{y}\tan\Lambda)^2 - \frac{1}{\beta}(\tilde{x}^2-\tilde{x}\tilde{y}\tan\Lambda)\right]\ell n[R_2-y_2]$$

$$-\frac{2\Theta_H k^2M^2}{\pi\beta^2}\,\tilde{x}\tilde{y}\,\ell n[R_2-\tilde{x}] \qquad \text{(A47)}$$

$$\nabla^2\psi_2^C = 0$$

BOUNDARY VALUE PROBLEM
IN SCALED COORDINATES.

$$\left.\frac{\partial\psi_2^C}{\partial z_o}\right|_{z_o=0} = 2\Theta_H k^2\beta(x_o - y_o\tan\Lambda_1)U(x_o - y_o\tan\Lambda_1)U(y_o) \qquad \text{(A48)}$$

Solution in physical coordinates

$$\varepsilon^2\psi_2^C = \frac{\Theta_H k^2}{2\pi\bar{\beta}}(\tilde{x}-\tilde{y}\tan\Lambda)^2 \ell n[R_2 - y_2] - \frac{\Theta_H k^2}{\pi}\left(\frac{\tilde{y}^2\tan\Lambda}{2} - \tilde{x}\tilde{y}\right)\ell n[R_2 - \tilde{x}]$$

The pressure coefficient that satisfies the boundary value problem of equations (A1), (A2) may now be expressed as a sum of the individual solutions

$$\bar{P}(\tilde{x},\tilde{y},o) = (\psi_o + \varepsilon\psi_1 + \varepsilon^2\psi_2)\, e^{\left(\frac{ikM^2\tilde{x}}{\beta^2}\right)} \qquad \text{(A49)}$$

$$\bar{P}(\tilde{x},\tilde{y},o) = C1 \cdot \ell n\left[(\tilde{x}^2+\beta^2\tilde{y}^2)^{1/2} - \left(\frac{\beta^2\tilde{y}+\tilde{x}\tan\Lambda}{\bar{\beta}}\right)\right] + C2\ y\ \ell n\left[(\tilde{x}^2+\beta^2\tilde{y}^2)^{1/2} - \tilde{x}\right] \qquad \text{(A50)}$$

where

$$C1 = -\frac{\Theta_H}{\pi\bar{\beta}}\left\{1+2ik(\tilde{x}-\tilde{y}\tan\Lambda) - \frac{ikM^2\tan\Lambda}{\beta^2\,\bar{\beta}^2}(\tilde{x}\tan\Lambda+\tilde{y}\beta^2) - \frac{k^2M^2}{4\beta^2\bar{\beta}^2}(\tilde{x}-\tilde{y}\tan\Lambda)^2\right.$$
$$+ \frac{k^2M^4\tan^2\Lambda}{4\,\beta^2\,\bar{\beta}^4}\left[(\tilde{x}-\tilde{y}\tan\Lambda)^2 - 2\left(\frac{\tilde{x}\tan\Lambda}{\beta}+\beta\tilde{y}\right)^2\right]$$
$$\left. - \frac{2k^2M^2}{\beta^2}\left[\frac{\beta^2}{2\bar{\beta}^2}(\tilde{x}-\tilde{y}\tan\Lambda)^2 - (\tilde{x}^2-\tilde{x}\tilde{y}\tan\Lambda)\right] - \frac{k^2}{2}(\tilde{x}-\tilde{y}\tan\Lambda)^2\right\} e^{\left(\frac{ikM^2\tilde{x}}{\beta^2}\right)}$$

$$C2 = -\frac{\Theta_H}{\pi}\left\{2ik + \left(\frac{2k^2M^2}{\beta^2} - k^2\right)x + \frac{k^2\tan\Lambda}{2}\tilde{y}\right\} e^{\left(\frac{ikM^2\tilde{x}}{\beta^2}\right)}$$

The expression for $\bar{P}(x,y,o)$ may be simplified by expanding the exponential, carrying out the indicated multiplication and collecting terms that are linear in x and y. The resulting expression then becomes

$$\bar{P}(\tilde{x},\tilde{y},o) = -\frac{\Theta_H}{\pi\bar{\beta}}\left[1 + 2ik(\xi-\xi_c) + \frac{ikM^2}{\bar{\beta}^2}(\xi-\xi_c)\right] \ell n\left[(\tilde{x}^2+\beta^2\tilde{y}^2)^{\frac{1}{2}} - \frac{\beta^2\tilde{y}+\tan\Lambda}{\bar{\beta}}\right]$$

$$-\frac{\Theta_H}{\pi}\left[2ik - k^2(\xi-\xi_c)\right]\tilde{y}\ \ell n\left[(\tilde{x}^2+\beta^2\tilde{y}^2)^{\frac{1}{2}} - \tilde{x}\right] \qquad \text{(A51)}$$

The limiting value of this expression for $\Lambda=0$ is equivalent to the expression developed by Landahl (reference 3) for the rectangular non-swept control surface. The above expression for $\Lambda=0$ is

$$\bar{P}(\tilde{x},\tilde{y},o) = -\frac{\Theta_H}{\pi\beta}\left[1 + 2ik(\xi-\xi_c) + \frac{ikM^2(\xi-\xi_c)}{\beta^2}\right] \ell n\left[\left((\xi-\xi_c)^2+\beta^2\tilde{y}^2\right)^{\frac{1}{2}} - \beta\tilde{y}\right]$$

$$-\frac{\Theta_H}{\pi}\left[2ik-k^2(\xi-\xi_c)\right]\tilde{y}\ \ell n\left[\left((\xi-\xi_c)^2+\beta^2\tilde{y}^2\right)^{\frac{1}{2}} - (\xi-\xi_c)\right] \qquad \text{(A52)}$$

Thus, the expression for $\bar{P}(x,y,o)$ appears to have the necessary characteristics to provide a proper solution of the swept hingeline boundary value problem and compares favorably with the widely accepted expression of Landahl for the zero sweep case.

APPENDIX B

DEVELOPMENT OF PRESSURE DISTRIBUTIONS TO SATISFY THE BOUNDARY CONDITIONS FOR A SWEPT LEADING EDGE CONTROL SURFACE

Pressure distributions are formulated using the asymptotic expansion process suggested by Landahl (reference 3). The analysis coordinate system shown in figure 48 represents a segment of a swept wing leading edge having a control surface that oscillates about a hingeline aft of the leading edge.

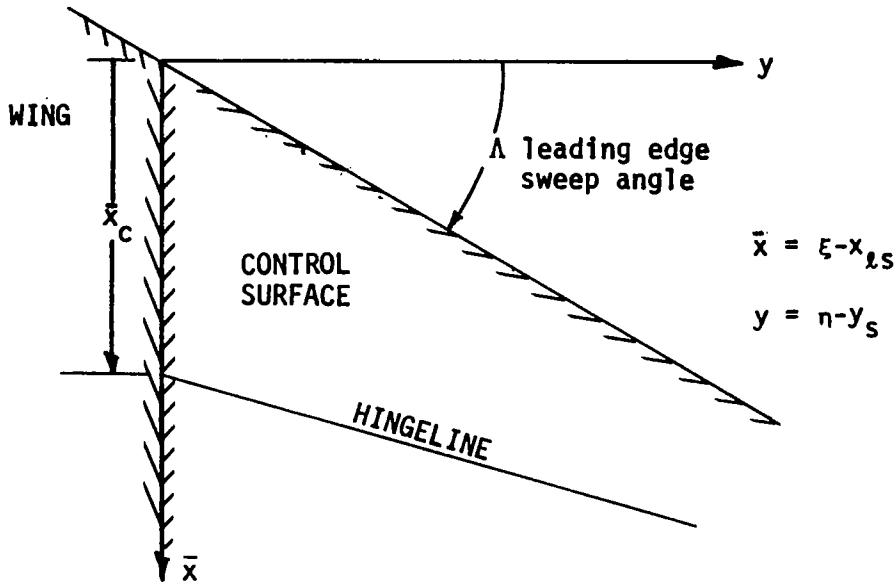

Figure 48: Analysis Coordinate System

Solutions of the mixed boundary value problem are obtained using the linearized partial differential equation of flow given as

$$\beta^2\phi_{\bar{x}\bar{x}} + \phi_{yy} + \phi_{zz} - 2ikM^2\phi_{\bar{x}} + k^2M^2\phi = 0 \qquad (B1)$$

The motion of the control surface is assumed to be sinusoidal and is defined in non-dimensional coordinates as

$$Z_c = \Theta_H(\bar{x} - \bar{x}_c)\, e^{ikt}$$

The boundary conditions resulting from the control surface motion are

$$\begin{cases} \dfrac{\partial \phi}{\partial z} = \dfrac{\partial z_c}{\partial \bar{x}} + ikz_c & \text{for} \quad y<0 \ \text{ on } \ z=0 \\ & \qquad \bar{x}>y \tan \Lambda \\ \dfrac{\partial \phi}{\partial z} = 0 & \text{for} \quad y<0 \ \text{ on } \ z=0 \\ & \qquad \bar{x}>y \tan \Lambda \\ \phi = 0 & \qquad \bar{x}<y \tan \Lambda \\ & \qquad \text{(ahead of leading edge)} \end{cases} \tag{B2}$$

The first two expressions may be combined into a single expression for the change in boundary condition across the control surface side edge

$$\begin{cases} \phi_z = (z_{c_{\bar{x}}} + ikz_c)\, U(y) \\ \phi_z = \Theta_H \left[(1-ik\bar{x}_c) + ik\bar{x}\right] u(y) \end{cases} \tag{B3}$$

where $U(y) = \begin{cases} 1 & y>0 \\ 0 & y<0 \end{cases}$

A transformation or scaling of coordinates is made to simplify the differential equation by defining

$$x_o = \bar{x}/\beta; \quad y_o = y; \quad z_o = z$$

that results in the flow equation

$$\phi_{x_o x_o} + \phi_{y_o y_o} + \phi_{z_o z_o} - \frac{2ikM^2}{\beta} \phi_{x_o} + k^2 M^2 \phi = 0 \tag{B4}$$

In the new coordinate system the equation for the leading edge becomes

$$x_o \beta = y_o \tan \Lambda$$

$$\text{or} \quad x_o = y_o \frac{\tan \Lambda}{\beta}$$

Defining a new angle, Λ_1, such that $\tan\Lambda_1=\frac{\tan\Lambda}{\beta}$ then the leading edge equation becomes $x_o=y_o\tan\Lambda_1$ and the boundary conditions in the new coordinate system are

$$\begin{cases} \phi = 0 & \text{for} \quad x_o<y_o\tan\Lambda_1 \quad \text{on} \quad z=0 \\ \frac{\partial\phi}{\partial z} = (\lambda+vx_o)U(y_o) & \text{for} \quad x_o>y_o\tan\Lambda_1 \quad \text{on} \quad z=0 \end{cases} \tag{B5}$$

where $\lambda = \Theta_H(1-ik\bar{x}_c)$

$v = \Theta_H\, ik\beta$

The first derivative term in equation (B4) is then removed by defining a new variable, ψ, defined as

$$\phi(x_o,y_o,z_o) = e^{ikM^2x_o/\beta}\,\psi(x_o,y_o,z_o) \tag{B6}$$

Insertion of equation (B6) into (B4) results in the transformed differential equation

$$\psi_{x_ox_o} + \psi_{y_oy_o} + \psi_{z_oz_o} + \left(\frac{kM}{\beta}\right)^2 \psi = 0 \tag{B7}$$

The transformed boundary conditions are then defined as

$$\begin{cases} \psi = 0 & x_o<y_o\tan\Lambda_1 \quad \text{on} \quad z=0 \\ \frac{\partial\psi}{\partial z_o} = (\lambda+vx_o)e^{-ikM^2x_o/\beta}\,U(y_o) & \text{for} \quad x_o>y_o\tan\Lambda_1 \end{cases} \tag{B8}$$

In order to study the problem in the vicinity of the leading edge corner all coordinates are stretched such that

$$(x_o,y_o,z_o)_{old} \rightarrow (\varepsilon x_o,\varepsilon y_o,\varepsilon z_o)_{new}$$

In terms of the stretched coordinates the boundary conditions become

$$\begin{cases} \psi = 0 & x_0 < y_0 \tan\Lambda_1 \quad \text{on} \quad z_0 = 0 \\ \dfrac{\partial \psi}{\partial z_0} = \varepsilon(\lambda + v\varepsilon x_0) e^{-ikM^2 \varepsilon x_0/\beta} U(y_0) & x_0 > y_0 \tan\Lambda_1 \quad \text{on} \quad z_0 = 0 \end{cases} \tag{B9}$$

Expanding the exponential and collecting terms of ε^n the second boundary condition is then defined as

$$\frac{\partial \psi}{\partial z_0} = \varepsilon\lambda U(y_0) + \varepsilon^2 (v - \frac{ikM^2\lambda}{\beta}) x_0 U(y_0) + O(\varepsilon^3) \tag{B10}$$

The variable ψ is also expanded in a series given as

$$\psi = \psi_0 + \psi_1 \varepsilon + \psi_2 \varepsilon^2 + \cdots \tag{B11}$$

and inserted in the differential equation and boundary conditions terms of like powers in ε are collected and define boundary value problems for which solutions are to be obtained whose sum will satisfy the flow conditions at the leading edge corner.

$$\begin{cases} \nabla^2 \psi_0 = 0 & \text{(zeroth order problem)} \\ \psi_0 = 0 & \text{on} \quad z_0 = 0 \quad x_0 < y_0 \tan\Lambda_1 \\ \dfrac{\partial \psi_0}{\partial z_0} = 0 & \text{on} \quad z_0 = 0 \quad x_0 > y_0 \tan\Lambda_1 \end{cases} \tag{B12}$$

$$\begin{cases} \nabla^2 \psi_1 = 0 & \text{(first order problem)} \\ \psi_1 = 0 & \text{on} \quad z_0 = 0 \quad x_0 < y_0 \tan\Lambda_1 \\ \dfrac{\partial \psi_1}{\partial z_0} = \lambda U(y_0) & \text{on} \quad z_0 = 0 \quad x_0 > y_0 \tan\Lambda_1 \end{cases} \tag{B13}$$

$$
\begin{cases}
\nabla^2\psi_2 = -\left(\dfrac{k^2M^2}{\beta^2}\right)\psi_o & \text{(second order problem)} \\
\psi_2 = 0 & \text{on } z=0;\ x_o<y_o\tan\Lambda_1 \\
\dfrac{\partial\psi_2}{\partial z_o} = \left(v - \dfrac{ikM^2\lambda}{\beta}\right) x_o U(y_o) & \text{on } z=0;\ x_o>y_o\tan\Lambda_1
\end{cases}
\tag{B14}
$$

Solution of the zeroth order boundary value problem results in an expression that is given by

$$
\psi_o = C\left[\left(\frac{1}{(\bar{x}-y\tan\Lambda)^{1/2}}\right) + \frac{ik}{\beta^2}(\bar{x}-y\tan\Lambda)^{1/2}\right] \tag{B15}
$$

where the coefficient, C, can only be determined by a global integration over the planform. Since the function contains a square root and inverse square root term that are available in the main lifting surface solution then this zeroth order solution will be ignored.

Solution of the First Order Boundary Value Problem

A rigid rotation of coordinates is made such that the coordinates are parallel and perpendicular to the leading edge as shown in figure 49 .

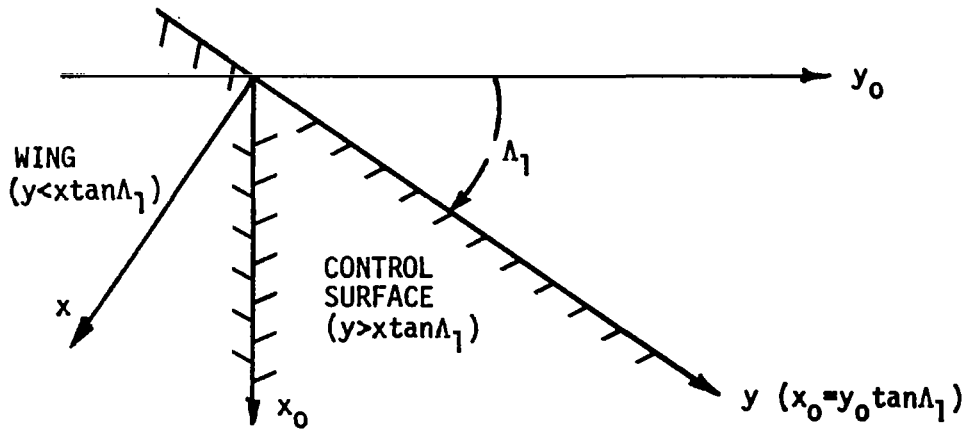

Figure 49: Rotated Coordinate System

The new coordinates are defined by

$$\begin{aligned} x &= x_o \cos \Lambda_1 - y_o \sin \Lambda_1 \\ y &= x_o \sin \Lambda_1 + y_o \cos \Lambda_1 \\ z &= z_o \end{aligned} \tag{B16}$$

and the old coordinates given in terms of the new coordinates are

$$\begin{aligned} x_o &= x \cos \Lambda_1 + y \sin \Lambda_1 \\ y_o &= - x \sin \Lambda_1 + y \cos \Lambda_1 \\ z_o &= z \end{aligned} \tag{B17}$$

The above transformation is a rigid rotation without stretching so that the orthogonality of the axes and scales are preserved. Thus the transformed first order boundary value problem is given as

$$\begin{cases} \psi_{1_{xx}} + \psi_{1_{yy}} + \psi_{1_{zz}} = 0 \\ \psi_1 = 0; \quad x<0 \quad \text{on} \quad z=0 \\ \dfrac{\partial \psi_1}{\partial z} = \lambda U(y - x\tan\lambda_1); \quad x>0 \quad \text{on} \quad z=0 \end{cases} \tag{B18}$$

A Fourier transform in the y direction is applied to reduce the problem to a two dimensional problem with a parameter. The transformed differential equation becomes

$$\bar{\psi}_{1_{xx}} + \bar{\psi}_{1_{zz}} - s^2 \bar{\psi}_1 = 0 \tag{B19}$$

Transformation of the off wing boundary condition yields

$$\bar{\psi}_1 = 0 \qquad x<0 \quad \text{on} \quad z=0$$

The second boundary condition is transformed by

$$\bar{\psi}_{1_z} = \frac{\lambda}{(2\pi)^{\frac{1}{2}}} \int_{-\infty}^{\infty} e^{-isy}\, U(y-x\tan\Lambda_1)\,dy$$

$$\bar{\psi}_{1_z} = \frac{\lambda}{(2\pi)^{\frac{1}{2}}} \int_{x\tan\Lambda_1}^{\infty} e^{-isy}\,dy = \frac{-\lambda}{is(2\pi)^{\frac{1}{2}}} \Bigg|_{x\tan_1}^{\infty} \quad \text{on} \quad z=0$$

The convergence at the upper limit is circumvented by considering s to be complex having $\mathrm{Imag}(s)<0$. Then the boundary condition is

$$\bar{\psi}_{1_z} = \frac{\lambda}{is(2\pi)^{\frac{1}{2}}}\, e^{-isx\tan\Lambda_1} \; ; \quad x>0 \quad \text{on} \quad z=0 \tag{B20}$$

Following Landahl in the construction of a solution of equation a trial solution is assumed to be of the form

$$\bar{\psi}_1 = A\int_{-\infty}^{x} e^{-|s|r_1 - is(x-x')\tan\Lambda_1} \cos\frac{\Theta_1}{2} \cdot \frac{1}{(r_1)^{\frac{1}{2}}}\,dx' \tag{B21}$$

where $\Theta_1 = \tan^{-1}\left(\frac{z}{x'}\right)$ and $r_1^2 = x'^2 + z^2$

The quantity A is determined by having $\bar{\psi}_1$ satisfy the boundary condition on the lifting surface (equation (B20)). Thus, the above expression is differentiated with respect to z by using the expression for the derivative in polar form

$$\frac{\partial}{\partial z} = \frac{\cos\Theta_1}{r_1}\,\frac{\partial}{\partial\Theta} + \sin\Theta_1\,\frac{\partial}{\partial r_1}$$

$$\frac{\partial \bar{\psi}_1}{\partial z} = -\frac{A}{2}\int_{-\infty}^{x} \frac{e^{-|s|r_1 - is(x-x')\tan\Lambda_1}}{r_1^{3/2}} \cdot \left\{\cos\theta_1 \sin\frac{\theta_1}{2} + \cos\frac{\theta_1}{2}\sin\theta_1\right\} dx'$$

$$- A|s|\int_{-\infty}^{x} \frac{e^{-|s|r_1 - is(x-x')\tan\Lambda_1}}{r^{1/2}} \sin\theta_1 \cos\frac{\theta_1}{2}\, dx' \qquad \text{(B22)}$$

The second integral vanishes for $z \to 0$ since $\theta_1 = 0$ or π. The derivative becomes

$$\left.\frac{\partial \bar{\psi}_1}{\partial z}\right|_{z=0} = -\frac{A}{2} e^{-isx\tan\Lambda_1} \lim_{z\to 0}\left\{\int_{-\infty}^{x} \frac{e^{-|s|r_1 + isx'\tan\Lambda}}{r_1^{3/2}} \sin\frac{3\theta_1}{2}\, dx'\right\} \qquad \text{(B23)}$$

The apparent singularity is removed by adding and subtracting $\dfrac{\sin\frac{3}{2}\theta_1}{r_1^{3/2}}$ within the expression to obtain

$$\lim_{z\to 0}\frac{\partial \psi_1}{\partial z} = -\frac{A}{2}\lim_{z\to 0}\left\{\int_{-\infty}^{x}\left[e^{-|s|r_1 + isx'\tan\Lambda_1} - 1.\right]\frac{\sin\frac{3}{2}\theta_1}{r_1^{3/2}}\, dx\right\} e^{-isx\tan\Lambda_1}$$

$$- \frac{A}{2}\lim_{z\to 0}\left\{\int_{-\infty}^{x} \frac{\sin\frac{3}{2}\theta_1}{r_1^{3/2}}\, dx'\right\} e^{-isx\tan\Lambda_1} \qquad \text{(B24)}$$

Landahl has demonstrated that the second integral vanishes for $z \to 0$. Since $\theta_1 \to 0$ for $x > 0$ and $\theta_1 \to \pi$ for $x < 0$, then the limit as $z \to 0$ of the right hand side becomes

$$\left.\frac{\partial\bar{\psi}_1}{\partial z}\right|_{z=0} = + \frac{A}{2} e^{-isx\tan\Lambda_1} \int_{-\infty}^{0} \frac{\left[e^{-|s||x'|+isx'\tan\Lambda_1} - 1\right]}{|x'|^{3/2}} dx'$$

$$\equiv + \frac{A}{2} e^{-isx\tan\Lambda_1} \int_{0}^{\infty} \frac{\left[e^{-x'[|s|+is\tan\Lambda_1]} - 1\right]}{x'^{3/2}} dx' \qquad \text{(B25)}$$

Integrating this expression by parts yields

$$\left.\frac{\partial\bar{\psi}_1}{\partial z}\right|_{z=0} = + \frac{A}{2} e^{-isx\tan\Lambda_1} \left\{ - 2\left[e^{-x[|s|+is\tan\Lambda_1]} - 1\right] \cdot (x')^{-\frac{1}{2}} \right|_0^{\infty}$$

$$- 2\,[|s|+is\tan\Lambda_1] \int_0^{\infty} \frac{e^{-x\,[|s|+is\tan\Lambda_1]}}{x'^{\frac{1}{2}}} dx' \Bigg\} \qquad \text{(B26)}$$

Since $$\int_0^{\infty} \frac{e^{-ax'}\,dx'}{x'^{\frac{1}{2}}} = 2 \int_0^{\infty} e^{-at^2}\,dt = \left(\frac{\pi}{a}\right)^{\frac{1}{2}}$$

then the expression for the derivative is

$$\left.\frac{\partial\bar{\psi}_1}{\partial z}\right|_{z=0} = - A\,(\pi[|s|+is\tan\Lambda_1])^{\frac{1}{2}}\, e^{-isx\tan\Lambda_1} \qquad \text{(B27)}$$

This expression for the derivative must be equal to the boundary condition equation (B20) that results in evaluating A as

$$A = - \frac{\lambda}{is\pi(2[|s|+is\tan\Lambda_1])^{\frac{1}{2}}} \qquad \text{(B28)}$$

Finally $\bar{\psi}_1$ becomes

$$\bar{\psi}_1 = -\frac{\lambda\, e^{-isx\tan\Lambda_1}}{i\pi s(2[|s|+is\tan\Lambda_1])^{1/2}} \int_{-\infty}^{x} \frac{e^{-|s|r_1+isx'\tan\Lambda_1}}{r_1^{1/2}} \cos\left(\frac{\theta_1}{2}\right) dx' \qquad \text{(B29)}$$

Taking the inverse transform of equation (B29) and interchanging the order of integration yields

$$\psi_1 = -\frac{\lambda}{2\pi^{3/2}} \int_{-\infty}^{x} \frac{\cos\left(\frac{\theta_1}{2}\right)}{r^{1/2}} \left[\int_{-\infty-i\gamma}^{\infty-i\gamma} \frac{e^{is[y+(x'-x)\tan\Lambda_1]-|s|r_1}}{is[|s|+is\tan\Lambda_1]^{1/2}} ds \right] dx' \qquad \text{(B30)}$$

Now, with $\rho = y + (x' - x)\tan\Lambda_1$, the inner integral becomes

$$F(\rho) = \int_{-\infty-i\gamma}^{\infty-i\gamma} \frac{e^{is\rho-|s|r_1}}{is[|s|+is\tan\Lambda_1]^{1/2}} ds \qquad \text{(B31)}$$

The integrand contains a non-integrable singularity, however, this integral may be evaluated if the singularity is softened by first taking a derivative with respect to ρ

$$F'(\rho) = \int_{-\infty-i\gamma}^{\infty-i\gamma} \frac{e^{is\rho-|s|r_1}}{\sqrt{|s|+is\tan\Lambda_1}} ds \qquad \text{(B32)}$$

Then $F'(\rho)$ may be evaluated for the limiting case of $\lim_{\gamma\to 0} F'(\rho)$ and obtain

$$F'(\rho) = \int_{-\infty}^{\infty} \frac{e^{is\,-|s|r_1}}{\sqrt{|s|+is\tan\Lambda_1}} ds \qquad \text{(B33)}$$

where the path of path of integration is along the s(Real) axis.

$$F'(\rho) = \int_0^\infty \frac{e^{is\rho-|s|r_1}}{\sqrt{s+is\tan\Lambda_1}}\,ds + \int_{-\infty}^0 \frac{e^{is\rho-|s|r_1}}{\sqrt{s+is\tan\Lambda_1}}\,ds \qquad \text{(B34)}$$

or

$$F'(\rho) = \int_0^\infty \frac{e^{is\rho-sr_1}}{\sqrt{s+is\tan\Lambda_1}}\,ds + \int_0^\infty \frac{e^{-is\rho-sr_1}}{\sqrt{s-is\tan\Lambda_1}}\,ds$$

$$= \int_0^\infty \frac{e^{-sr_1}}{\sqrt{s}}\left[\frac{e^{is\rho}}{\sqrt{1+i\tan\Lambda_1}} + \frac{e^{-is\rho}}{\sqrt{1-i\tan\Lambda_1}}\right] ds$$

Observing that $1+i\tan\Lambda_1 = \sqrt{1+\tan^2\Lambda_1}\; e^{i\Lambda_1} = \sec\Lambda_1 e^{i\Lambda_1}$ then upon combining the expressions we obtain

$$F'(\rho) = 2\sqrt{\cos\Lambda_1}\;\; R_e\left\{\int_0^\infty \frac{e^{-sr_1}}{\sqrt{s}}\; e^{i(s\rho-\Lambda_1/2)}\, ds\right\} \qquad \text{(B35)}$$

$$F'(\rho) = 2\sqrt{\cos\Lambda_1}\;\; R_e\left\{e^{-i\Lambda_1/2}\int_0^\infty \frac{e^{-s(r_1-i\rho)}}{\sqrt{s}}\, ds\right\}$$

$$= 2\sqrt{\cos\Lambda_1}\;\; R_e\left\{e^{-i\Lambda_1/2}\sqrt{\frac{\pi}{r_1-i\rho}}\right\}$$

$$\left(\text{Since } \int_0^\infty \frac{e^{-as}}{\sqrt{s}}\, ds = \sqrt{\frac{\pi}{a}}\right)$$

$$F'(\rho) = 2\sqrt{\pi}\;\; \sqrt{\cos\Lambda_1}\;\;\; R_e\left\{\frac{e^{-i\Lambda_1/2}}{\sqrt{r_1-i\rho}}\right\} \qquad \text{(B36)}$$

Now $F(\rho)$ may be obtained by an integration of $F'(\rho)$ as follows:

$$F(\rho) = 2\sqrt{\pi}\sqrt{\cos\Lambda_1}\int_{\mu}^{\rho} \mathrm{Re}\left\{\frac{e^{-i\Lambda_1/2}}{\sqrt{r_1-it}}\right\}dt \tag{B37}$$

$$= 2\sqrt{\pi}\sqrt{\cos\Lambda_1}\ \mathrm{Re}\left\{e^{-i\Lambda_1/2}\, 2i\sqrt{r_1-it}\ \Big|_{t=\mu}^{\rho}\right\}$$

$$= -4\sqrt{\pi}\sqrt{\cos\Lambda_1}\ \mathrm{Im}\left\{e^{-i\Lambda_1/2}\sqrt{r_1-it}\ \Big|_{t=\mu}^{\rho}\right\}$$

$$= -4\sqrt{\pi}\sqrt{\cos\Lambda_1}\ \mathrm{Im}\left\{e^{-i\Lambda_1/2}\sqrt{r_1-i\rho}\right\} + 4\sqrt{\pi}\sqrt{\cos\Lambda_1}\ \mathrm{I_m}\left\{e^{-i\Lambda_1/2}\sqrt{r_1-i\mu}\right\} \tag{B38}$$

Since the lower limit, μ, is an arbitrary limit then value of μ is selected such that the second term vanishes; that is, we select μ such that

$$\mathrm{Im}\left\{e^{-i\Lambda_1/2}\sqrt{r_1-i\mu}\right\} \equiv 0 \tag{B39}$$

now

$$r_1-i\mu = \sqrt{r_1^2+\mu^2}\ \ e^{-i\tan^{-1}\left(\frac{\mu}{r_1}\right)}$$

and

$$\mathrm{Im}\left\{e^{-i\Lambda_1/2}\sqrt{r_1-i\mu}\right\} = \mathrm{Im}\left\{\sqrt[4]{r_1^2+\mu^2}\ \ e^{-i\left(\Lambda_1+\tan^{-1}\left(\frac{\mu}{r_1}\right)\right)/2}\right\}$$

$$= \sqrt[4]{r_1^2+\mu^2}\ \left[-\sin\left(\left(\Lambda_1+\tan^{-1}\left(\frac{\mu}{r_1}\right)\right)/2\right)\right]$$

Thus μ is selected such that $\mu = -r_1 \tan \Lambda_1$ and consequently $F(\rho)$ is given as

$$F(\rho) = -4\sqrt{\pi}\sqrt{\cos\Lambda_1}\ \mathrm{Im}\left\{e^{-i\Lambda_1/2}\sqrt{r_1^2 - i\rho}\right\} \tag{B40}$$

and the expression for ψ_1 given in equation (B30) may be put in the form

$$\psi_1 = -\frac{\lambda}{2\pi^{3/2}}\int_{-\infty}^{x}\frac{\cos(\Theta_1/2)}{\sqrt{r_1}}\,F(\rho)\,dx' \tag{B41}$$

or

$$\psi_1 = \frac{2\lambda}{\pi}\int_{-\infty}^{x}\frac{\cos(\Theta_1/2)}{\sqrt{r_1}}\,\mathrm{Im}\left[e^{-i\Lambda_1/2}\sqrt{r_1 - i\rho}\;dx'\right]$$

and since $\mathrm{Im}(\bar{Z}) = \mathrm{Im}(x-iy) \equiv -y \equiv -\mathrm{Im}(x+iy)$ then ψ_1 becomes

$$\psi_1 = -\frac{2\lambda}{\pi}\int_{-\infty}^{x}\frac{\cos(\Theta_1/2)\sqrt{\cos\Lambda_1}}{\sqrt{r_1}}\,\mathrm{Im}\left[e^{i\Lambda_1/2}\sqrt{r_1 + i\rho}\right]dx' \tag{B42}$$

now replacing ρ by $\rho = y + (x'-x)\tan\Lambda_1$

$$\psi_1 = -\frac{2\lambda}{\pi}\int_{-\infty}^{x}\frac{\cos(\Theta_1/2)}{\sqrt{r_1}}\,\mathrm{Im}\left\{e^{i\Lambda_1/2}\sqrt{r_1\cos\Lambda_1 + i(y\cos\Lambda_1 + (x'-x)\sin\Lambda_1)}\right\}dx'$$

Now let $\eta = y\cos\Lambda_1 - x\sin\Lambda_1$ and ψ_1 becomes

$$\psi_1 = -\frac{2\lambda}{\pi}\int_{-\infty}^{x}\frac{\cos(\Theta_1/2)}{\sqrt{r_1}}\,\mathrm{Im}\left\{e^{i\Lambda_1/2}\sqrt{r_1\cos\Lambda_1 + ix'\sin\Lambda_1 + i\eta}\right\}dx' \tag{B43}$$

The value of ψ_1 on $z\to 0$ may now be established by noting that $\lim_{z\to 0} r_1 = |x'|$ and that the integral from $-\infty$ to 0 is equal to zero since $\theta_1 = \pi$ for $x'<0$ on $z=0$, thus the expression for ψ_1 on $z=0$ becomes

$$\psi_1 = -\frac{2\lambda}{\pi}\int_0^x \sqrt{\frac{1}{x'}}\,\mathrm{Im}\left\{e^{i\Lambda_1/2}\sqrt{x'\cos\Lambda_1+ix'\sin\Lambda_1+i\eta}\right\}dx' \tag{B44}$$

Rather than attempting to evaluate this integral in its present form introduce a new function $\bar{\psi}_1$ such that

$$\bar{\psi}_1 + i\psi_1 = -\frac{2\lambda}{\pi}e^{i\Lambda_1/2}\int_0^x \frac{\sqrt{x'\cos\Lambda_1+ix'\sin\Lambda_1+i\eta}}{\sqrt{x'}}\,dx' \tag{B45}$$

and note that ψ_1 has the same definition as before in that it is equal to the imaginary part of the integral.

Now with $e^{i\Lambda_1/2} = e^{i\Lambda_1}\cdot e^{-i\Lambda_1/2}$

$$\bar{\psi}_1 + i\psi_1 = -\frac{2\lambda e^{i\Lambda_1}}{\pi}\int_0^x \frac{\sqrt{x'+i\eta e^{-i\Lambda_1}}}{\sqrt{x'}}\,dx'$$

$$= -\frac{2\lambda e^{i\Lambda_1}}{\pi}\int_0^x \sqrt{1+\frac{i\eta e^{-i\Lambda_1}}{x'}}\,dx' \tag{B46}$$

The integral may be evaluated by making a substitution of $x' = \frac{1}{\tau}$ and integrating the expression by parts to yield

$$\bar{\psi}_1 + i\psi_1 = -\frac{2\lambda}{\pi}\left\{e^{i\Lambda_1}\sqrt{x(x+a)} + \frac{i}{2}\,\mathrm{log}\left[\frac{\sqrt{x+a}+\sqrt{x}}{\sqrt{x+a}-\sqrt{x}}\right]\right\} \tag{B47}$$

where $a = i\eta e^{-i\Lambda_1}$ and $\eta = y\cos\Lambda_1 - x\sin\Lambda_1$

The function ψ_1 is the Imaginary part of the equation and is given in stretched rotated coordinates and may be expressed in the original stretched coordinates by transforming back out of the rotated coordinate system by using

$$x = x_o \cos \Lambda_1 - y_o \sin \Lambda_1$$

$$y_o = y \cos \Lambda_1 - x \sin \Lambda_1 = \eta$$

$$\bar{\psi}_1 + i\psi_1 = -\frac{2\lambda}{\pi}\left\{e^{i\Lambda_1}\sqrt{(x_o\cos\Lambda_1 - y_1\sin\Lambda_1)(x_o+iy_o)\cos\Lambda_1}\right.$$
$$\left. + \frac{iy_o}{2}\,\ell og\left[\frac{\sqrt{x_o+iy_o}+\sqrt{x_o-y_o\tan\Lambda_1}}{\sqrt{x_o+iy_o}-\sqrt{x_o-y_o\tan\Lambda_1}}\right]\right\} \qquad \text{(B48)}$$

Now making a new definition $q = y_o/x_o$ and replacing x_o by $\bar{x}/\beta\varepsilon$ where $\bar{x}$ is physical coordinates, the above equation becomes

$$\bar{\psi}_1 + i\psi_1 = -\frac{2\lambda}{\pi}\,\frac{\bar{x}}{\beta\varepsilon}\left\{e^{i\Lambda_1}\cos\Lambda_1\sqrt{(1-\beta_1 q)(1+iq)}\right.$$
$$\left. + \frac{iq}{2}\,\ell og\left[\frac{\sqrt{1+iq}+\sqrt{1-\beta_1 q}}{\sqrt{1+iq}-\sqrt{1-\beta_1 q}}\right]\right\} \qquad \text{(B49)}$$

where $\beta_1 = \tan \Lambda_1$

Then $\varepsilon\psi_1$ may be obtained by evaluating the imaginary part of the above equation

$$\varepsilon\psi_1 = \lambda\ \mathrm{Im}\left\{-\frac{2}{\pi}\,\frac{\bar{x}}{\beta}\,e^{i\Lambda_1}\sqrt{(1-\beta_1 q)(1+iq)}\right.$$
$$\left. + \frac{iq}{2}\,\ell og\left[\frac{\sqrt{1+iq}+\sqrt{1-\beta_1 q}}{\sqrt{1+iq}-\sqrt{1-\beta_1 q}}\right]\right\} \qquad \text{(B50)}$$

After some maniupulations the expression becomes

$$\varepsilon\psi_1 = -\frac{2\lambda}{\pi}\frac{\bar{x}}{\beta}\cos^2\Lambda_1\sqrt{1-\beta_1 q}\left[\beta_1\sqrt{\frac{\sqrt{1+q^2}+1}{2}} + sgn(q)\sqrt{\frac{\sqrt{1+q^2}-1}{2}}\right]$$

$$-\frac{2\lambda}{\pi}\frac{\bar{x}}{\beta}\frac{q}{4}\log\left[\frac{\sqrt{1+q^2}+1-\beta_1 q+\sqrt{2}\sqrt{1-\beta_1 q}\sqrt{\sqrt{1+q^2}+1}}{\sqrt{1+q^2}+1-\beta_1 q-\sqrt{2}\sqrt{1-\beta_1 q}\sqrt{\sqrt{1+q^2}+1}}\right] \qquad \text{(B51)}$$

Secondary Order Boundary Value Problem

The second order boundary value problem may be stated as

$$\begin{cases} \nabla^2\psi_2 = -\dfrac{k^2M^2}{\beta^2}\psi_o \\ \psi_2 = 0; \quad z=o \text{ and } x_o<y_o\tan\Lambda_1 \\ \dfrac{\partial\psi_2}{\partial z_o} = C_2\, x_o\, U(y_o); \quad z=o,\ x_o\, y_o \tan\ 1 \end{cases} \qquad \text{(B52)}$$

where $$C_2 = \left(\nu - \frac{ikM^2\lambda}{\beta}\right)$$

$$\nu = i\Theta_H k\beta$$

$$\lambda = \Theta_H(1 - ik\bar{x}_o)$$

This problem is separated into two parts by the following procedure

$$\begin{cases} \nabla^2\psi_2 = -\dfrac{k^2M^2}{\beta^2}\psi_o \\ \psi_2 = 0 \quad \text{on} \quad z=o; \quad x_o<y_o\tan\Lambda_1 \\ \dfrac{\partial\psi_2}{\partial z} = 0 \quad \text{on} \quad z=o; \quad x_o>y_o\tan\Lambda_1 \end{cases} \qquad \text{(B53)}$$

$$\begin{cases} \tilde{\nabla}^2\psi_2 = 0 \\ \psi_2 = 0 \quad \text{on} \quad z=0; \quad x_0<y_0 \tan \Lambda_1 \\ \dfrac{\partial\psi_2}{\partial z} = C_2\, x_0\, U(y_0) \quad \text{on} \quad z=0; \quad x_0>y_0 \tan \Lambda_1 \end{cases} \tag{B54}$$

Since it is indicated in equation (B12) that ψ_0 contains functions that do not provide for any change in boundary conditions across the control surface side edge then it follows that ψ_0 is a regular function and thus the solution of the boundary value problem of equation (B53) must also be a regular function that will be obtained from the global solution portion of the solution process.

A solution, ψ_2, of equation (B54) is taken to be given as

$$\psi_2 = \frac{C_2}{\lambda} \int_{\beta_1 y_0}^{x_0} \psi_1(\eta, y_0, z_0)\, d\eta \tag{B55}$$

where $\beta_1 = \tan \Lambda_1$

The function ψ_2 satisfies the differential equation since ψ_1 was obtained on that basis. Also, $\psi_2=0$ on $z_0=0$ for $x_0<\beta_1 y_0$ since $\psi_1=0$ for $x_0<\beta_1 y_0$, and

$$\left.\frac{\partial\psi_2}{\partial z_0}\right|_{z=0} = C_2\,(x_0 - \beta_1 y_0)\, U(y_0)$$

due to the fact that

$$\left.\frac{\partial\psi_1}{\partial z_0}\right|_{z=0} = \lambda\, U(y_0) \quad \text{for} \quad x_0 > \beta_1\, y_0.$$

The second order solution, ψ_2, may be obtained using a modified form of equation (B48) to define ψ_1 within the integrand

$$\psi_2 = -\frac{2\,C_2}{\pi}\,\mathrm{Im}\left\{\int_{\beta_1 y_o}^{x_o} e^{i\Lambda_1}\cos\Lambda_1\,\sqrt{(\eta-\beta_1 y_o)(\eta+iy_o)} + \frac{iy_o}{2}\,\ell og\left[\frac{\sqrt{\eta+iy_o}+\sqrt{\eta-\beta_1 y_o}}{\sqrt{\eta+iy_o}-\sqrt{\eta-\beta_1 y_o}}\right] d\eta\right\} \tag{B56}$$

To shorten the notation let

$$\nu_o = \sqrt{\eta + iy_o}$$

$$\nu_1 = \sqrt{\eta - \beta_1 y_o}$$

$$\psi_2 = -\frac{2C_2}{\pi}\,\mathrm{Im}\left\{e^{-i\Lambda_1}\cos\Lambda_1 \int_{\beta_1 y_o}^{x_o} \nu_o\nu_1 d\eta + \frac{iy_o}{2}\int_{\beta_1 y_o}^{x_o} d\eta\left(\frac{\nu_o+\nu_1}{\nu_o-\nu_1}\right) d\eta\right\} \tag{B57}$$

Replacing $e^{i\Lambda_1}\cos\Lambda_1$ by $\frac{i}{i+\beta_1}$ and evaluating the two integrals results in the expression

$$\psi_2 = -\frac{2C_2}{\pi}\,\mathrm{Im}\left\{\frac{i}{i+\beta_1}\left[\frac{2x_o+(i-\beta_1)y_o}{4}\,\nu_o\nu_1 - \frac{y_o^{\,2}(i+\beta_1)^2}{8}\,\ell og\left(\frac{\nu_o+\nu_1}{\nu_o-\nu_1}\right)\right] + \frac{iy_o}{2}\left[\frac{2x_o+y_o(i-\beta_1)}{2}\,\ell og\left(\frac{\nu_o+\nu_1}{\nu_o-\nu_1}\right) - \nu_o\nu_1\right]\right\} \tag{B58}$$

Upon collecting like terms the expression becomes

$$\psi_2 = -\frac{C_2}{\pi}\,\mathrm{Im}\left\{\frac{2x_o-y_o(i+3\beta_1)}{2(1-i\beta_1)}\,\nu_o\nu_1 + y_o\left(ix_o - \frac{(1+3\beta_1 i)}{4}\,y_o\right)\ell og\left(\frac{\nu_o+\nu_1}{\nu_o-\nu_1}\right)\right\} \tag{B59}$$

where $\nu_o = \sqrt{x_o + iy_o}$

$\nu_1 = \sqrt{x_o - \beta_1 y_o}$

Thus, expressions for the solutions of the first and second order boundary value problems are now defined by equations (B48) and (B59), and it only remains to obtain the pressure coefficient in terms of these solutions. By definition, the pressure coefficient C_p is given in physical coordinates $\bar{x}$, y by

$$C_p(\bar{x},y,0) = -2\left\{\phi_{\bar{x}}(\bar{x},y,0) + ik\phi(\bar{x},y,0)\right\} \tag{B60}$$

where $\phi(\bar{x},y,0)$ obtained by the ε expansion process is given as

$$\phi(\bar{x},y,0) = e^{ikM^2\bar{x}/\beta^2}(\psi_0 + \varepsilon\psi_1 + \varepsilon^2\psi_2 + \ldots)$$

$$= \sum_{j=0}^{\infty}\left[e^{ikM^2\bar{x}/\beta^2}\psi_j\varepsilon^j\right] \tag{B61}$$

Then

$$\phi_{\bar{x}} = \sum_{j=0}^{\infty}\left[\frac{\partial(\psi_j\varepsilon^j)}{\partial\bar{x}} + \frac{ikM^2}{\beta^2}\psi_j\varepsilon^j\right]e^{ikM^2\bar{x}/\beta^2}$$

$$\phi_{\bar{x}}+ik\phi = \sum_{j=0}^{\infty}\left[\frac{\partial(\psi_j\varepsilon^j)}{\partial\bar{x}} + \frac{ik}{\beta^2}\psi_j\varepsilon^j\right]e^{ikM^2\bar{x}/\beta^2} \tag{B62}$$

Therefore

$$C_p = -2\sum_{j=0}^{\infty}\left(\frac{\partial(\psi_j\varepsilon^j)}{\partial\bar{x}} + \frac{ik}{\beta^2}\psi_j\varepsilon^j\right)e^{ikM^2\bar{x}/\beta^2} \tag{B63}$$

Now ψ_1 may be restated in stretched and scaled coordinates as being

$$\psi_1 = -\frac{2\lambda}{\pi}\,\mathrm{Im}\left\{ e^{i\Lambda_1}\cos\Lambda_1\,\sqrt{x_o-\beta_1 y_o}\,\sqrt{x_o+iy_o} + \frac{iy_o}{2}\,\ell og\left[\frac{\sqrt{x_o+iy_o}+\sqrt{x_o-\beta_1 y_o}}{\sqrt{x_o+iy_o}-\sqrt{x_o-\beta_1 y_o}}\right]\right\} \tag{B64}$$

Upon redefining

$$\nu_o = \sqrt{x_o + iy_o}$$

$$\nu_1 = \sqrt{x_o - {}_1 y_o}$$

$$e^{i\Lambda_1}\cos\Lambda_1 = \frac{i}{i+\beta_1}$$

$$\psi_1 = -\frac{2\lambda}{\pi}\,\mathrm{Im}\left\{\frac{i}{i+\beta_1}\,\nu_o\nu_1 + \frac{iy_o}{2}\,\ell og\left[\frac{\nu_o+\nu_1}{\nu_o-\nu_1}\right]\right\}$$

and the expression given in physical coordinates $(\bar{x},y)$ is obtained by replacing x_o by $\frac{\bar{x}}{\beta\varepsilon}$, y_o by $\frac{y}{\varepsilon}$ and β_1 by $\frac{\tan\Lambda}{\beta}$ to yield

$$\varepsilon\psi_1 = -\frac{2\lambda}{\pi}\,\mathrm{Im}\left\{\frac{i}{i\beta+\tan\Lambda}\,\bar{\nu}_o\bar{\nu}_1 + \frac{iy}{2}\,\ell og\left(\frac{\bar{\nu}_o+\bar{\nu}_1}{\bar{\nu}_o-\bar{\nu}_1}\right)\right\} \tag{B65}$$

where $\bar{\nu}_o = \sqrt{\bar{x}+i\beta y}$

$$\bar{\nu}_1 = \sqrt{x-y\tan\Lambda}$$

Equation (B65) along with its derivative with respect to $\bar{x}$ may be inserted into equation (B63) to give the pressure coefficient due to the first order solution as

$$C_p^{(1)} = \left\{ \frac{4\lambda}{\pi \bar{\nu}_1 \bar{\beta}^2} \operatorname{Im}\left([\beta + i\tan\Lambda]\bar{\nu}_o \right) + \frac{4\lambda i k}{\pi\ \beta^2} \operatorname{Im}\left[\frac{i}{i\beta + \tan} \bar{\nu}_o \bar{\nu}_1 \right] \right.$$

$$\left. + \frac{2\lambda i k y}{\pi \beta^2} \operatorname{Im}\left(i\ \ell og \left[\frac{\bar{\nu}_o + \bar{\nu}_1}{\bar{\nu}_o - \bar{\nu}_1} \right] \right) \right\} \cdot e^{ikM^2 \bar{x}/\beta^2} \qquad \text{(B66)}$$

Collecting terms and evaluating the imaginary parts of the equation results in the pressure coefficient given in physical coordinates due to the first order solution given as

$$C_p^{(1)} = \frac{\lambda}{\pi} \left\{ \frac{2\sqrt{2}}{\bar{\beta}_\ell^{\,2}} \left(\frac{1}{\sqrt{\bar{x} - y\tan\Lambda}} + \frac{ik}{\beta^2} \sqrt{\bar{x} - y\tan\Lambda} \right) \right.$$

$$\cdot \left(\beta\ Sgn(y, \bar{x}) \sqrt{\sqrt{\bar{x}^2 + \beta^2 y^2} - \bar{x}} + \tan\Lambda \sqrt{\sqrt{\bar{x}^2 + \beta^2 y^2} + \bar{x}} \right)$$

$$\left. + \frac{iky}{\beta^2}\ \ell og \left[\frac{\sqrt{\bar{x}^2 + \beta^2 y^2} + \bar{x} - y\tan\Lambda + \sqrt{2}\sqrt{\bar{x} - y\tan\Lambda}\ \sqrt{\sqrt{\bar{x}^2 + \beta^2 y^2} + \bar{x}}}{\sqrt{\bar{x}^2 + \beta^2 y^2} + \bar{x} - y\tan\Lambda - \sqrt{2}\ \sqrt{\bar{x} - y\tan\Lambda}\ \sqrt{\sqrt{\bar{x}^2 + \beta^2 y^2} + \bar{x}}} \right] \right\}$$

$$\cdot\ e^{ikM^2 \bar{x}/\beta^2} \qquad \text{(B67)}$$

where $\bar{\beta}_\ell = \sqrt{\beta^2 + \tan^2\Lambda}$ $\qquad \bar{x} = \xi - x_{\ell s}$

$y = n - y_s$

$\lambda = \Theta_H(1 - ik\bar{x}_c)$

$\bar{x}, y$ = physical coordinates

The pressure coefficient due to the second order term may be obtained by using equation (B55) , equation (B63) , equation (B65) and applying the above procedure to yield

$$C_p^{(2)}(\bar{x},y,0) = \frac{C_2}{\pi}\left\{\frac{4\bar{\nu}_1}{\beta\bar{\beta}_\ell^2}\left[\tan\Lambda + \left(\frac{ik}{\beta^2}\right)\left(\frac{2\bar{x}\tan\Lambda-(3\tan^2\Lambda+\beta^2)}{4}\right)\right]\bar{\mu}_2\right.$$

$$+ \frac{4\bar{\nu}_1\ Sgn\ (\bar{x},y)}{\bar{\beta}_\ell^2}\left[1 + \left(\frac{ik}{\beta^2}\right)\frac{\bar{\nu}_1^2}{2}\right]\bar{\mu}_3$$

$$+ \left(\frac{ik}{\beta^2}\right)\frac{y^2}{2}\ Sgn\ (\bar{x},y)\ \tan^{-1}\left(\frac{2\bar{\mu}_3\bar{\nu}_1}{\bar{\tau}-\bar{\nu}_1^2}\right)$$

$$\left. + \frac{y}{\beta}\left[1+\left(\frac{ik}{\beta^2}\right)\left(\bar{x}-\frac{3y\tan\Lambda}{4}\right)\right]\ \ell og\left[\frac{\bar{\tau}+\bar{\nu}_1^2+2\bar{\nu}_1\bar{\mu}_2}{\bar{\tau}+\bar{\nu}_1^2-2\bar{\nu}_1\bar{\mu}_2}\right]\right\}\cdot e^{ikM^2\bar{x}/\beta^2} \qquad \text{(B68)}$$

where

$$\bar{\beta}_\ell = \sqrt{\beta^2+\tan^2\Lambda_\ell}$$

$$\bar{\nu}_1 = \sqrt{\bar{x}-y\tan\Lambda_\ell} \qquad \bar{x} = \xi - x_{\ell s}$$

$$\bar{\tau} = \sqrt{\bar{x}^2+\beta^2y^2} \qquad y = \eta - y_s$$

$$\bar{\mu}_2 = \sqrt{\frac{\bar{\tau}+\bar{x}}{2}}$$

$$\bar{\mu}_3 = \sqrt{\frac{\bar{\tau}-\bar{x}}{2}}$$

$$C_2 = \nu - \frac{ikM^2\lambda}{\beta}$$

The sum of equations (B67) and (B68) will provide proper change in boundary conditions at the corner of a leading edge control surface. These expressions need to be modified such that the planform boundary conditions are satisfied at the edges of the planform while maintaining the strength of the singularities along the side edges of the control surface. The functions that satisfy these constraints are described in the main section of the document following the loading function developments of Landahl.

APPENDIX C

A CAUTION REGARDING PLANFORMS WITH DISCONTINUOUS EDGES, AND A PROVISION FOR INCLUDING EFFECTS OF AIRFOIL THICKNESS VIA LOCAL LINEARIZATION

Suggestions are made for modifying analytical procedures used in obtaining loadings on discontinuous planform shapes, and for modifying lifting surface boundary conditions $\bar{w}/V$ such that the physical flow pressure distributions are more readily simulated by the theoretical pressure distributions.

Modification of Planforms Having Discontinuous Shapes

Analytical difficulties may be encountered in predicting the aerodynamic loadings on planforms having analytic discontinuities in the planform shape definition. Figure 50 represents a typical analysis planform where first derivative discontinuities in the shape definition exist and may provide inconsistent results if the spanwise distribution of collocation stations contain a control point located at or very near the spanwise discontinuity station.

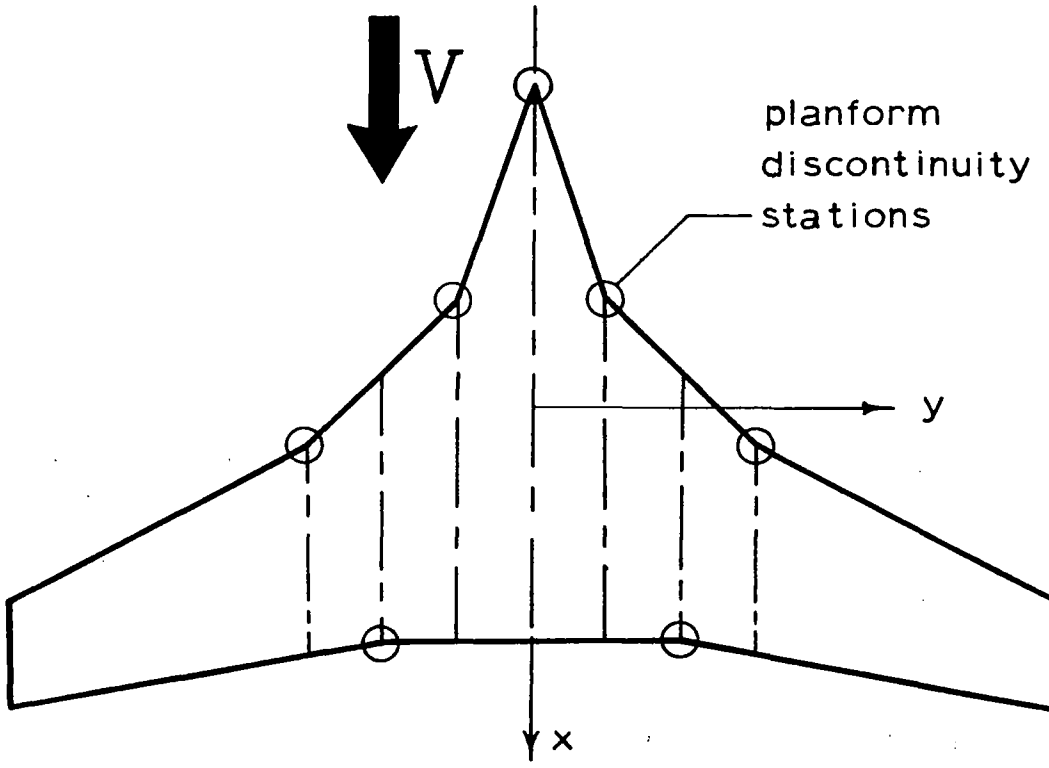

Figure 50.- Typical Analysis Configuration with a Discontinuous Shape Definition

The mathematically derived downwash sheets obtained from an evaluation of the downwash integral will exhibit singularities whenever collocation stations are located at the planform spanwise discontinuity stations. The singularities are due to the over-simplified manner in which the pressure distributions are assumed to exist over the planform. The assumed pressure functions are distributed continuously over the surface in such a manner that the planform is completely covered regardless of the analytic continuity of the planform definition. If the planform definition contains sharp breaks or discontinuities in its first derivative definition, then the pressure distributions and resulting spanwise loadings will also exhibit discontinuities at the same spanwise stations. It is the discontinuous first derivative of spanwise loadings that cause the numerical problems and produce singularities in the predicted downwash sheets. The spanwise loading discontinuities may be removed by using a suitable pressure distribution that is analytically continuous in its spanwise direction. However, no such distributions have been formulated nor used within the present program development since it is obvious that there are other means available for obtaining reasonable results other than overemphasizing the effects of localized flow in regions of planform discontinuities. The problem of downwash singularities may be circumvented by smoothing the planform discontinuities or by keeping the spanwise location of collocation stations well away from the troublesome regions. However, numerical problems do exist and the analyst should be cognizant of the potential problem and to what extent that the downwash distributions may be distorted in the regions of planform discontinuities.

The extent of downwash distortion may be determined by evaluating the downwash integral equation for the steady flow case given the following form:

$$W(x, y) = \int_{-s}^{s} \frac{\partial}{\partial \eta} \left\{ f(\eta) \int_{x_\ell}^{x_t} g(\xi,\eta) \left[1 + \frac{x-\xi}{\sqrt{(x-\xi)^2+\beta^2(y-\eta)^2}} \right] d\xi \right\} \frac{d\eta}{y-\eta} \qquad \text{(C1)}$$

In this example, $f(\eta)$ is taken to be the spanwise pressure function corresponding to an ellipse, $f(\eta) = \sqrt{s^2 - \eta^2}$; and $g(\xi,\eta)$ is the chordwise pressure function given as

$$g(\xi,\eta) = [\, x_t(\eta) - \xi \,]^{1/2} \,/\, [\, \xi - x_\ell(\eta) \,]^{1/2}$$

Also, the planform being evaluated is a delta wing having a discontinuous planform definition at the center line.

Performing the indicated differentiation with respect to η in equation (C1) and retaining only the essential terms that contribute to the singularity problem results in the following expression:

$$\overline{W}(x, y) = \int_{-s}^{s} \left\{ \int_{x_\ell}^{x_t} f(\eta) \frac{\partial g(\xi,\eta)}{\partial \eta} \left[1 + \frac{x-\xi}{\sqrt{(x-\xi)^2+\beta^2(y-\eta)^2}} \right] d\xi \right\} \frac{d\eta}{y-\eta} \qquad (C2)$$

The $\frac{\partial g(\xi,\eta)}{\partial \eta}$ term has a finite discontinuity at the planform center line having equal but opposite signs on either side of the center line.

To shorten the expression let the chordwise integral be defined as:

$$H(\eta) = \int_{x_\ell}^{x_t} f(\eta) \frac{\partial g(\xi,\eta)}{\partial \eta} \left[1 + \frac{x-\xi}{\sqrt{(x-\xi)^2+\beta^2(y-\eta)^2}} \right] d\xi \qquad (C3)$$

And let $H_\ell(\eta)$ be $H(\eta)$ when the left hand side derivative of $\frac{\partial g(\xi,\eta)}{\partial \eta}$ used in equation (C3); also let $H_r(\eta)$ be $H(\eta)$ of equation (C3) using the right hand side derivative of $\frac{\partial g(\xi,\eta)}{\partial \eta}$

Then the shortened form of equation (C2) becomes:

$$\overline{W}(x, y) = \int_{-s}^{s} H(\eta) \frac{d\eta}{y-\eta} \qquad (C4)$$

Equation (C4) may be evaluated by adding and subtracting the function $H_\ell(\eta)$ over the integration interval $0 \leq \eta \leq s$.

$$\overline{W}(x, y) = \int_{-s}^{0} H_\ell(y) \frac{d\eta}{y-\eta} + \int_{0}^{s} H_\ell(\eta) \frac{d\eta}{y-\eta} \qquad (C5)$$

$$- \int_{0}^{s} H_\ell(\eta) \frac{d\eta}{y-\eta} + \int_{0}^{s} H_r(\eta) \frac{d\eta}{y-\eta}$$

The second and third integrals of (C5) are evaluated by making a continuous extention of the definition of $\frac{\partial g(\xi,\eta)}{\partial \eta}\Big|_{\ell}$ across the centerline to the right hand tip at $\eta = s$.

The integrals may be combined to provide the expression

$$\bar{W}(x,y) = \int_{-s}^{s} H_{\ell}(\eta)\,\frac{d\eta}{y-\eta} - \int_{0}^{s} H_{\ell}(\eta)\,\frac{d\eta}{y-\eta} + \int_{0}^{s} H_{r}(\eta)\,\frac{d\eta}{y-\eta} \qquad \text{(C6)}$$

Singularities at $\eta = y$ are removed from the integral and evaluated separately as shown by the following:

$$\begin{aligned}\bar{W}(x,y) = {} & \int_{-s}^{s} [\, H_{\ell}(\eta) - H_{\ell}(y) \,]\,\frac{d\eta}{y-\eta} + H_{\ell}(y) \int_{-s}^{s} \frac{d\eta}{y-\eta} \\ & - \int_{0}^{s} [\, H_{\ell}(\eta) - H_{\ell}(y) \,]\,\frac{d\eta}{y-\eta} - H_{\ell}(y) \int_{0}^{s} \frac{d\eta}{y-\eta} \\ & + \int_{0}^{s} [\, H_{r}(\eta) - H_{r}(y) \,]\,\frac{d\eta}{y-\eta} + H_{r}(y) \int_{0}^{s} \frac{d\eta}{y-\eta}\end{aligned} \qquad \text{(C7)}$$

The only terms containing singularities (with the restriction that the downwash stations are contained in the interval $-s < y < s$) are the terms having an integral form of

$$\int_{0}^{s} \frac{d\eta}{y-\eta} \qquad \text{(C8)}$$

Equation (C7) may then be expressed as having singular and non-singular terms that take the form of:

$$\bar{W}(x,y) = [\, H_{r}(y) - H_{\ell}(y) \,]\,\ln|y| + \text{Regular Terms} \qquad \text{(C9)}$$

and the limiting value of $\bar{W}(x,y)$ tends to infinity as $y \rightarrow 0$.

Thus, the downwash sheet will exhibit unrealistically large values of downwashes whenever a downwash chord is placed near a planform discontinuity station and is due solely to the manner in which the pressure loadings are assumed to exist on the boundaries of the planform.

There is an obvious solution to this problem (see reference 8) in that the derivative of the spanwise loadings may be made continuous by smoothing the planform discontinuities. An example of how smoothing of planform discontinuities affects the downwash distribution is shown in figure 51.

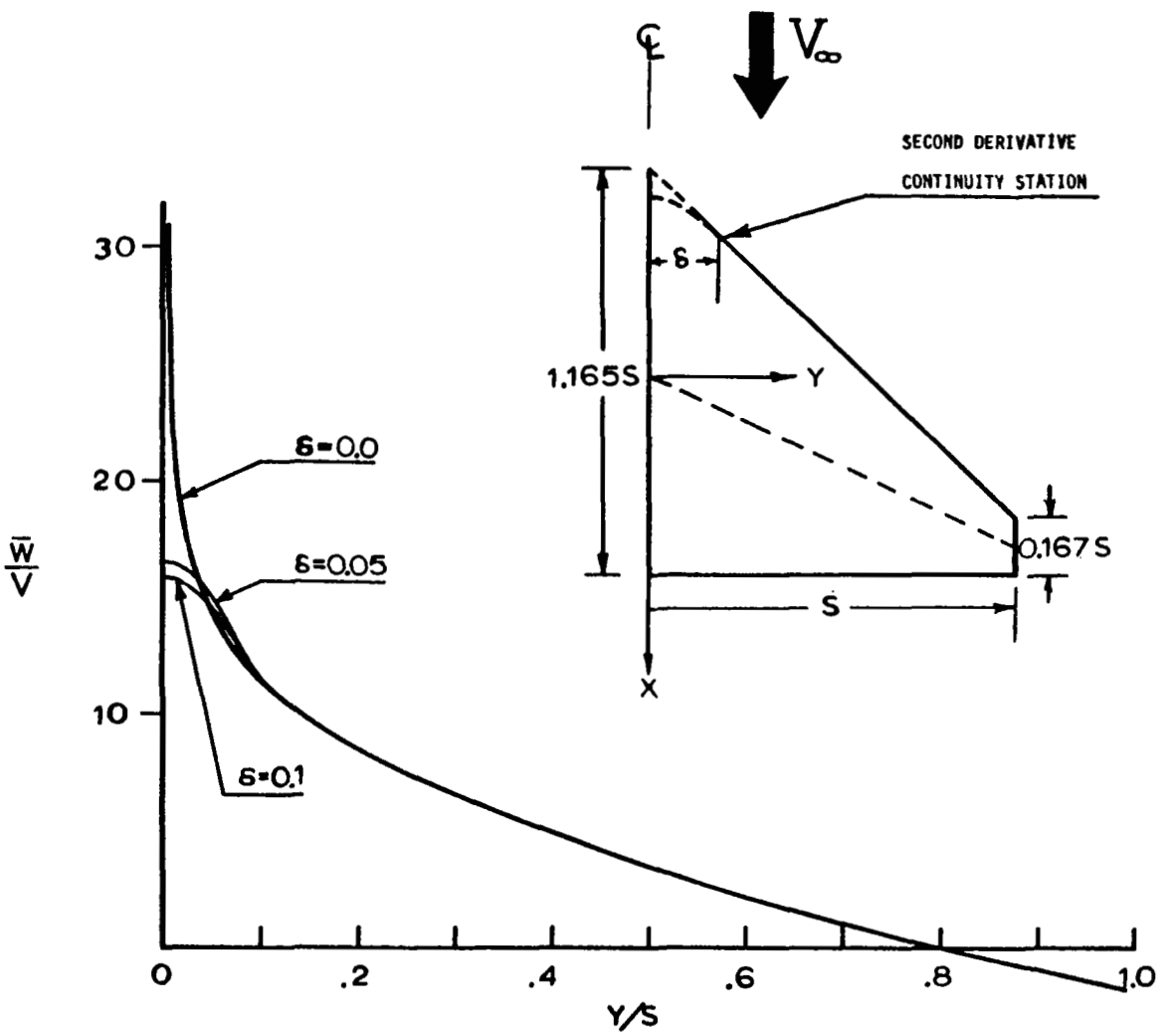

Figure 51.- Spanwise Downwash Distribution Resulting from Various Apex Smoothing Values

The clipped delta planform shown in figure 51 has been modified in the region of the apex at the centerline to produce a continuous first derivative definition of the planform across the centerline. The method selected to smooth the shape definition is one of applying a function having a continuous first derivative that is zero at the centerline and is also continuous in the second derivative at the spanwise matching station. This particular smoothing function provides derivative continuity with the least distortion in planform definition. Downwash values obtained at spanwise stations along the 50% chordline are shown in the lower part of figure 51. The downwash distribution near the planform centerline does become singular for the pointed apex case. However, the downwashes take on more realistic values whenever the apex discontinuity is removed by applying a small amount of smoothing.

The spanwise distortion in downwash sheet is only slightly affected by redefining the planform shape. However, caution should be exercised in applying large amounts of smoothing since the redefined shape may provide a poor approximation of the original planform shape.

The above discussion has been presented to identify a potential problem that may arise in predicting the loadings on discontinuous planforms and to suggest a method to alleviate the problem. The suggested smoothing technique is not available within the present computer program, however, an alternate method is suggested such that reasonable results may be obtained without redefining the planform shape.

An alternate method suggested by other authors is one of applying engineering judgement to the placement of spanwise collocation stations in regions of planform discontinuities. The downwash distribution shown in figure 51 indicates that the distributions are only slightly affected at small distances away from the discontinuity station. The amount of distortion will be the greatest near the centerline of a highly swept planform since this is the location where the largest difference in the spanwise loading derivative exists. Planforms having leading and trailing edges defined by a combination of straight line segments for which differences in spanwise slopes are small

will produce even smaller distortions in the downwash description than is observed for the centerlines station. Consequently, it is suggested that the placement of the spanwise collocation stations (downwash chords) is such that the stations are located at least a small distance away from any planform discontinuity station.

Although application of planform smoothing or positioning of collocation stations may appear to be an artificial method to bypass the source of the problem, these methods will provide reasonable results for the aerodynamic loadings without being overly encumbered by localized flow conditions that contibute only in a small way to final load definitions.

Suggested Modification of Boundary Conditions $\bar{w}/V$

From an operational standpoint, it appears that if a local linearization is used, that is if the linearized boundary conditions $\bar{w}/V$ are modified to include local velocities due to airfoil thickness the resulting theoretical pressure distributions will simulate the physical flow conditions more accurately. Lifting surface theory solutions using assumed mode-kernel function approach usually provide results that correlate well with experimental results. An example of the correlation of theoretical-experimental results is presented for the analysis planform shown in figure 52.

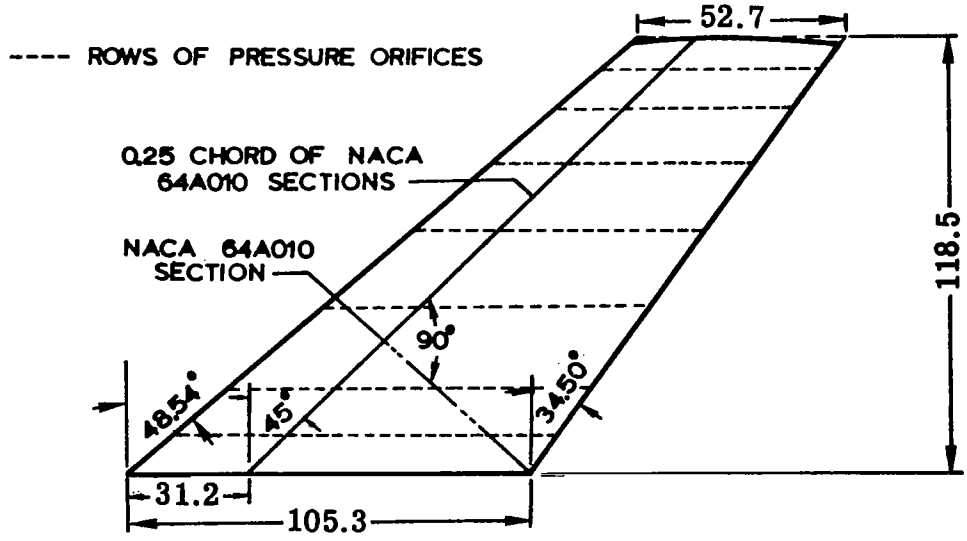

Figure 52.- Experimental Planform of NACA RM A51G31 (dimensions in cm)

Chordwise pressure distributions were obtained at seven spanwise locations as indicated in the figure. The comparisons of theoretical-experimental results are shown in figure 53 for the pressure chord located at y/s = .831 for M = 0.80 and α = 4°.

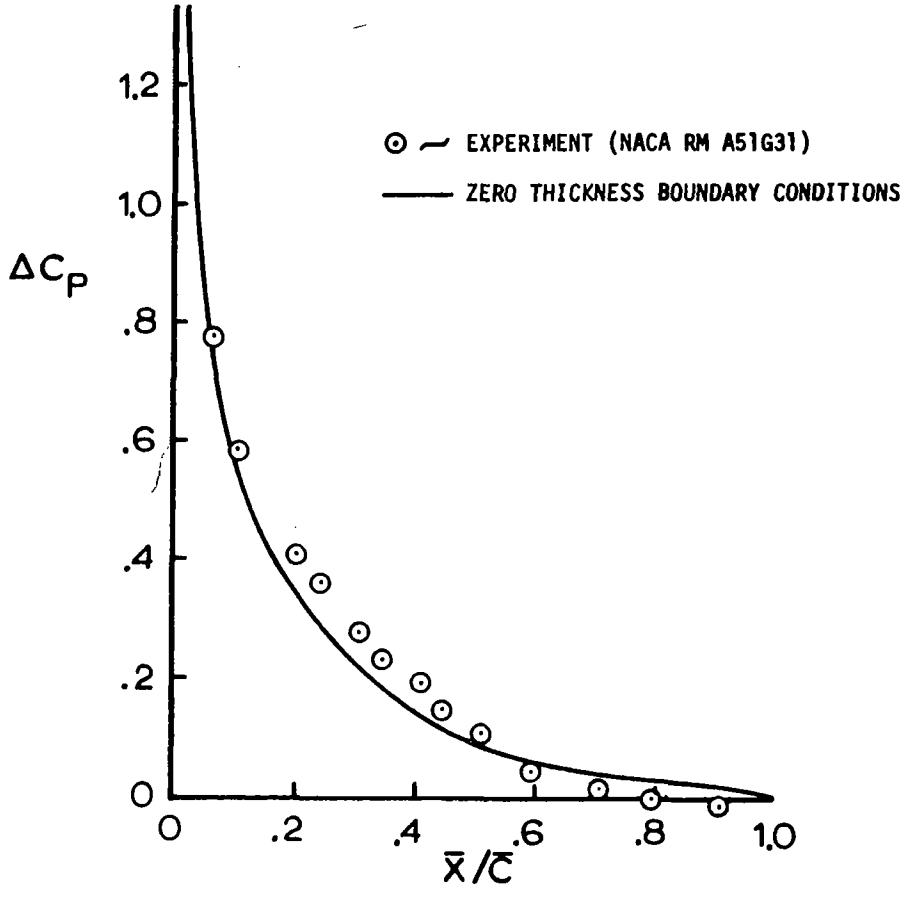

Figure 53.- Experimental and Zero Thickness Theoretical Pressure Distribution at y/s = 0.831, M = 0.80, α = 4°

The resulting theoretical pressure distribution was obtained using the standard linearized boundary conditions applicable for zero thickness lifting surfaces. It appears that a reasonable correlation is obtained on the average in that the theoretical distribution does approximate the experimental values in an average sense over the length of the streamwise chord. Theoretical pressures forward of the midchord are smaller than experimental values and are greater than experimental values for stations aft of the midchord.

The analysis was revised using a modification on the lifting surface boundary conditions such that the local velocity due to symmetrical thickness distribution is used instead of applying the uniform velocity distribution of a zero thickness lifting surface.

That is, the boundary condition of the integral equation was obtained from the definition

$$\bar{W}_j(x,y,0) = \frac{1}{V}\frac{Dz}{Dt} = \frac{1}{V}\left[\frac{\partial z_j}{\partial t} + \frac{\partial z_j}{\partial x}\frac{\partial x}{\partial t}\right]$$

where z_j represents the displacement of the surface and is a function of time(t).

$\frac{\partial z_j}{\partial x}$ — the slope of the surface at (x,y).

$\frac{\partial x}{\partial t}$ is usually taken to be equal to the remote velocity V, and for a zero thickness airfoil section this may be correct. However, physical experiments are conducted on finite thickness airfoil sections having local velocities that are not uniform over the chord length.

Consequently, the $\frac{\partial x}{\partial t}$ term should represent the local flow velocity V_{Local} at collocation stations in making a comparison between theoretical and real flow results.

The modified boundary conditions applicable to finite thickness airfoil sections are then defined as:

$$\bar{W}_j(x,y,0) = \frac{1}{V}\left[\frac{\partial z_j}{\partial t} + \frac{\partial z_j}{\partial x} V_{Local}\right]$$

V_{Local} is defined as being the steady streamwise velocity distribution that differs from V due to thickness effects only, and may be obtained from experimental results or by using the theoretical distributions of reference 17.

Theoretical results shown in figure 54 represent analyses using zero thickness and finite thickness boundary conditions and it is evident that in this case more accurate simulation of the physical flow results are obtained using local boundary conditions that incorporate finite thickness effects.

Theoretical pressure distributions forward of the midchord station approach the experimental values in a better fashion than do the results using zero thickness boundary conditions. Also, the theoretical distributions near the trailing edge predict the change in sign in pressures as indicated in the experimental results.

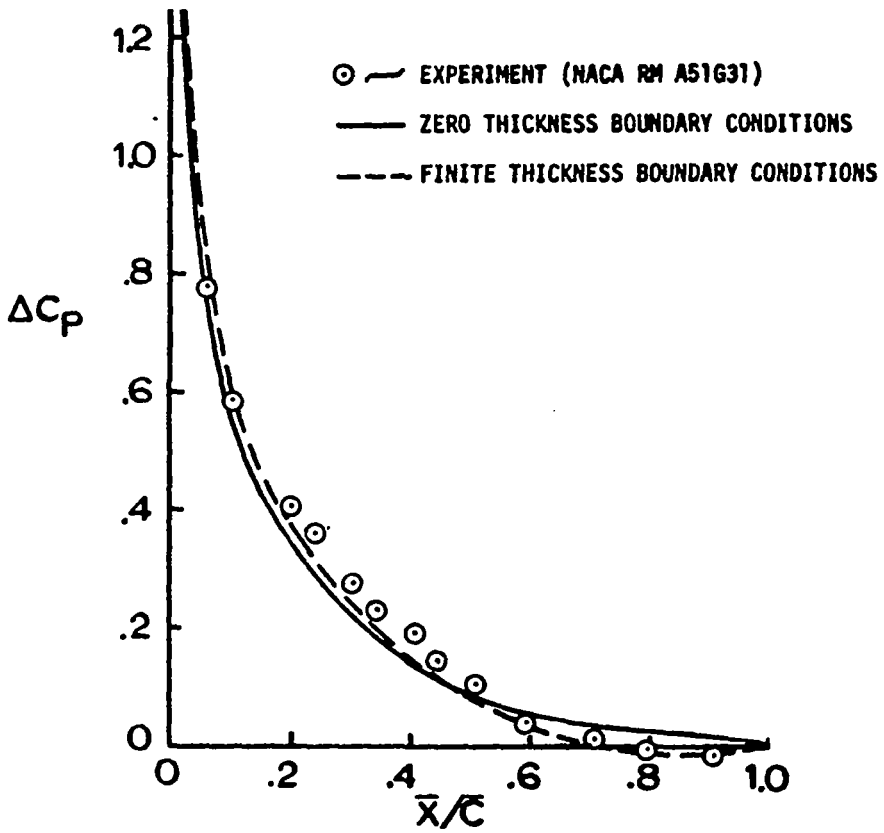

Figure 54.- Comparison of Pressure Distributions Predicted by Zero Thickness and Finite Thickness Boundary Conditions at a Semi-Span Station $y/s = 0.831$, for $M = 0.80$ and $\alpha = 4°$

Although no large changes appear in the distribution using the modified boundary conditions, it does appear that the physical flow conditions are more accurately simulated at least for this steady flow test configuration.

Validity of applying local linearization of boundary conditions within the unsteady case may be questioned on the basis that the kernel function has not been changed to reflect the local linearization effects.

However, a numerical experiment has been accomplished to evaluate the effects of local linearization on the unsteady pressure distributions using the test configuration shown in figure 55.

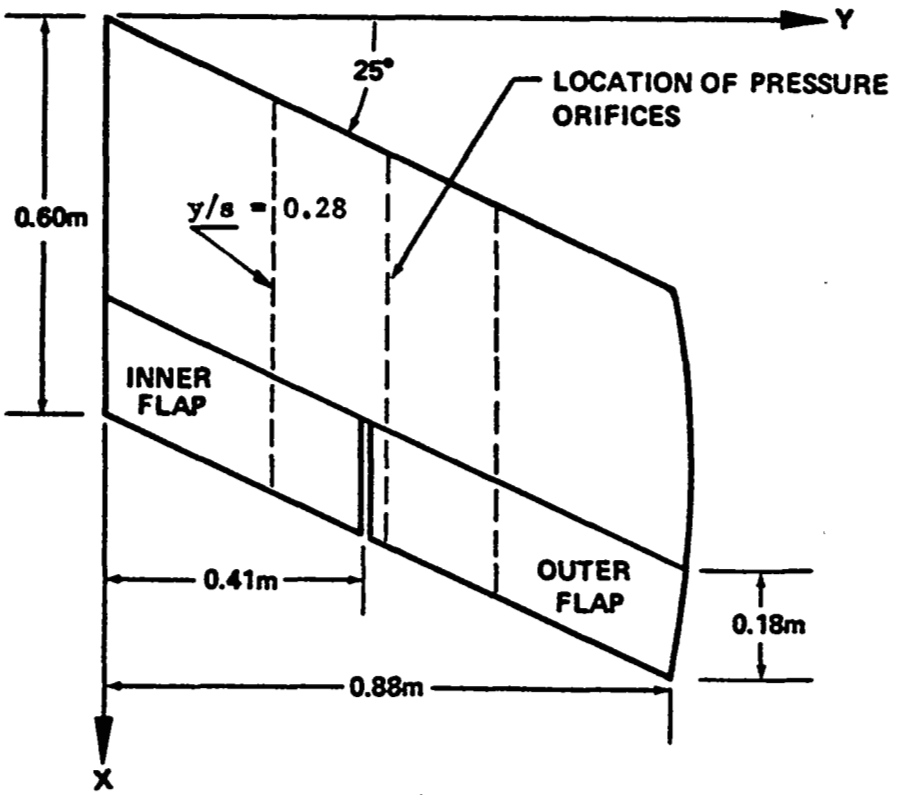

Figure 55 - Experimental Planform of Side-by-Side Control Surface Arrangement Showing Spanwise Location of Pressure Measuring Stations.

Results of this investigation are shown in figure 56 for the in-phase part of the resulting pressure distributions and the out-of-phase part is presented in figure 57.

The theoretical pressure distributions of the in-phase part approach the experimental values in a better fashion than do the results using zero thickness boundary conditions. The out-of-phase theoretical distributions remain almost invariant over the control surface and are changed only by very small amounts forward of the hingeline.

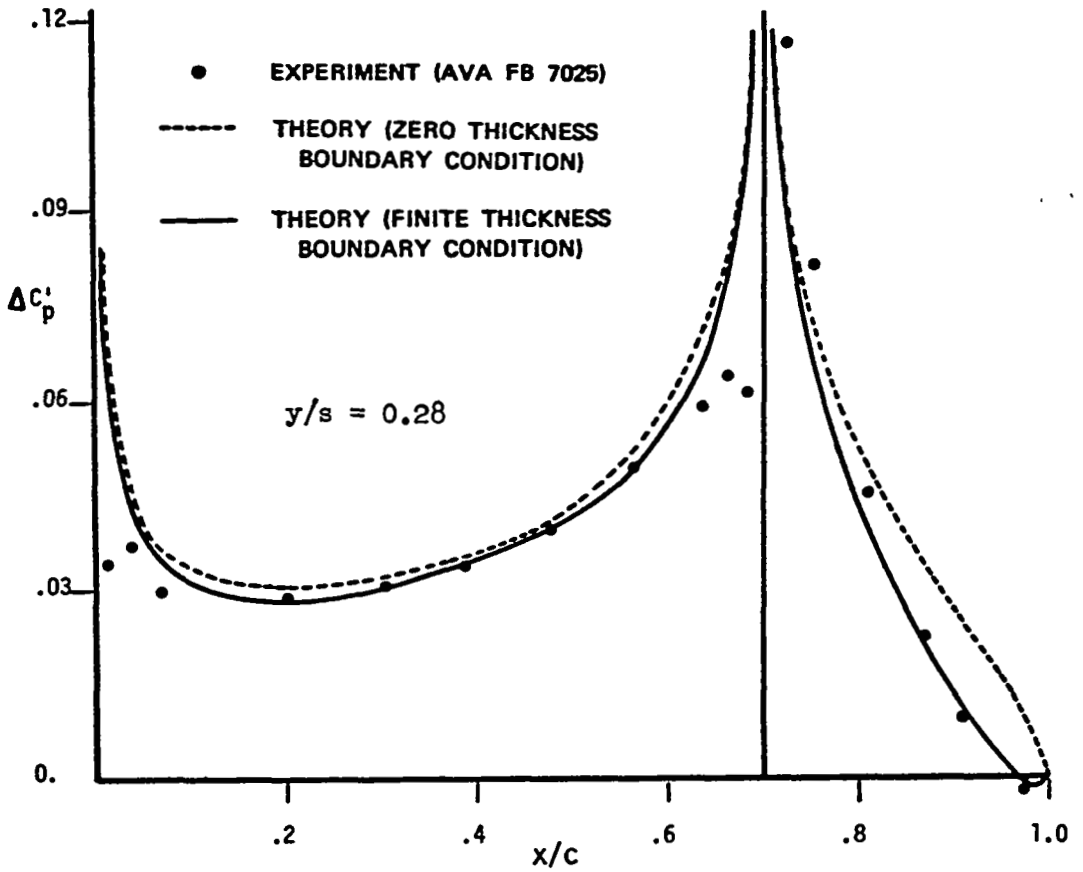

Figure 56 - In-Phase Pressure Distribution for Both Flaps Oscillating with the Same Phase and Amplitude. $\delta_f = 0.82^\circ$, $k = 0.372$, $M \cong 0.0$

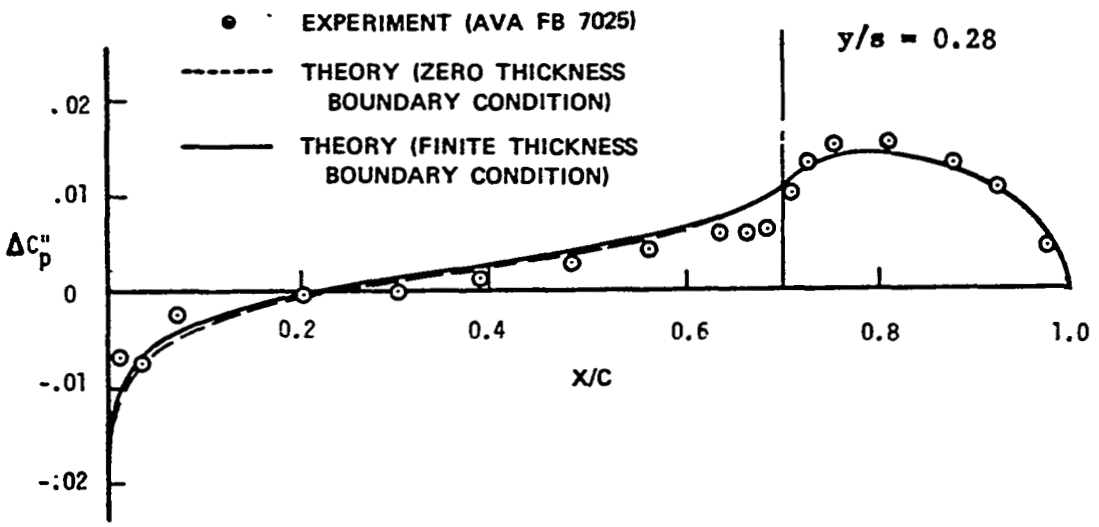

Figure 57 - Out-of-Phase Pressure Distribution for Both Flaps Oscillating with the Same Phase and Amplitude. $\delta_f = 0.82^\circ$, $k = 0.372$, $M \cong 0.0$

It should be noted that the validity of including local linearization effects within the boundary conditions can not be generalized on the basis of this single example.

However, it appears that the physical flow conditions may be more accurately simulated and may contribute significantly to the successful design of energy absorbing Stability Augmentation Systems provided that good correlation between experimental and theoretical results can be established over the frequency range of interest.

A program option is available for modifying the boundary conditions within the analysis and the data format along with limitations are given in reference 4.

REFERENCES

1. A. H. Flax, "Reverse Flow and Variation Theorems of Lifting Surface in Nonstationary Compressible Flow," J. Aeron. Sci., pp. 120-126, 1953.

2. J. H. Berman, P. Shyprykevich and J. B. Smedfjeld, "Unsteady Aerodynamic Forces in General Wing/Control Surface Configuration in Subsonic Flow," AFFDL-TR-67-117.

3. M. Landahl, "Pressure Loading Functions for Oscillating Wings with Control Surfaces," AIAA Journal, Vol. 6, No. 2, February 1968.

4. M. C. Redman and W. S. Rowe, "Prediction of Unsteady Aerodynamic Loadings Caused by Leading Edge and Trailing Edge Control Surface Motions in Subsonic Compressible Flow--Computer Program Description," NASA CR-132634, May 1975.

5. H. G. Kussner," General Lifting Surface Theory," Luftfahrforschung, Vol. 17, No. 11/12, Dec. 10, 1940. Also discussed in Aerodynamic Flutter, I. E. Garrick, editor. AIAA Selected Reprints, Vol. V.

6. C. E. Watkins, H. L. Runyan and D. S. Woolston, "On the Kernel Function of the Integral Equation Relating the Lift and Downwash Distributions of Oscillating Finite Wings in Subsonic Flow," NACA Rep. 1234.

7. P. T. Hsu, "Calculation of Pressure Distributions for Oscillating Wings of Arbitrary Planform in Subsonic Flow by the Kernel Function Method," MIT ASRL T.R. 64-1.

8. H. Multhopp, "Methods for Calculating the Lift Distribution of Wings (Subsonic Lifting-Surface Theory)," ARC R & M 2884.

9. B. Laschka, "Zur Theorie der Harmonish Schwingenden Tragenden Flache bez Unterschallstromung," Z. Flugwiss 12, pp. 265-292, 1963.

10. H. Ashley and W. S. Rowe, "Unsteady Aerodynamic Loading of Wings with Control Surfaces," Z. Flugwiss 18, September/October, pp. 321-330, 1970.

11. H. Ashley, "Subsonic Oscillatory or Steady Airloads on Wings with Control Surfaces and Other Discontinuities," SUDAAR No. 336, December 1967.

12. B. Darras and R. Dat, "Application de la Theorie de la Surface Portante a des Ailes Munies de Gouvernes," TIRE A Part, T.P. n. 889, 1970.

13. R. J. Zwaan, "On a Kernel-Function Method for the Calculation of Pressure Distributions on Wings with Harmonically Oscillating Control Surfaces in Subsonic Flow," NLR TR 70123 U.

14. W. S. Rowe, B. A. Winther and M. C. Redman, "Unsteady Subsonic Aerodynamic Loadings Caused by Control Surface Motions," J. or Aircraft, Vol. 11, No. 1, pp. 45-54, January 1974.

15. R. T. Medan, "Steady, Subsonic, Lifting Surface Theory for Wings with Swept, Partial Span, Trailing Edge Control Surfaces," NASA TN D-7251, April 1973.

16. B. L. Hewitt, "AGARD-CP-80-71 Symposium on Unsteady Aerodynamics for Aeroelastic Analyses of Interfering Surfaces," Part II, pp. 14-1 to 14-48.

17. H. Forsching, H. Triebstein and J. Wagener, "AGARD-CP-80-71 Symposium on Unsteady Aerodynamics for Aeroelastic Analyses of Interfering Surfaces," Part II, pp. 15-1 to 15-12.

18. B. E. Tinling and J. K, Dickson, "Tests of a Model Horizontal Tail of Aspect Ratio 4.5 in the AMES 12-foot Pressure Wind Tunnel," NACA RM A9G13.

19. A. D. Hammond and B. A. Keffer, "The Effect at High Subsonic Speeds of a Flap-Type Aileron on the Chordwise Pressure Distribution Near Mid-Semispan of a 35° Sweptback Wing of Aspect Ratio 4 Having NACA 65A006 Airfoil Section," NACA RM L53C23.

20. V. Beals and W. P. Targoff, "Control Surface Oscillatory Coefficients Measured on Low Aspect Ratio Wings," WADC TR No. 53-64.

21. R. B. White and M. T. Landahl, "Effect of Gaps on the Loading Distribution of Planar Lifting Surfaces," AIAA Journal, pp. 626-631, April 1968.

22. I. Abel and M. C. Sandford, "Status of Two Studies on Active Control of Aeroelastic Response," NASA TM X-2909, September 1973.

23. A. G. Rainey, C. L. Ruhlin and M. C. Sandford, "Active Control of Aeroelastic Response," AGARD-CP-119, pp. 16-1 to 16-8.

24. I. H. Abbott and A. E. VonDoenhoff, "Theory of Wing Sections, McGraw-Hill Book Company, 1949.

*U.S. GOVERNMENT PRINTING OFFICE: 1975 - 635-275/8